Electronic Spectra of Carbon Chain Molecules

— C_4H, C_4D and C_3N —

炭素鎖分子の電子スペクトル
− C_4H, C_4D, C_3N −

Kennosuke Hoshina

①

Electronic Spectra of Carbon Chain Molecules

— C_4H, C_4D and C_3N —

Kennosuke Hoshina

Department of Pure and Applied Sciences,
The Collage of Arts and Sciences,
The University of Tokyo

March 1997

Contents

Chapter 1. General Introduction

Chapter 2. Laser-Induced Fluorescence Spectroscopy of the C_4H and C_4D Radicals in Supersonic Free Jets

Chapter 3. Dispersed Fluorescence Spectra from $\widetilde{B}^2\Pi_i$ of the C_4H and C_4D Radicals.

Chapter 4. Laser Induced Fluorescence Spectroscopy of C_3N.

Chapter 5. Conclusions *168*

Chapter 1

General Introduction

1.1 Spectroscopy of Carbon Chain Molecules.

Molecular spectroscopy in gas phase

Molecular spectroscopy of isolated molecules in the gas phase is a basis of science investigating the fundamental unit of substance, "molecules", and simultaneously is a powerful detection technique of molecules by using electromagnetic wave (in the microwave, infrared, visible and ultra-violet region) corresponding to the energy separations between individual quantum states (rotational, vibrational and electronic states) based on quantum theory[1,2]. Excellence of molecular spectroscopy as a detection technique of molecules is that it does not require isolation of species to be studied and thus allows us to detect molecules as "they are". Systems in which molecular spectroscopy exercise its merit is extensive: astronomical objects, atmosphere, combustion, and plasma. In such systems violent or moderate chemical reactions are taking place continuously, in which short-lived molecules exist. Short lived molecules are chemically unstable but physically stable, namely chemically reactive. They can exist only in the middle of chemical reactions, thus they also are called "intermediate species" and cannot be isolated under normal conditions. Detection of such short-lived molecules is quite important as a mean to trace chemical reactions and probe the physical environment of the system, because most of the chemical reaction in gas phase consist of many chain reactions involving short-lived molecules. Molecular spectroscopy provides a mean to answer to these needs.

Depletion of stratospheric ozone is a well known but serious example for this kind of chemical reactions. Although many reactions are involved in this problem, the following chain reaction called ClOx cycle is considered to be taking one of the most important roles for ozone depletion[3]

$$\mathrm{Cl + O_3 \rightarrow ClO + O_2}$$

$$\mathrm{ClO + O \rightarrow Cl + O_2} \qquad \text{net} \qquad \mathrm{O_3 + O \rightarrow 2O_2}$$

Here ClO is a short lived molecule, and its spectroscopic data is required to detect or discuss photochemical reactions involving this molecule in the atmosphere[4,5]. Thus spectroscopic study of molecules based on laboratory experiment is necessary in understanding familiar phenomena involving chemical reactions. Simultaneously most of these short-lived molecules are called "free radicals" which have spectroscopic interest in its energy structure because they have an unpaired electron. By accumulating spectroscopic data on various molecules and providing explanations of physical properties of individual molecules, "Molecular Spectroscopy" constitutes an important field in supporting powerfully the related areas in science.

Carbon Chain Molecules (Why Carbon Chain Molecules?)

"Carbon chain molecules", I am considering, C_n, C_nX(X=H, N, O, S, Si...), HC_nX(X=N, O, S), belong to short-lived molecules mentioned above, involved in the middle of chemical reactions under carbon-rich conditions. Previous spectroscopic studies on carbon chain molecules are summarized in Table 1.1, which indicates mainly the first observations of the transitions of carbon chain molecules (four-atomic or more). Left hand side of the Table describes electronic transitions between the ground state and the electronic excited states (observed in the visible to UV region) and right hand side the rotational transitions (microwave region) or vibrational transitions (IR region) within the electronic ground state.

Carbon chain molecules cannot be considered without referring to the astronomical observations. It can be said that at the beginning of these investigations carbon chain molecules were paid attention particularly by astronomers. Actually carbon chain molecules whose existence were first proved by astronomical observations are not rare. For example, well known C_3 emission in the near UV region has already been observed from a comet in 1882[6] about a half century before molecular spectroscopy was established in 1930's. Also during past 20 years searches for new longer carbon chain molecules had been carried out enthusiastically by radio telescope looking towards interstellar media as readily seen in Table.I In the late 1970s five new

Table 1.1 Previous Spectroscopic works about Carbon Chain Molecules.

	Electronic Excited States	Ground States
	C_3 emission (1882)	
year		
1960	C_3 CCN CNC ('64)	
|	(HCCN) ('65)	
1970		$\underline{HC_3N}$ ('71)
	C_4H ** ('75)	$\underline{HC_5N}$,('75')
		$\underline{HC_7N}$, $\underline{HC_9N}$ ('77, '78)
		$\underline{C_4H}$, $\underline{C_3N}$ ('77,'78)
1980	HCCS ('80)	
		$\underline{C_3O}$ ('83)
	(HCCO) ('84)	HCCN ('84)
	$\boxed{C_{60}\ ('85)}$	$\underline{C_3H}$ ('85)
		$\underline{C_5H}$, $\underline{C_6H}$ ('86)
		$\underline{CCS}$, $\underline{C_3S}$ ('87)
		$\underline{C_4H}$ (v=1, 2)
		HCCO
		$\underline{SiC_4}$ ('89)
1990		C_7 (90)
		C_4 ('91, '91)
		HC_3O ('92)
	C_nH_m, $C_nH_m^-$ ** ('93)	C_6 C_4S, C_5S ('93)
	C_6, C_8, ..., C_{14} ** ('95)	C_{13} HC_4O, HC_4S, HC_5S ('94)
	C_6^-, C_8^-, ... ,C_{20}^- **	C_4O, C_5O,...,C_9O ('95)
	C_6H, C_8H,...,$C_{16}H$ **	
	C_4, C_4^- ** ('96)	C_7H, $\underline{C_8H}$, C_9H, $C_{11}H$ ('96)
	C_4^-	$HC_{11}N$, $HC_{13}N$
	C_6^-, C_8^- *	C_5N
	HCCO	
	C_4H, C_3N, HCCN, CCS (PDN-LIF spctroscopy)	

* gas phase low resolution
** matrix isolation
( ) not confirmed

underlines
observed both laboratory and intersteller media

carbon chain molecules had been discovered in succession by radio telescopes. C_4H and C_3N, the molecules treated in this thesis, had already been known for about 20 years, and their discovery in interstellar media was the first detection of carbon chain free radicals containing three or four carbon atoms. Therefore their abundance in interstellar clouds are relatively larger than other free radicals and conversely these historical background indicates the importance of carbon chain molecules for astronomical interest.

Carbon chain molecules are a subject with great interest also in combustion chemistry or plasmas, as short-lived intermediate species in the growing processes in forming large carbon clusters such as graphite, diamonds and C_{60}. In spite of the great interest, existence and behavior of carbon chain molecules in such systems are not well unraveled. For instance, in chemical vapor deposition (CVD) synthesis of diamond in C_2H_2/O_2 flame, C_2 and CH are detected by UV emission in flame, and reactions relating C_2 and CH are reported to have important roles in diamond synthesis[7]. Much larger carbon chain molecules such as C_n, C_nH ($n \geqq 3$) must be expected to be involving in this synthesize process. C_{60}, which attracts attentions of all scientists' since its discovery in 1985[8], is efficiently synthesized in combustion and plasma. But formation mechanism of C_{60} from carbon atoms or carbon-containing molecules has been a still unresolved question. Investigations of carbon chain molecules in the combustion or plasma including synthesis of C_{60} must provide a important information to solve this question.

Electronic transitions or electronic states of carbon chain molecules have been scarcely known, in spite of various needs for spectroscopic data on these carbon chain molecules. On the other hand a number of studies of rotational transitions and some of vibrational transitions of C_n series in the ground states have been reported. Comparison between the right and left sections in Table. 1.1 clearly shows lack of data on electronic states of carbon chain molecules. For triatomic molecules spectroscopic studies on electronic excited state on carbon chain molecules are vigorously carried out by Herzberg and Ramsay, and co-workers in 1960s by using grating spectrometer with photographic plates. But strangely, in 1970s and 1980s new discoveries of electronic transitions or electronic states of carbon chain molecules are almost missing, althoug new carbon chain molecules had been detected constantly by microwave spectroscopy and IR absorption spectroscopy in the ground state. One of the reasons for this lack of study on the electronic transition is that it was difficult to produce carbon chain molecules with enough concentrations to be detected, and the choice of an appropriate detection method is also difficult while various techniques have been considered to observe electronic transitions: photo detection, mass detection, ion detection.

In the middle of 1990s three experimental strategies have succeeded to observe new systems of electronic transitions of carbon chain molecules by solving the problems: (1) absorption spectrum of mass selected carbon chain molecules in a rare gas matrix by the group of J.P. Meier(Basel Univ. in Switzerland)[9-11]; (2) mass-selected photofragment or resonance photodetachment spectroscopy by the group of D.M. Neumark (Univ. of California, Berkeley) [12-14]; (3) laser induced fluorescence spectroscopy combined with a pulsed-discharge nozzle(PDN) developed in our laboratory [15,16]. In 1993 Meier's group reported absorption spectra of C_nH_m and $C_nH_m^-$ series in Ne matrix from an interest related to the Diffuse Interstellar Bands(DIBs)[9], consisting of many absorption lines superimposed on the visible and near-infrared of stars located on the far side of interstellar clouds. After that, in 1995, they succeeded in observing electronic transitions of C_{2n}^-(2n=4-20), C_{2n} (2n=6-12) and C_nH (2n=6-12) series. The matrix isolation method has an advantage that it can isolate short-lived molecules with high concentration, but has a difficulty in identification due to low spectral resolution. Both our and Neumark's systems employ PDN as molecular generation source, which gave a breakthrough in looking for longer carbon chain molecules by laboratory microwave spectroscopy in 1992 by Ohshima and Endo[17]. In 1996 group of Neumark observed electronic transitions of carbon cluster anions, C_n^- (n=4,6,8) by mass-selected photodetatchment spectroscopy[12,13] and HCCO by photofrgment spectroscopy of neutralized mass-selected $HCCO^-$[14], where spectra of C_4^- and HCCO were rotationally resolved. Their system has advantage in spectroscopy on carbon chain ionic species and investigations for dissociation dynamics as it has very high sensitivity. On the other hand, our method is laser induced fluorescence(LIF) spectroscopy of products in discharge plasma by using PDN. LIF spectroscopy is one of a familiar highly sensitive detection method established along the development of tunable lasers in 1970s and still one of the most powerful method for spectroscopic studies on not only electronic excited states but also the ground state[18-20]. LIF spectroscopy has possibility to be easily applied to investigations in combustion or atmosphere. At all events spectroscopic studies on electronic states of carbon chain molecules have just started in recent years, and electronic transitions of even longer carbon chain molecules should be discovered subsequently in the near future.

In this thesis I will present electronic spectra of C_4H and C_3N, which have been discovered in earliest years of the spectroscopic studies on carbon chain molecules in 1977 and 1978, and I also include a study on an isotopomer C_4D by using the system with pulsed discharge nozzle and laser induced fluorescence spectroscopy. I measured two kinds of electronic spectra, (1)Laser induced fluorescence excitation spectra (called LIF spectra) and (2) dispersed fluorescence spectra (called DF spectra). From the LIF spectra we could clarify rotational and vibrtional structures of the electronic excited state ($\tilde{B}^2\Pi_i$) and recognize relaxation processes electronically excited C_4H and C_3N. Vibrational structures of the ground state ($\tilde{X}^2\Sigma^+$) and first excited electronic state ($\tilde{A}^2\Pi_i$) of C_4H and C_3N were also observed in the DF spectra. Electronic, vibrational and rotational energy structures of four- or five- atomic linear molecules, such as C_4H and C_3N, are expected to be characteristic due to its high symmetry and plural-bending vibrational modes, and are of particular spectroscopic interest. But experimental data of such kind of molecules have been quite limited. Therefore, the observation of electronic-vibrational transitions of C_4H and C_3N must, I believe, provide new spectroscopic trend. At the same time, these observations of the electronic transitions including information on relaxation processes of C_4H and C_3N, must contribute to understanding astronomical and other environments involving chemical reactions of carbons.

1.2 Astronomical Interest of Carbon Chain Molecules

Carbon chain molecules such as C_4H and C_3N have been identified only in interstellar medium other than laboratory. There are some unresolved astronomical observation which are considered to be very important for understanding the interstellar chemistry. I introduce here two attractive astronomical topics related to electronic structure of carbon chain molecules, "Diffuse Interstellar Bands (DIBs)" and "vibrationally excited C_4H".

Diffuse Interstellar bands Diffuse Interstellar Bands (DIBs) have been observed in spectra recorded towards stars that are partially obscured by an interstellar medium as shown in Fig.1.1. There are now over 100 known bands[21-25] and it is now clear from the band width, depths, and shapes, that these lines are unlikely to come from a single carrier. Although many candidates have been proposed as carriers, such as gas-phase carbon chains[26], fullerenes[27] and dust grains[28], none of which succeeded in making definite assignment of unidentified DIBs. In 1983 Bell *et al.* suggested that the observed density of C_4H in the Orion gas arm were sufficient enough to explain strong diffuse bands and recommended that C_4H was a candidate for a strong DIBs at 4428 Å[29]. Based on their proposition, Kobolweski calculated transition energies of C_4H by an *ab initio* calculation in 1994 and derived a negative result that the C_4H $\tilde{B}^2\Pi$ - $\tilde{X}^2\Sigma^+$ transition was about 3890 Å[30] which was not consistent with 4428 Å. Therefore, observation of the gas-phase electronic spectrum of C_4H has been required to judge this issue. Quite recently, Sarre suggested that large "carbon ring" molecules including 14-30 carbon atoms were good candidates for diffuse bands at 6614 and 5797 Å[31]. Laboratory experiments for carbon ring molecules are also required.

Vibrationally excited C_4H Several vibrationally excited molecules have been detected in the carbon star envelop IRC+10216$^{*)}$ by radio telescopes. These are abundant species such as HCN (v_2=1,2)[32,33], CS (v=1)[34] ,SiS (v=1)[35,36], HC_3N (v_7=1)[37], and C_4H (v_7=1,2)[35,38]. Among these molecules, C_4H is particularly

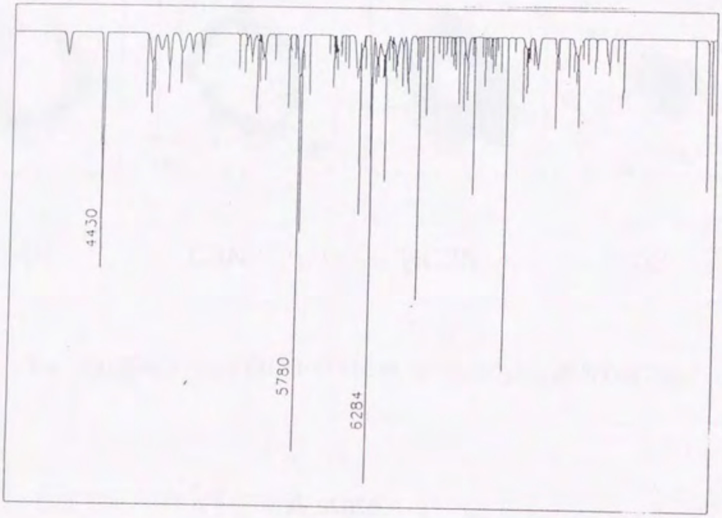

Fig. 1.1 Diffuse Interstellar Bands

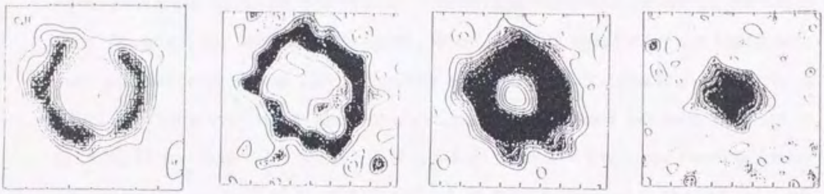

C4H C3N HC3N SiS

Fig.1.2(a) Distribution in IRC+10216 [C4H ref. 58, HC_3N, C_3N, SiS ref.59]

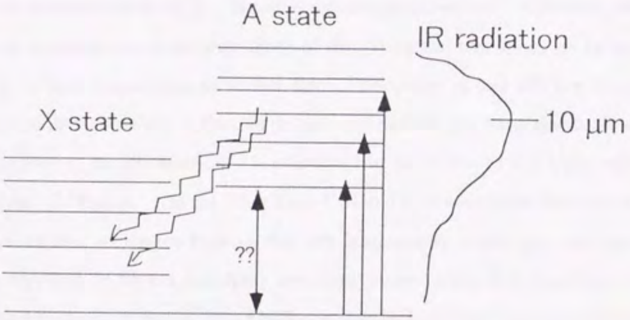

Fig.1.2(b) Excitation mechanism of C_4H.

excited so that signals of the ν_7 and $2\nu_7$ states have intensities as large as 1/3 and 1/6 of that of the ground state[39]. Fig.1.2(a) show distributions of C_4H and other molecules in the carbon star envelope, IRC+10216. As physical conditions depend on the radius from the carbon star located in the center, HC_3N and C_3N distribute in the region with same physical conditions as C_4H. However signals in the vibrationally excited state of HC_3N (v=1) are very weak, and no vibrationally excited state has been detected in IRC+10216 for C_3N[40]. Since HC_3N and C_3N have low frequency bending modes (HC_3N ν_7=223 cm^{-1}[41], C_3N ν_5=131 cm^{-1} which were determined in the present work (Chapter 4)) like C_4H (ν_7=118 cm^{-1} and $2\nu_7$=235 cm^{-1} (Chapter 3), they also must be excited efficiently. In order to explain the exceptionally excited C_4H, Yamamoto *et al.* proposed an excitation mechanism which was derived from the particular electronic structure of C_4H: radiation of dusts in carbon star envelope with its peak at 10 μm induces electronic transitions from the ground state to the "low-lying $\tilde{A}^2\Pi_i$ state", and the following emission populates them in vibrationally excited states including ν_7, $2\nu_7$ as schematically described in Fig.1.2(b). The two transition steps are electronic transitions while the relaxation from ν_7, $2\nu_7$ to v=0 is vibrational transitions. Generally, electronic transition moments are larger than those of the vibrational transitions by factor of 10^4, resulting in large populations in ν_7 and $2\nu_7$. The reason of less efficient excitation in HC_3N and C_3N is that these molecules do not have suitable low-lying electronic states for the absorption of the IR radiation. It is known that HC_3N has its first electronic excited state at the UV region. On the other hand C_4H and C_3N have been considered to have similar electronic structures because they are isoelectronic molecules with each other. C_3N is expected to have a low-lying electronic excited state $A^2\Pi$ like C_4H. But no experimental approach for $\tilde{A}^2\Pi$ of both the species have been reported until now. I will describe the first observation of $\tilde{A}^2\Pi_i$ state of C_4H and C_3N in Chapter 3 and 4.

---

*)Interstellar medium

IRC+10216 is a late type carbon star which is well known to be the brightest celestial body emitting at the wavelength region, 10-20 μm. Chemical reactions are different from the inner region to the outer region of the envelope due to the variations of temperature and density: chemical equilibrium reactions at a relatively high temperature are dominant in the inner region, neutral-neutral reactions in the intermediate region, and photochemical and ion-molecule reactions in the outer region. C_4H and C_3N are observed in the outer region.

1.3 Linear polyatomic molecules and Vibronic Interactions

Linear polyatomic molecules are interesting with complex energy structures due to its high symmetry about their molecular axis. Although most of the physical quantities associated with angular momenta are "degenerated" due to the symmetry along molecular axis in linear molecules, the degeneracy is lifted by a strong coupling between electronic and vibrational motions, generally called the "vibronic interaction", leading to a breakdown of the Born-Oppenheimer approximation. The results of vibronic interaction in linear polyatomic molecules are represented by the Renner-Teller effect[42] and the Herzberg-Teller effect[43] as follows.

Renner-Teller effect. This effect is important for a degenerate electronic state of linear molecules, where the vibrational angular momentum induced by a degenerate vibrational mode couples with the electronic angular momentum, resulting in further splittings of the vibrational levels. Thus Renner-Teller effect occur within the degenerate electronic state.

Herzberg-Teller effect. This effect is important for both degenerate and non-degenerated electronic states, where a close lying electronic states of a polyatomic molecule may be mixed by excitation of a vibrational mode. Thus this effect induces interstate interactions such as those between Π and Σ, and often distorts the vibrational potential function or causes intensity borrowing of an electronic transition.

The theoretical treatment of the vibronic interactions of triatomic linear molecules has been well established[42-47] and many spectroscopic studies of triatomic molecules including "Carbon Chain Molecules" such as C_3[48,49], CCN[50], CNC[51] have been carried out and discussed based on the theory. In linear polyatomic molecules there are three angular momenta of interest:

L: the total orbital momentum of the electrons. (Λ)

S: the total spin angular momentum of the electrons. (Σ)

G: the vibrational angular momentum of the nuclei. (l)

G is associated with the degenerate bending vibrations (N-2 bending modes exist for N-atom linear molecules. See Appendix 1.1 where normal vibrational modes are schematically described for C_4H and C_3N). Projections of these angular momenta along the molecular axis, are called, Λ, Σ, and l, respectively as shown in parentheses. For a given value of the bending vibrational quantum number v, l takes the values v, v-2, v-4,...,-v. The electronic states of a linear molecule are labeled by Σ, Π, Δ,... for $\Lambda=0, \pm 1, \pm 2,...$ If the bending potential is harmonic and there is no coupling between the electronic motion and the bending vibration, that is the molecule behaves within the Born-Oppenheimer approximation, the various degrees of freedom mentioned above can be separated and the wave function is written in the form,

$$|\Lambda,n,l,\Sigma\rangle = \exp(i\Lambda\theta)\rho_{n|l|}(r)\exp(il\phi)\Phi_{spin} \qquad (1.1)$$

where n equals v+1, r is the amplitude of the degenerate bending vibration mode, ϕ is an azimuthal angle of the bending plane, and θ is azimuthal angle of the unpaired electron. $\rho_{n|l|}(r)\exp(il\phi)$ is the wavefunction for the two dimensional harmonic oscillator[52] and Φ_{spin} is the spin wavefunction, which is neglected for a singlet electronic state and has an expectation value along the molecular axis, $\Sigma=\pm 1/2$, for doublet electronic states. (From equation (1.1) electronic transitions must satisfy the $\Delta l=0$ selection rule)

Λ and Σ are good quantum numbers. $\Omega=\Lambda+\Sigma$ is also a good quantum number for molecules without excitation of the bending mode. However when a bending mode is excited in a degenerate electronic state, such as $l \neq 0$ vibrational states in a Π electronic state, angular momenta L and G couple and Λ and l are not good quantum numbers any more. In this case, $K=|\Lambda+l|$, Σ, and $P=\Lambda+l+\Sigma$ are good quantum numbers, and such "vibronic states" are generally labeled by Σ, Π, Δ,... for $K=0, \pm 1, \pm 2,...$, and actually vibronic couplings caused by the Renner-Teller effect or the Herzberg-Teller effect mix the same K vibronic states, namely between the same representations such as $\Sigma \leftrightarrow \Sigma$ or $\Pi \leftrightarrow \Pi$.

Let us consider vibronic states in a $^2\Pi$ electronic state, to which $\tilde{B}\,^2\Pi_i$ state of C_4H and C_3N belong. The $^2\Pi$ electronic state has an angular momentum of electron $\Lambda=\pm1$ and that of an unpaired spin $\Sigma=\pm1/2$. Vibronic states given by an excitation of a bending mode by a quantum number v=0,1,2 are expressed as ^2K_P, similar to the notation $^2\Lambda_\Omega$ for diatomic molecules,

$$\begin{array}{llllll}
v=0 & |\Lambda=\pm1,l=0\rangle|\Sigma=\mp\tfrac{1}{2}\rangle & K=1 & P=\tfrac{1}{2} & ^2\Pi_{1/2} \\
 & |\Lambda=\pm1,l=0\rangle|\Sigma=\pm\tfrac{1}{2}\rangle & K=1 & P=\tfrac{3}{2} & ^2\Pi_{3/2} \\
v=1 & |\Lambda=\pm1,l=\mp1\rangle|\Sigma=\pm\tfrac{1}{2}\rangle & K=0 & P=\tfrac{1}{2} & ^2\Sigma_{(1/2)} \\
 & |\Lambda=\pm1,l=\mp1\rangle|\Sigma=\mp\tfrac{1}{2}\rangle & K=0 & P=\tfrac{1}{2} & ^2\Sigma_{(1/2)} \\
 & |\Lambda=\pm1,l=\pm1\rangle|\Sigma=\mp\tfrac{1}{2}\rangle & K=2 & P=\tfrac{3}{2} & ^2\Delta_{3/2} \\
 & |\Lambda=\pm1,l=\pm1\rangle|\Sigma=\pm\tfrac{1}{2}\rangle & K=2 & P=\tfrac{5}{2} & ^2\Delta_{5/2} \\
v=2 & |\Lambda=\pm1,l=0\rangle|\Sigma=\mp\tfrac{1}{2}\rangle & K=1 & P=\tfrac{1}{2} & ^2\Pi_{1/2} \\
 & |\Lambda=\pm1,l=0\rangle|\Sigma=\pm\tfrac{1}{2}\rangle & K=1 & P=\tfrac{3}{2} & ^2\Pi_{3/2} \\
 & |\Lambda=\pm1,l=\mp2\rangle|\Sigma=\mp\tfrac{1}{2}\rangle & K=1 & P=\tfrac{1}{2} & ^2\Pi_{1/2} \\
 & |\Lambda=\pm1,l=\mp2\rangle|\Sigma=\mp\tfrac{1}{2}\rangle & K=1 & P=\tfrac{3}{2} & ^2\Pi_{3/2} \\
 & |\Lambda=\pm1,l=\pm2\rangle|\Sigma=\mp\tfrac{1}{2}\rangle & K=3 & P=\tfrac{5}{2} & ^2\Phi_{5/2} \\
 & |\Lambda=\pm1,l=\pm2\rangle|\Sigma=\mp\tfrac{1}{2}\rangle & K=3 & P=\tfrac{7}{2} & ^2\Phi_{7/2}
\end{array}$$

The above wavefunctions are still under the Born-Oppenheimer approximation and also can be written by the decoupled form $|\Lambda\rangle|l\rangle$. They constitute basis functions, and the vibronic states in a vibrational state v are degenerate without the vibronic interactions. (In reality since $^2\Pi$ electronic state has a spin angular momentum, the degeneracy is lifted by the spin-orbit interaction. See the theory in Chapter 2.) Hamiltonian of the vibronic interaction is expressed as,

$$H' = V_1 r\cos(\theta-\phi) + V_2 r\cos 2(\theta-\phi)$$

The first term, which has nonzero matrix elements between the $|\Delta \mathrm{v}|=1$, $\Delta K=0$, $\Delta\Lambda=\pm1$, and $\Delta l=\mp1$ states, causes the Herzberg-Teller effect, and the second term, which has nonzero matrix elements between the $|\Delta \mathrm{v}|=0$, $\Delta K=0$, $\Delta\Lambda=\pm2$, and $\Delta l=\mp2$ states, gives the first order contribution of the Renner-Teller effect.

Therefore, for example, two $^2\Sigma$ states of v=1 in a $^2\Pi$ electronic state have nonzero matrix elements of the Renner-Teller effect $\langle \Lambda = \pm 1, l = \mp 1, \Sigma | H' | \Lambda = \mp 1, l = \pm 1, \Sigma \rangle$, and split into two with eigen wavefunctions of $|\Sigma^{\pm}\rangle = \frac{1}{\sqrt{2}}\left[|\Lambda = \pm 1, l = \mp 1, \Sigma\rangle \pm |\Lambda = \mp 1, l = \pm 1, \Sigma\rangle \right]$ as shown in Fig.1.3. The Herzberg-Teller effect may occur when a $^2\Sigma$ state exists, for example, between Σ(K=0) vibronic states of v=1 in the $^2\Pi$ electronic state and the Σ(K=0) vibronic state in v=0 in the $^2\Sigma$ electronic state. Its matrix element can be written as $\langle \Lambda = \pm 1, l = \mp 1, \Sigma | H' | \Lambda = 0, l = 0, \Sigma \rangle$. Σ^+ state has a nonzero matrix element while Σ^- does not. As a result, only Σ^+ vibronic states are affected by the Herzberg-Teller effect and shifted as shown in Fig.1.3, where the $^2\Sigma$ electronic state is supposed to lie above the $^2\Pi$ electronic state.

In the case of four or five atom-linear molecules, like C_4H and C_3N, vibronic interaction takes place by more a complicated form than the case of a triatomic molecules because degrees of freedom of the degenerate bending mode increase as number of atoms increase. Theory of the vibronic interaction for four-atomic molecules was discussed by Petelin and Kiselev[53,54], but experimental observations of vibronic structures of four or five atom-molecules are limited. Recently Tang and Saito[55] observed microwave spectra of four atomic linear molecule, HCCS, and derived higher order vibronic interaction terms between the two degenerate bending modes, which have not been considered for triatomic molecules, in order to explain precisely determined molecular constants. Considering the lack of spectroscopic data of vibronic structures of four or five atom linear molecules, our observation of vibronic states of C_4H and C_3N laeds to further understanding of this spectroscopic target.

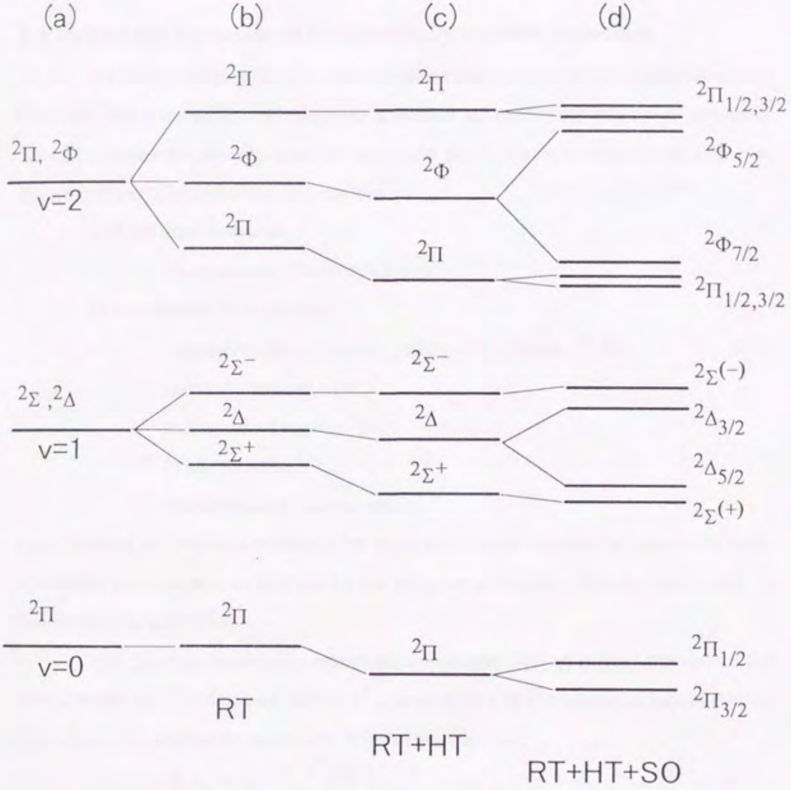

Fig.1.3 Level splittings of a $^2\Pi$ electronic state.
(a) unpertubed, (b) only the Renner-Teller effect, (c) Renner-Teller effect and Herzberg-Teller effect on an assumption that $^2\Sigma^+$ electronic state lies above, and (d) Renner-Teller effect, Herzberg-Teller effect and spin-orbit interaction.

1.4 Relaxation Processes of Electronically Excited Molecules

Excited molecules do not remain excited states even under the isolated condition (collision free condition), and there are a number of interesting relaxation processes. These processes are distinguished to two main paths: Radiative transitions and non-Radiative transitions including dissociations:

1) Radiative transitions

Fluorescence, Phosphorescence

2) non-Radiative transitions

Intramolecular vibrational energy redistribution (IVR)

Internal conversion (IC)

Intersystem Crossing (ISC)

Predissociation

Autoionization, Isomarization

Laser induced fluorescence studies in jet cooled conditions provide evidences for these non-radiative processes, in addition to the radiative processes through observation of fluorescence time profiles.

The radiation process is a spontaneous emission from an excited state |s> to the ground states {|g>} and natural lifetime τ^0_{rad} associated with the relaxation rate of excited molecules are expressed by using Einstein's A coefficient as,

$$1/\tau^0_{rad} = \sum_g A_{sg} = \sum_g \frac{64\pi^4\nu^3}{3hc^3}\left(\frac{g_g}{g_s}\right)\left|\mu_{sg}\right|^2 \tag{1.2}$$

and the time profile is expressed as a single exponential decay,

$$I(t) = I_0 \exp(-\frac{1}{\tau^0_{rad}}t) \tag{1.3}$$

where $|\mu|^2$ is a transition dipole moment, and g is the degeneracy of the states. Generally for most of molecules, especially for larger molecules, non-radiative transitions occur competitively to the radiative transition, where non-diabatic processes with other vibronic states take place through the vibronic coupling, the spin-orbit coupling, and the anhrmonic interaction, leading to IC (spin-allowed transitions by operators of nuclear motions, $\partial/\partial Q$), ISC (spin-forbidden transitions by the operator H_{SO}) and IVR(within the same electronic state), respectively, as schematically shown in Fig.1.4 where |s> and |i> are basis states within the BO approximation. These processes are more important for large molecules with high density of states {|i>} accessible from |s> due to high degrees of freedom. In the model of Fig.1.4, zero order state |s> is prepared by laser excitation, and is subsequently mixed with dark states {|i>}(n states), and eigen states are produced as the form,

$$|\varphi_n\rangle = a_n|s\rangle + b_i^n \sum_i |i\rangle \tag{1.5}$$

The rate of this relaxation process is given by Fermi's golden rule,

$$W = \frac{2\pi}{h}\rho\overline{|v_{si}|^2} \tag{1.6}$$

where ρ is the density of states of |i> and v_{si} is an interaction matrix element. Thus the time profile is expressed as,

$$I(t) = I_0 \exp\left\{-\left(\frac{1}{\tau_{rad}^0} + W\right)t\right\} \tag{1.7}$$

If |i> states are those of repulsive potential or correlate to a dissociation coordinate, most of the molecules dissociate into fragments, leading to a substantial decrease of population. In most of the cases involving dissociation, since W is much larger than $1/\tau^0_{rad}$ the fluorescence lifetime becomes $1/W(<\tau^0_{rad})$ or in an extreme case fluorescence cannot be observed. HCCO is a latter type of molecules, because Mordaunt *et al.* have recently observed $\tilde{C}^2\Pi(^2A")$- $\tilde{X}\,^2A"$ transition of HCCO[14] around 34000 cm^{-1} by monitoring the CH and CO fragments, in which both IC and ISC lead to non-diabatic transitions to pridissociation. However we could not observed any LIF signal in the same region under the optimized conditions for the HCCO production[57]. However if |i> states belong to bound states, the molecule keep the excitation energy in $|\varphi_n(t)\rangle$ states even after the relaxation, and thus the fluorescence time profile has an additional component to (1.7), according to probability of finding |s> in $|\varphi_n(t)\rangle$ as,

$$\begin{aligned} I(t) &= |<s|\varphi_n(t)>|^2 \\ &= \sum_i |a_{si}|^4 \exp\left(-\frac{1}{\tau_i}t\right) + 2\sum_{i \neq i'} |a_{si}|^2\,|a_{si'}|^2 \exp\left\{-\frac{1}{2}\left(\frac{1}{\tau_i}+\frac{1}{\tau_{i'}}\right)t\right\}\cos\omega_{ii'}t \end{aligned} \qquad (1.8)$$

The first term causes unusually long lifetime decay called the "Douglas effect"[56], and the second term causes a "Quantum beat". If the number of |i> is large, $|a_{si}|^4$ and $|a_{si}|^2|a_{si'}|^2$ are approximated by 1/n. Detail features of the time profile expressed by equation (1.8) vary for individual molecules according to the density of states of {|i>}. HCCS is one of such type of molecules. In the fluorescence time profile of HCCS (24000-27000 cm^{-1}) in $\tilde{B}^2\Pi_i$, Kouguchi *et al.* have observed various decay patterns which depended on the excitation energies, which can be expressed by equation of (1.7) and (1.8)[16], caused by IC to highly vibrationally excited states of the ground state. The finding suggested the increase of the density of states |i> as an increase of the excitation energy.

I will discuss the relaxation processes and the energy flow of C_4H and C_3N in Chapters 2 and 4 based on the fluorescence time profiles. Fluorescence time profiles of C_4H and C_3N contain both short and long decay components with quantum beat on it: the former corresponds to the fluorescence from $\tilde{B}^2\Pi_i$ relaxing to high vibrational states of $\tilde{X}^2\Sigma^+$ and $\tilde{A}^2\Pi_i$ through IC(equation (1.7)), and the latter to the fluorescence from the eigen states (equation (1.8)). Short decay component of C_4H (10-20 ns)is much faster than that of $C_3N(\approx 120$ ns), and long decay component of C_4H is very weak compared with that of C_3N. These results are consistent with the fact that density of states ($\propto$ n) of C_4H is larger than C_3N. Long lived components are about 2-3 μs for both C_4H and C_3N.

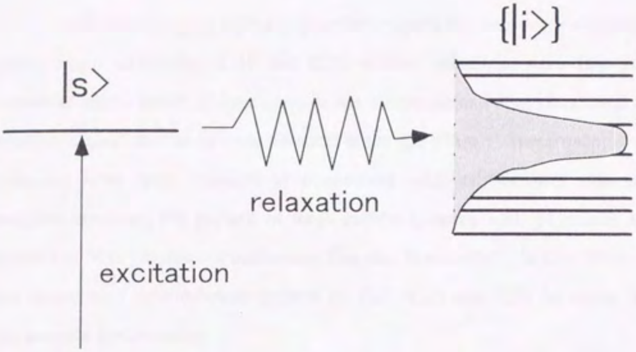

Fig.1.4 Schematic diagram of non-radiative relaxation in zero-order model. |s> and |i> are zero order states.

1.5 The aim and scope of the thesis

The main purpose of the present investigation is to observe electronic spectra of carbon chain molecules, C_4H and C_3N, whose existence were first recognized in interstellar media about 20 years ago, while electronic and also vibrational transitions of these molecules have never been detected in the gas phase. Spectroscopic data on these molecules have been required in connection with astronomical interests, chemical reactions involving the growth of large carbon clusters, and, of course spectroscopic interests of linear molecules containing four and five atoms. In this thesis I present the first observation of electronic spectra of C_4H, C_4D and C_3N by using laser induced fluorescence spectroscopy.

Chapter 2 explains observations of electronic spectra of C_4H and C_4D $\tilde{B}^2\Pi_i$ - $\tilde{X}^2\Sigma^+$ system by LIF spectroscopy in the region of 24000-25000 cm^{-1}. Molecular constants for 20 vibronic states of C_4H and 17 of C_4D were determined, and partial vibrational assignments were carried out. I will discuss vibronic interactions which depends on each bending mode from the vibrational and rotational structures. Relaxation processes of the $\tilde{B}^2\Pi_i$ state were discussed based on the fluorescence time profiles and obtained a conclusion that radiations and fast internal conversions occur competitively in the $\tilde{B}^2\Pi_i$ state rather than the dissociation. Nature of the local perturbations which were found in most of the vibronic states in the $\tilde{B}^2\Pi_i$ was considered. Finally, I disproved the proposition that C_4H might be a carrier of DIBs at 4430 Å which was not consistent with the present observation.

Chapter 3 explains observation of the dispersed fluorescence spectra of C_4H and C_4D from the $\tilde{B}^2\Pi_i$ state, and describes vibrational structures of the ground state $\tilde{X}^2\Sigma^+$ and the low-lying first electronic excited state $\tilde{A}^2\Pi_i$. The ν_7 (CCC bending) mode of $\tilde{X}^2\Sigma^+$ and the ν_6 (CCC bending) mode of $\tilde{A}^2\Pi_i$ were assigned, and the origin of the $\tilde{A}^2\Pi_i$ state was estimated to be 150 $cm^{-1}$for C_4H and 160 cm^{-1} for C_4D.

Chapter 4 describes observations of the electronic spectra of the C_3N, $\tilde{B}^2\Pi_i$ - $\tilde{X}^2\Sigma^+$ system in the region 28600-29200 cm^{-1} by LIF spectroscopy. Molecular constants of $\tilde{B}^2\Pi_i$ were determined from rotational analyses and relaxation processes from the $\tilde{B}^2\Pi_i$ state were discussed. Dispersed fluorescence spectra from the $\tilde{B}^2\Pi_i$ state were also observed. The DF spectra showed clearly distinguishable structures assigned to the fluorescence to the ground state and the first excited electronic state, $\tilde{A}^2\Pi_i$. The origin of the $\tilde{A}^2\Pi_i$ state were determined to be 1846 cm^{-1}. All the spectroscopic data of C_3N were compared with those of C_4H which is an isoelectonic molecule. The last chapter includes summary of the results obtained in the present investigation.

Referesces

1. G. Herzberg, "MOLECULAR SPECTRA AND MOLECULAR STRUCTURE" I-III(1966)
2. C.H. Towns and A.L. Schawlow, "MICRAWAVE SPECTROSCOPY", Dover Publications, Inc. New York(1975).
3. J.M.Mario and F.S. Rowland, Nature, **249**, 810 (1974)
4. S. Crewell, R. Fabian, K. Kunzi, H. Nett, T. Wehr, W. Read, and J. Waters, Geophys. Res. Lett. **22**, 1489 (1995).MW detection
5. Y. Matsumi, S.M. Shamsuddin, and M. Kawasaki, J. Chem. Phys., **101**, 8268 (1994).
6. W. Huggins, Proc. Soc. London **33**, 1 (1882).
7. K Komaki, M. Yanagisawa, I. Yamamoto and Y. Hirose, Jpn. J. Appl. Phys. **32**, 1814 (1993)
8. H.W. Kroto, J.R.Hearth, S.C.O'Brien, R.F. Curl, and R.E.Smally, Nature, **318**, 162 (1985).
9. J. Fulara, D. Lessen, P. Freivogel, and J.P Meier, Nature, **366**, 439 (1993).
10. P. Frivogal, J. Fulara, M. Jakobi, D. Forney, and J.P. Maier, J. Chem. Phys., **103**, 54 (1995).
11. P. freivogal, M. Grutter, D. Forney , and J.P. Maier, Chem. Phys. Lett. **249**, 92 (1996).
12. Y. Zhao, E. de Beer, C. Xu, T. Taylor and D. M. Neumark, J. Chem. Phys. **105**, 4905 (1996).
13. Y. Zhao, E. de Beer, and D.M. Neumark, J. Chem. Phys., **105**, 2575 (1996).
14. D.H. Mordaunt, D.L. Osborn, H. Choi, R.Y. Bise, and D.M. Neumark, J. Chem. Phys., **105,** 6078 (1996)
15. H. Kohguchi, Y. Ohshima, and Y. Endo, Chem. Phys. Lett. **256**, 635 (1996)
16. H. Kohguchi, Y. Ohshima, and Y. Endo, accepted to J. Chem. Phys.
17. Y. Ohshima and Y. Endo, J. Mol. Spectrosc., **153**, 627 (1992).
18. E. Rohlfing and J.E.M. Goldsmith, J. Chem. Phys., **90**, 6804 (1989).
19. E. Rohlfing, J. Chem. Phys., **91**, 4531 (1989).
20. "Molecular dynamics and spectroscopy by stimulated emission pumping", H.L. Dai and R.W. Field, World Scientific Publishing Co. 1995.
21. G.H.Herbig, Astrophys. J. **196**, 129 (1975).
22. F. Sanner, R. Snell, and B.P. Vanden, astrophys. J. **226**, 460 (1978).
23. G.H. Herbig, Astrophys. J. **331**, 999 (1988).
24. C. Jobin, J.P. Maillard, L. d'Hendecourt, and A. Leger, Nature, **346**, 729 (1991).
25. G.H. Herbig and K.D. Leka, Astrophys. J. **382**, 193 (1991).
26. A.E. Douglas, Nature, **269**, 130 (1977).
27. J.P. Hare and H.W. Kroto, Acct. Chem. Res. **25**, 106 (1992).
28. Polycyclic aromatic Hydrocarbons and Astrophysics (eds A. Leger, L. d'Hendecourt and N. Boccara) (reidel, Dordrecht, 1987).
29. M.B. Bell, P.A. Feldman, and H.E. Mattews, Astrophys. J. **273**, L35 (1983).
30. M. Kolbuoszewski, Astrophys. J., **432**, L63 (1994).

31. P.J. Sarre, private communion & T.H. Kerr, R.E. Hibbins, J.R. miles, S.J. Fossey, W.B. Somerville, and P.J. Sarre, Mon. Not. R. astron. Soc. **283**, L105 (1996).

32. L.M. Ziurys, B.E. Turner, Astron. Astrophys., Letters, **300**, L19 (1986).

33. R. Lucas, A. Omont, S. Gulloteau, and Q.R. Nguyen, Astron. Astrophys., **154**, L12 (1986).

34. B.E. Turner, Astron. Astrophys. **182**, L15 (1987).

35. M. Guelin, J. Cernicharo, S. Navarro, D.R. Woodward, C.A. Gottlieb, P. Thaddeus, Astron. Astrophys., **182**, L37(1987).

36. B.E. Turner, Astron. Astrophys., **183**, L23(1987).

37. J. Cernicharo, M. Guelin, and C. Kahane,

38. S. Yamamoto, S. Saito, M. Guelin, M. Cernicharo, H. Suzuki, and M. Ohishi, Astrophys. J. **323**, L149 (1987).

39. H. Mikami, S. Yamamoto, S. Saito, and M. Guelin, Astron. Astrophys. **217**, L5 (1989).

40. K.M.T. Yamada, J. Mol. Spectrosc., **116**, 384 (1986).

41. M.C. McCathy, C.A. Gottlieb, P. Thaddeus, M. Horn, and P. Botschwina, J. Chem. Phys., **103**, 7820 (1995).

42. R.Renner, Z.Phys. **92**, 172 (1934)

43. G. Herzberg and E. Teller, Z. Phys, Chem, **B 21**, 410 (1933).

44. J.A. Pople and H.C. Longuet-Higgins, Mole. Phys., **1**, 327 (1958).

45. J.A. Pople, Mol. Phys., **3**, 16 (1960).

46. J.T. Houge, J. Chem. Phys., **36**, 519 (1962).

47. J.F. Aarts, Mol. Phys. **35**, 1785 (1978).

48. L. Gausset, G. Herzberg, A. Lagerqvist, and B. Rosen, Disc. Faraday Soc. **35**, 113 (1963).

49. L. Gausset, G. Herzberg, A. Lagerqvist, and B. Rosen, Astrophys. J. **142**, 45 (1965).

50. A.J.Merer and D.N.Travis, Can. J. Phys., **43**, 1795(1965).

51. A.J.Merer and D.N.Travis, Can. J. Phys., **44**, 353(1966).

52. C. Di Lauro and I.M. Mills, J. Mol. Spectrosc. **21,** 386 (1966).

53. A.N. Petelin and A.A. Kiselev, Int. J. Quantum Chem., VI, 701 (1972).

54. A.A. Kiselev, Can. J. Phys., **56,** 615 (1977).

55. J. Tang and S. Saito, J. Chem. Phys., **105,** 8020 (1996).

56. A.E. Douglas, J. Chem. Phys. **45**, 1007 (1966).

57. Y. Ohshima and Y. Endo, J. Mol. Spectrosc., **159**, 458 (1993).

58. M. Guelin, R. Lucas, and J. Cernicharo, Astron. Asyrophys., **280**, L19 (1993).

59. J.H. Bieging and M. Tafalla, Astrophys. J. **105**, 576 (1993).

Appendix 1.1

Vibration Modes of C_4H and C_3N

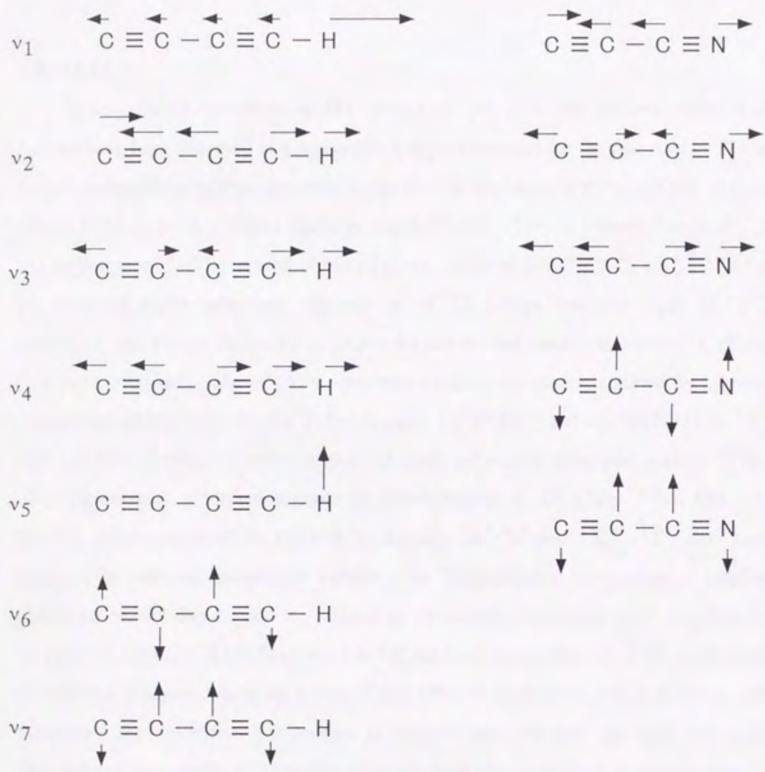

Chapter 2.

Laser-Induced Fluorescence Spectra of the C_4H and C_4D radicals in a Supersonic Jet

ABSTRACT

Laser-induced fluorescence(LIF) spectra of the C_4H and its isotopomer C_4D radicals have been observed in a supersonic free jet expansion for the first time. The jet cooled molecules have been generated by an electric discharge of 0.5% of C_2H_2 or C_2D_2 diluted in Ar by using a pulsed discharge nozzle(PDN). Twenty vibronic bands of C_4H and seventeen of C_4D have been observed in the region of 24000-25000 cm^{-1}. Most of the observed bands have been assigned to of $^2\Pi$-$^2\Sigma$ type and two types of $^2\Sigma$-$^2\Sigma$ transitions, and precise molecular constants for the excited electronic states of C_4H and C_4D were obtained. The effective spin-orbit coupling constants modified by vibronic interactions determined from the $^2\Pi$ bands were -14.7644(80) and -10.9926(35) cm^{-1} for C_4H and C_4D, leading a conclusion that the observed excited electronic state is $\tilde{B}^2\Pi_i$, which agrees with a prediction made by Sobolewski *et al.* [*J. Chem. Phys.* **102**, 394 (1995)]. Observation of two types of $^2\Sigma$-$^2\Sigma$ bands, $^2\Sigma^+$-$^2\Sigma^+$ and $^2\Sigma^{(\pm)}_{1/2}-{}^2\Sigma^+$, have been explained by vibronic interactions including the Renner-Teller interactions of bending vibrational modes they belong to. Although vibrational structure is very complicated, we assigned the ν_5(CCH bending) and ν_6(CCC bending) progression of $\tilde{B}^2\Pi_i$ state based on rotational analyses, where the Renner-Teller effect is large for ν_5, and small for ν_6, and determined the vibrational frequencies as ω_6=191 and 184 cm^{-1} for C_4H and C_4D. Fluorescence time profile is composed of strong short (10-20 ns) and very weak long (2-3 μs) time decay components, which indicate C_4H in $\tilde{B}^2\Pi_i$ state goes to a fast relaxation process to nonradiative states through internal conversion and does not dissociate by the near UV absorption at 400-417 nm.

2.1 Introduction.

The linear carbon-chain molecule C_4H(CCCCH) is one of the C_nH series molecules, which are important as intermediate species in interstellar chemistry[1-12] or in combustion chemistry involving growth of larger carbon clusters such as C_{60} or graphite. C_4H was first identified at a carbon star envelope, IRC+10216, in 1977[8]. The discovery of C_4H was simultaneously the first spectroscopic identification of long carbon chain radicals or unstable molecules, C_nX (X=H, N, O, S, $n \geqq 3$). So far C_3H-C_9H [1-17], C_3N [18], C_5N [19] and C_3S-C_5S [20-22] have been known in the interstellar clouds or by laboratory experiments at the present time in 1996. Since 1977 C_4H have been well studied as one of the most important species to prove interstellar conditions because this molecule has been detected by radiotelescopes in many of the important astronomical sources associated to the circulation of the interstellar matters: at a diffuse cloud such as the Orion arm[3], a dark molecular cloud, TMC-1[4-7], and also carbon-rich circumsteller envelope, IRC+10216[8-11].

Laboratory detection of C_4H were performed by Gottlieb *et al.* in 1983[23], after six years from the first identification in circumstellar envelope, by microwave spectroscopy in discharge flow of C_2H_2/Ar. In 1987 Yamamoto *et al.*[24] investigated vibrationally excited states of the lowest-bending mode, ν_7 (Π) and $2\nu_7$ (Δ,Σ), and simultaneously succeeded in assigning some unidentified lines observed in IRC+10216 to vibrationally excited C_4H. C_4D have been detected by laboratory microwave spectroscopy in 1988[25]. Therefore, molecular constants for lower vibrational levels of the ground state have been determined precisely except for the vibrational energy.

The electronic states have been a subject of great interest from both astronomical and spectroscopic point of view. It has been expected that C_4H has the first electronic excited state $\tilde{A}^2\Pi$ at a little above the ground state, because the $\tilde{A}^2\Pi$ state is 3612 cm^{-1} above the $\tilde{X}^2\Sigma^+$ state for C_2H[26], and this order is reversed and the ground state is $^2\Pi$ for C_6H[12]. Yamamoto *et al.* proposed that the low-lying $\tilde{A}^2\Pi$ state contributes to specific vibrational excitation of C_4H in the carbon star envelope IRC+10216[27]. They also suggested the possibility of strong vibronic interactions between $\tilde{X}^2\Sigma^+$ and $\tilde{A}^2\Pi$

due to this accidentally small energy gap based on the rotational structure of the ν_7 state. The second or other electronic excited states were expected to exist in region from violet to UV. Bell *el al.*[3] suggested that electronic transition of C_4H is a good candidate for diffuse interstellar bands (DIBs) in the near UV region. Recently, Fulara *et al.*[28] indicated that unsaturated C_nH_m species are good candidates for Diffuse Interstellar Bands(DIBs). According to a most recent *ab initio* calculation by Soboleowski and Adamowicz[29] (CASSCF/DZVP), excitation energies of the lowest three electronic states at the $^2\Sigma^+$ ground state optimized geometry for C_4H have been expected to be 0.07eV(565 cm^{-1}, $1^2\Pi$), 3.04eV(24519 cm^{-1}, $2^2\Pi$) and 4.17eV(33633 cm^{-1}, $3^2\Pi$).

In spite of the importance and attraction of the electronic structure of this molecule, spectroscopic approaches other than the microwave studies have been very limited, only to rare gas matrix isolated experiments. The group of Graham[30,31] reported absorption spectrum of C_4H, which were produced in photolysis of C_4H_2, in Ar or Ne matrix in IR, visible and UV regions, and they assigned some vibrational modes of the ground state, C-H and two C≡C stretchings in 1990 and electronic excited state $^2\Pi_r$ with its origin at 33800 ± 60 cm^{-1} in 1975. However no experimental observation in the gas phase have not been reported until now for both IR and UV spectra. Recently Maier *et al.* [32,33] have observed visible absorption spectra of other longer chain series, $C_{2n}H$(n=3-6), in which band origins of $^2\Pi \leftarrow X^2\Pi$ have been determined to be 18854 cm^{-1}(C_6H), 15848 cm^{-1}(C_8H), 13852 cm^{-1}($C_{10}H$) and 12492 cm^{-1}($C_{12}H$), respectively.

In this chapter, we present first observation of the electronic spectrum of C_4H and isotopomer C_4D in the gas phase by using LIF spectroscopy. The observed excited state was the second excited electronic state, $\tilde{B}^2\Pi_i$, lying near in the UV region. Since LIF spectra are rotationally resolved, precise molecular constants including excitation energy and vibronic symmetry of the excited states could be determined. The present observation of $\tilde{B}^2\Pi_i$ state provides new propositions with following meaning: (1)The first is astronomical interest: transition energy of C_4H can compared with the data on UV absorption or emission of interstellar materials, such as DIBs. Also the relaxation process in the excited state, whether it mainly dissociates or not, gives a restriction for the existence of C_4H in interstellar medium. (2)The second is spectroscopic interest: spectroscopic data of the vibronic structure of four or five-atomic linear radicals, in which complicated interactions due to the vibronic effect and the spin-orbit coupling are expected, have been very scarce. C_4H(CCCCH) is an example showing such rare spectroscopic behaviors, property which will be commonly observed for large linear radicals.

2.2 Experimental.

2.2.1 Production of C_4H and C_4D.

We used a pulsed discharge nozzle (PDN) to produce short lived radicals, which has been applied successfully for generation of various unstable molecules including carbon-chain molecules such as C_nS[22-24], C_nO[34,35] and C_nN[19] in Fourier-transform microwave spectroscopy in supersonic expansion, and quite recently to laser spectroscopy of HCCS[36] and CCN[37]. Schematic diagram of the PDN is shown in Fig.2.1(a). The PDN used in the present study is composed of a pulsed valve (General Valve co.) with a 0.8 mm orifice and a unit of electrodes and insulators in front of it, where the inner electrode is a cathode and the outer is an anode. The pulsed valve was operated at a repetition rate of 10Hz. Just after the sample gas was pulsed out through the nozzle, pulsed DC discharge(1.0-1.5 kV with 20μs duration) was invoked between the two electrodes. Timing chart for synchronization is shown in Fig. 2.1(b). Discharge products thus generated were adiabatically cooled in a subsequent supersonic expansion. The rotational temperature estimated from rotationally resolved spectra was about 5K in the present study.

The C_4H and C_4D radicals were produced by discharges of gas mixtures, 0.5-1.0% of C_2H_2 or C_2D_2 diluted in Ar. The stagnation pressure was kept at 2.5-3.5 atm and the typical background pressure in the vacuum chamber is about $3\text{-}4\times10^{-5}$ Torr, which may be compared with the case of the condition optimized for C_3, $6\text{-}7\times10^{-5}$ Torr. We also tried a discharge of a gas mixture, 0.5% of C_4H_2 diluted in Ar. In the C_4H_2/Ar discharge the signal intensities of C_4H were almost the same as that of C_2H_2, while the signals of C_3, which overlap with some of the C_4H vibronic bands, became a little stronger under the C_4H optimized condition. Therefore, we mainly used the C_2H_2/Ar samples in the present measurement.

2.2.2 Laser Induced Fluorescence Spectra.

The excitation UV laser beam was obtained by a frequency doubling of the output of a pulsed dye laser (Lambda Physik Scanmate) by a KDP crystal. The dye laser was pumped by the 2nd harmonic of a Q-switched Nd^{3+}:YAG laser (Quanta-Ray GCR-3, 10Hz) which synchronized to pulse valve. The resulting resolution of the tunable UV laser was about 0.03 cm^{-1}. The laser dye used was Styryl 9, covered almost the full region in 24000-2500cm^{-1}. The output beam was expanded nine times through a beam expander and then attenuated to avoid saturation, and crossed the jet 40mm downstream from the PDN with a delay time of 80μs from the discharge. The scattered light caused by the discharge can be elminated during this delay time, and then only the background noise caused by the discharge is weak phosphorescence of metastable atoms[37].

Laser-induced fluorescence was collected at right angle of the laser propagation by the two planoconvex lenses(f=90 and f=120) focused onto an iris put on the quartz window, and detected by a photomultiplier(PMT, Hamamatsu R928) through a low-pass glass filter(HOYA Y-44 or 42). PMT signal was then preamplified(×25), averaged by a boxcar integrator(SR250), and stored in a personal computer(PC, NEC PC 9801BX).

When weak bands of $C_4H(D)$ were covered with strong C_3 signals, it was impossible to find out the $C_4H(D)$ from the LIF spectrum. In such case we used another measurement system to extract only the C_4H signals, in which preamplified PMT signal were fed in a digital oscilloscope (Lecroy 9350A) with a sampling rate of 1 GHz (or 500 MHz), and converted to digital signals. The fully digitized time profile (1pt./ns) was transferred to another PC(DELL OptiPlex GXMT 5100) at a repetition rate of 10Hz, and integrated over a certain region in the time domain signal. Fortunately, lifetime of C_3($\tau \sim$250 ns) is much longer than that of C_4H ($\tau \sim$20 ns), we integrated this time profile over two regions, 0-50 ns and 100-150 ns, where the former includes C_4H and C_3 while the latter includes only C_3. Then spectrum of C_4H could be extracted from the LIF spectrum of the first gate by subtracting the second gate with a suitable factor.

Fluorescence time profiles which were used to discuss relaxation processes in the excited states were measured through this system by an accumulation of 500 shots. In this case we used a home made fast preamplifier (250 MHz).

Calibration of the laser wavenumber was made by simultaneously observing absorption spectra of the hot I_2 vapor (20 Torr, 500 ℃, 30 cm path length) using the fundamental dye laser output. The relative uncertainty could be kept less than 0.008 cm^{-1}. Etalon fringe (FSR=1.1cm^{-1}) was also monitored simultaneously to ensure the linearity of frequency scan.

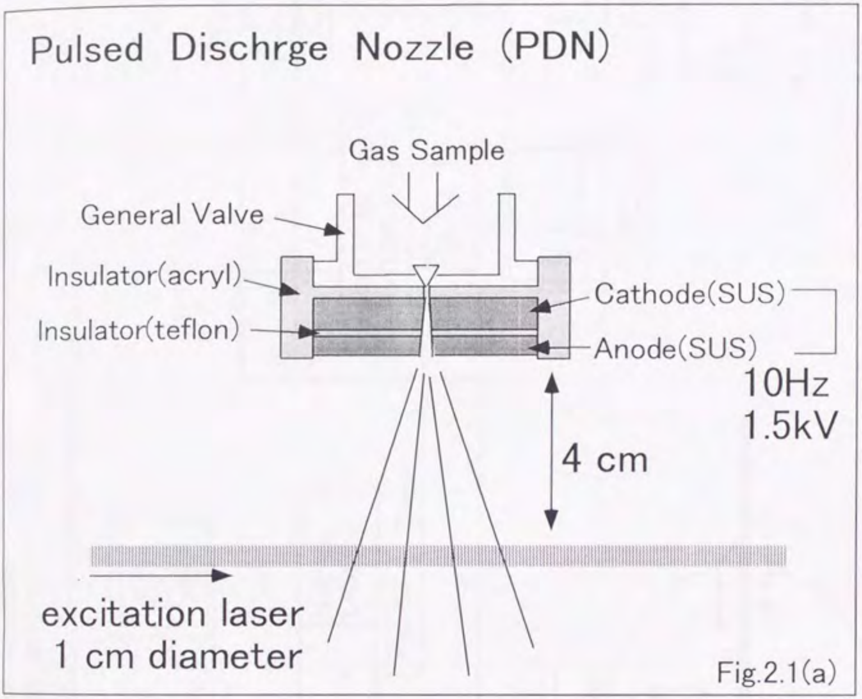

Fig.2.1(a)

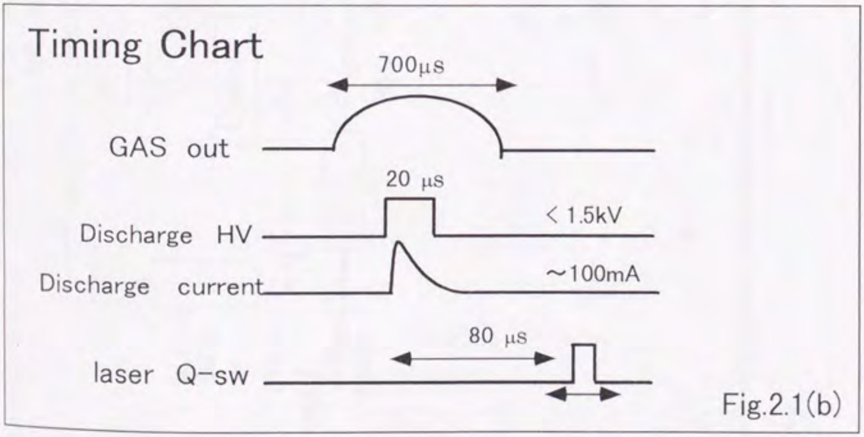

Fig.2.1(b)

Fig.2.1 (a) Schematic diagram of Pulsed Discharge Nozzle and a timing chart of synchronization of pulsed vulve, dischrge HV and excitationa laser.

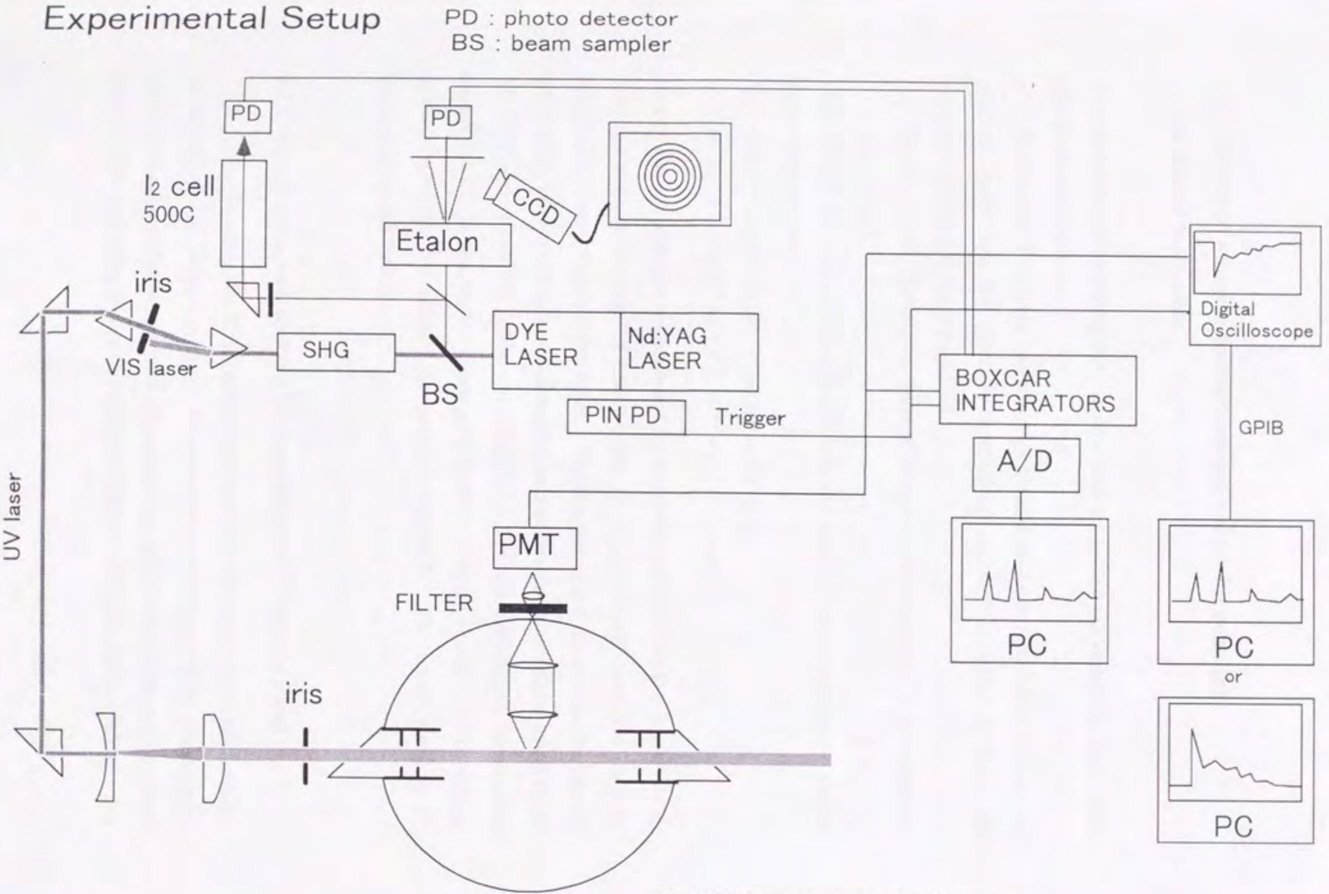

Fig.2.2 Schematic diagram of LIF system.

2.3 Theory of vibronic interaction and spin-orbit coupling for linear molecules.

2.3.1 Hamiltonian including the vibronic interaction and the spin-orbit interaction and its matrix elements.

The theory of vibronic interaction of linear polyatomic molecules in degenerate electronic state were first given by Renner[48], and then expanded by Pople and Longuet-Higgings[49] and Hougen[50].

Hamiltonian of $^2\Pi$ electronic states of linear polyatomic molecules is expressed as,

$$H = H_{rot} + H' \qquad (2.1)$$

where H' indicates a perturbation Hamiltonian including the vibronic interaction and the spin-orbit interaction,

$$\begin{aligned} H' &= V_1' r\cos(\theta-\phi) + V_2' r^2 \cos 2(\theta-\phi) + AL_zS_z \\ &= V_1(Q_+e^{-i\theta} + Q_-e^{i\theta}) + V_2(Q_+{}^2e^{-2i\theta} + Q_-{}^2e^{2i\theta}) + AL_zS_z \end{aligned} \qquad (2.2)$$

where r and ϕ indicate the amplitude and the azimuthal angle of a bending mode, θ is the azimuthal angle of the unpaired electron, and $Q_\pm = \sqrt{\mu r}\exp(\pm i\theta)$ represent the polar normal coordinates of the bending mode. The first and second terms cause the vibronic interactions, corresponding to Herzberg-Teller and Renner-Teller effects respectively. The third term shows the spin-orbit interaction. For this perturbation Hamiltonian, since $K=|\Lambda+l|$, Σ, and $P=\Lambda+l+\Sigma$ are good quantum numbers, the effect of the vibronic interaction can be distinguished by quantum number K. The matrix elements are summarized in Appendix 2.1.

2.3.2 Vibronic states with K=0 in a $^2\Pi$ electronic state: $^2\Sigma$ vibronic states.

$^2\Sigma$ vibronic states of a $^2\Pi$ electronic state arise when a bending vibrational mode are excited with an odd quantum number. We have observed two types of $^2\Sigma$ vibronic states which have quite different rotational structures with each other, which are originated from different magnitude of vibronic interactions of the bending modes they belong. For

C_4H, which has three bending vibrational modes, ν_5, ν_6, ν_7, vibronic states have Σ symmetry when $v_5+v_6+v_7$=odd and $K= l_5+ l_6+ l_7+\Lambda=0$. Λ and l_i represent projections of the electron and vibrational angular momenta along the linear axis, where Λ is ± 1 because the electronic state considering is Π. To simplify the discussion, we now consider only one particular bending mode in the following arguments, like triatomic molecules. Then the wavefunction of $^2\Sigma$ states with vibrational quantum number v in Π electronic state is expressed as $\left|\Sigma^{\pm}\right\rangle = 1/\sqrt{2}\left[\left|\Lambda = \pm 1, l = K \mp 1\right\rangle \pm \left|\Lambda = \mp 1, l = K \pm 1\right\rangle\right]$ with K=0, where Σ is a projection of the electron spin angular momentum onto the molecular axis, and +/- signs refer to the symmetry of orbital part of wavefunction with respect to reflection in a plane containing molecular axis. In electronic transition, $\Sigma^{+/-}$- $\Sigma^{+/-}$ is allowed while $\Sigma^{+/-}$- $\Sigma^{-/+}$ is forbidden. Σ^+ and Σ^- have diagonal matrix elements of the Renner-Teller effect and offdiagonal elements of the spin-orbit interaction for H' in equation (2.1),

$$\begin{array}{c} \Sigma^+ \\ \\ \Sigma^- \end{array} \begin{bmatrix} \dfrac{\varepsilon\omega(\mathrm{v}+1)}{2} & A_{eff}\Sigma \\ A_{eff}\Sigma & -\dfrac{\varepsilon\omega(\mathrm{v}+1)}{2} \end{bmatrix} \tag{2.3}$$

Where ω is a vibrational frequency and ε is a Renner parameter. Degeneracy of Σ states are lifted by the Renner-Teller effect and Σ^+ and Σ^- are mixed with each other by the spin-orbit interaction in the $^2\Pi$ electronic state. Therefore the ± symmetry label of $^2\Sigma$ vibronic states is not strictly defined when $\varepsilon\omega(v+1)$ is small compared with $A\Sigma$, and generally labeled by the ± sign in parentheses: $^2\Sigma^{(+)}$ and $^2\Sigma^{(-)}$. Hougen [40] derived a expression of the rovibrational energy of $^2\Sigma$ vibronic states in a $^2\Pi$ electronic state of linear triatomic molecules. According to Hougen's definition, the vibronic term energy including a higher order term is expressed as,

$$\begin{aligned} E(^{\kappa}\Sigma) &= \omega\left(1-\frac{1}{8}\varepsilon^2\right)(v+1)+r \\ E(^{\mu}\Sigma) &= \omega\left(1-\frac{1}{8}\varepsilon^2\right)(v+1)-r \end{aligned} \tag{2.4}$$

and when Aso>>BJ, the rotational energies are expressed in Hund's case (b) form as,

$$\begin{aligned} &F_1(\Sigma^\kappa, N) = B_{eff}^{\kappa} N(N+1) + \tfrac{1}{2}\gamma_{eff}^{\kappa}(N+1) \\ &F_2(\Sigma^\kappa, N) = B_{eff}^{\kappa} N(N+1) - \tfrac{1}{2}\gamma_{eff}^{\kappa} N \\ &F_1(\Sigma^\mu, N) = B_{eff}^{\mu} N(N+1) + \tfrac{1}{2}\gamma_{eff}^{\mu}(N+1) \\ &F_2(\Sigma^\mu, N) = B_{eff}^{\mu} N(N+1) - \tfrac{1}{2}\gamma_{eff}^{\mu} N \end{aligned} \tag{2.5}$$

where

$$\begin{aligned} &r\sin 2\beta = \tfrac{1}{2}\,\varepsilon\omega(\mathrm{v}+1) \\ &r\cos 2\beta = \tfrac{1}{2}\,A_{eff} \\ &r = \tfrac{1}{2}\sqrt{A_{eff}{}^{2} + \varepsilon^{2}\omega^{2}(\mathrm{v}+1)^{2}}\,. \end{aligned} \tag{2.6}$$

κ levels always lie above μ levels, and κ and μ levels correspond to whether $^2\Sigma^+$ or $^2\Sigma^-$. B_{eff} is an effective rotational constant and γ_{eff} is not a conventional spin rotation interaction constant but also an effective splitting constant defined by,

$$\begin{aligned} &B_{eff}^{\kappa} = B_{v}\left[1 + (B_{v}/2r)\cos^{2}2\beta\right] \\ &B_{eff}^{\mu} = B_{v}\left[1 - (B_{v}/2r)\cos^{2}2\beta\right] \end{aligned} \tag{2.7}$$

$$\begin{aligned} &\gamma_{eff}^{\kappa} = 2B_{v}\left[1 - |\sin 2\beta| + (B_{v}/2r)\cos^{2}2\beta\right] \\ &\gamma_{eff}^{\mu} = 2B_{v}\left[1 - |\sin 2\beta| - (B_{v}/2r)\cos^{2}2\beta\right] \\ &0 \le \gamma_{eff}^{\kappa}, \gamma_{eff}^{\mu} \le 2B \end{aligned} \tag{2.8}$$

and B_v is the original rotational constant of the vibronic state.

Using Hougen's parameter β, the eigen wavefunctions of matrrix (2.3) are written as,

$$\begin{aligned} &\Sigma^{(+)} = \frac{1}{\sqrt{2}}\left[\left(|\cos\beta| + |\sin\beta|\right)\Sigma^{+} + \left(|\cos\beta| - |\sin\beta|\right)\Sigma^{-}\right] \\ &\Sigma^{(-)} = \frac{1}{\sqrt{2}}\left[\left(|\cos\beta| - |\sin\beta|\right)\Sigma^{+} - \left(|\cos\beta| + |\sin\beta|\right)\Sigma^{-}\right] \end{aligned} \tag{2.9}$$

According to equations (2.4)-(2.8), the rotational structure and symmetry about reflection in a plane are expected to be quite different whether Renner-Teller effect of the bending mode is strong or not. We consider here two limiting cases. When Renner-Teller effect is strong, $\varepsilon\omega(\mathrm{v}+1) \gg A\Sigma$, or $|\sin 2\beta|$ is close to 1 and $|\cos 2\beta|$ close to zero. In this case eigen wavefunctions in equation (2.9) become to,

$$\begin{aligned} \Sigma_{1/2}^{(+)} &= \frac{1}{\sqrt{2}}\left[\Sigma^{+} + \Sigma^{-}\right] \\ \Sigma_{1/2}^{(-)} &= \frac{1}{\sqrt{2}}\left[\Sigma^{+} - \Sigma^{-}\right] \end{aligned} \qquad (2.10)$$

which indicate that the off diagonal elements of the matrix (2.3), is negligible compared to diagonal elements, and the Σ^+-Σ^- mixing is small. The rotational structures are similar to that of a $^2\Sigma$ state of diatomic molecules with no spin-orbit interaction, because γ_{eff} becomes almost zero. Conventional spin rotation interaction constant could be added if necessary. We labeled these $^2\Sigma$ states by Σ^+ and Σ^- to distinguish them from following $^2\Sigma^{(\pm)}$ states.

On the other hand, when the Renner-Teller effect is weak, that is $\varepsilon\omega(v+1) << A\Sigma$, an efficient mixing between Σ^+ and Σ^- occurs. In this case, $|\sin 2\beta|$ is close to zero and $|\cos 2\beta|$ close to 1, leading to $|\sin\beta| = |\cos\beta| \cong 1/\sqrt{2}$. Eigen functions are thus,

$$\begin{aligned} \Sigma^{(+)} &\approx \Sigma^{+} \\ \Sigma^{(-)} &\approx \Sigma^{-} \end{aligned} \qquad (2.11)$$

$\Sigma_{1/2}^{(+)}$ and $\Sigma_{1/2}^{(-)}$ notations are based on the Hund's case(c) rotatinal strucutre, where 1/2 indicates projection of the total angular momentum onto the molecular axis. Since γ_{eff} becomes considerably large, $\sim$2B, the rotational structure is similar to case (b) $^2\Sigma$ with large spin splittings. The splittings are also called the ρ-type doubling. Or the rotational structure is similar to that of $\Omega=1/2$ states of case(c) of diatomic molecules. Therefore, the rotational structure is considerably different from usual $^2\Sigma$ states in this case.

2.3.3 Vibronic states with K=v+1 and $0 \neq K \neq v+1$.

$^2\Pi$ vibronic states of v=0 or $^2\Delta$ vibronic states of v=1 in the $^2\Pi$ electronic state belong to this type. Vibronic states with K=v+1 have no matrix element of the first order Renner-Teller effect. The vibrational term energy including the second order Renner-Teller effect is expressed as,

$$E = \omega(\mathrm{v}+1) \pm A_{eff} - \frac{1}{8}\varepsilon^2 \omega K(\mathrm{v}+1) \qquad (2.12)$$

The rotational energy structure is little affected by the vibronic interaction and is similar to those of diatomic molecules, except for its spin splitting constant,

$$A_{eff} = A\left[1 - \frac{\varepsilon^2}{8}K(K+1)\right] \tag{2.13}$$

where A is the true spin-orbit coupling constant without the vibronic interaction.

For vibronic states with $0 \neq K \neq v+1$, the first order Renner-Teller effect have to be considered. For example, $^2\Pi$ vibronic states of v=2 belongs to this type, in which there are four wavefunctions interacting by the Renner-Teller effect and the spin-orbit interaction: $|\Lambda = \pm 1, l = 0\rangle$ and $|\Lambda = \pm 1, l = \mp 2\rangle$. If the Renner-Teller effect is small, only the spin-orbit interaction is considered as a perturbation. Thus the rotational structure is similar to K=v+1 vibronic states: $^2\Pi$ vibronic states form a spin-orbit pair separated by A_{eff}. But when the Renner-Teller effect is large, the above two sets of wavefunctions interact through the first order Renner-Teller effect, and the spin-orbit coupling becomes a minor perturbation in this case: $^2\Pi$ vibronic states form Renner-Teller pair with a small spin splitting, which is much smaller than A_{eff}.

2.4 Observation and Identification of C_4H and C_4D.

An expanded laser-induced fluorescence spectra observed in a C_2H_2/Ar discharge in the region of 24000-25000cm^{-1} is shown in Fig.2.3(a). A lot of vibronic bands appeared in this region and all of them were ascribed to discharge products. Several strong bands were assigned to the C_3 $\tilde{A}$ - $\tilde{X}$ system[38-40], with lifetimes, typically $\tau \sim 250$ns. In the same energy region, we found new bands labeled [A] to [O], all showing similar behaviors, such as short lifetimes $\tau \sim 20$ ns or production conditions as described in the experimental section. Similarly, Fig.2.3(b) shows LIF spectrum observed in a C_2D_2/Ar discharge, where other new bands labeled [a] to [k] were observed, while [A] to [O] were not observed. Thus the new species must contain at least one hydrogen atom. In addition, in a discharge of a mixture of C_2H_2 /C_2D_2/Ar, no new bands other than the former two series were observed. Therefore, we conclude that the carrier of these new bands are molecules composed of several carbon atoms and one hydrogen(deuterium) atom, namely C_nH(C_nD), because if the species contains more than two hydrogen atoms there must be at least three isotopomers, such as X-HH, X-HD and X-DD. Considering that C_nH molecules have one unpaired electron, we can determine the transition types for the observed bands as due to a doublet linear molecule from their rotational structures. Actually, C_nH (n=2-9) series detected so far were all analysed as doublet linear molecules.

Our identification of the present molecules to be C_4H and C_4D has been confirmed by rotational analyses of some vibronic bands, for example [C] and [e], which were observed only in the C_2H_2/Ar and C_2D_2/Ar discharge, respectively, and both have very simple structures. Figs.2.4(a) and (b) show high resolution LIF spectra of bands [C] and [e]. These bands have no Q-branches and consisted of only P and R- branches. While they are rotationally resolved, spin splittings were considered to be not distinguished in the present spectral resolution. Therefore bands[C] and [e] can be assigned to $^2\Sigma$-$^2\Sigma$ type transitions. Rotational assignment also can be made as shown in Figs.2.4(a) and (b). In the $^2\Sigma$-$^2\Sigma$ transition, since P(N''+1) and R(N''-1) transitions have the common rotational levels in the excited state, we could determine rotational constant of the ground

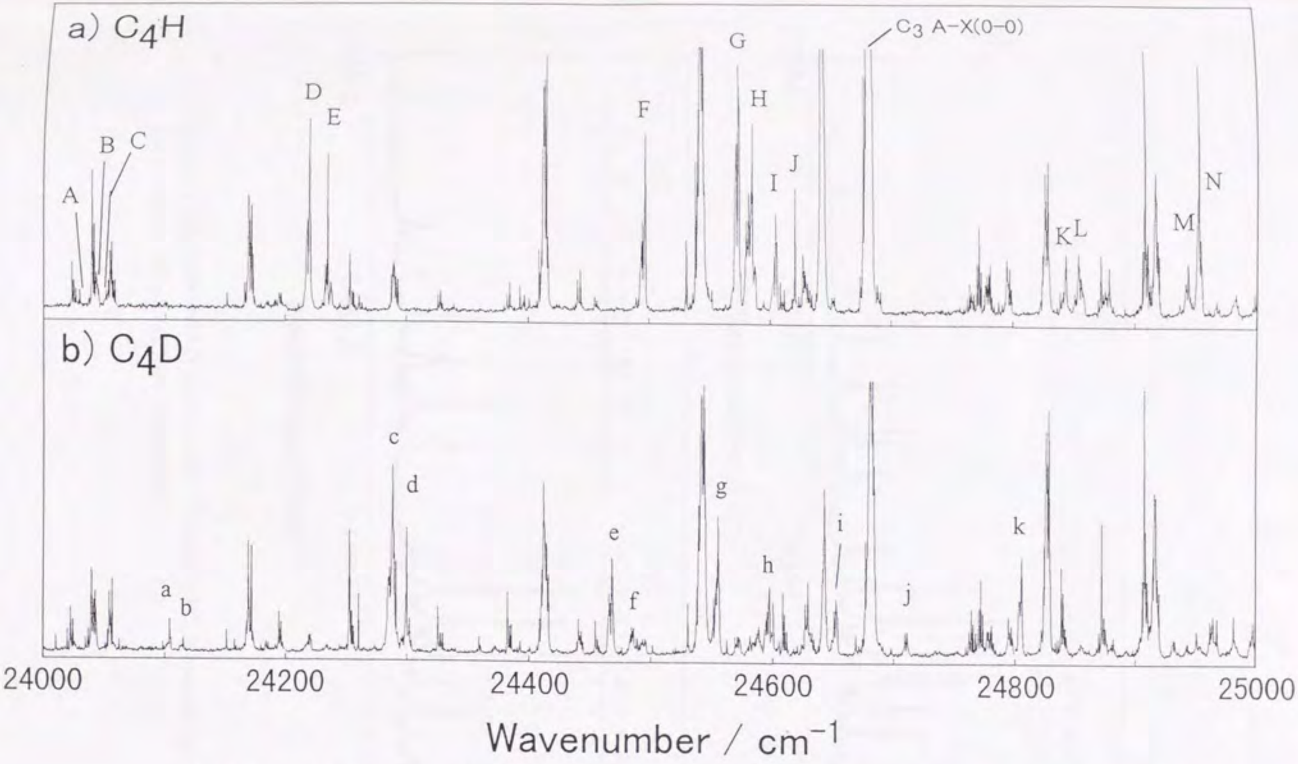

Fig.2.3 Expanded Laser Induced Fluorescence spectra obtained in (a)C_2H_2/Ar discharge and (b)C_2D_2/Ar discharge in the region of 24000-25000cm^{-1}. Laser resolution is about 0.15 cm_{-1}. Signals labeled by A-O and a-k are relatively strong signals of C_4H and C_4D respectively, and most of other strong bands belong to C_3 A-X system.

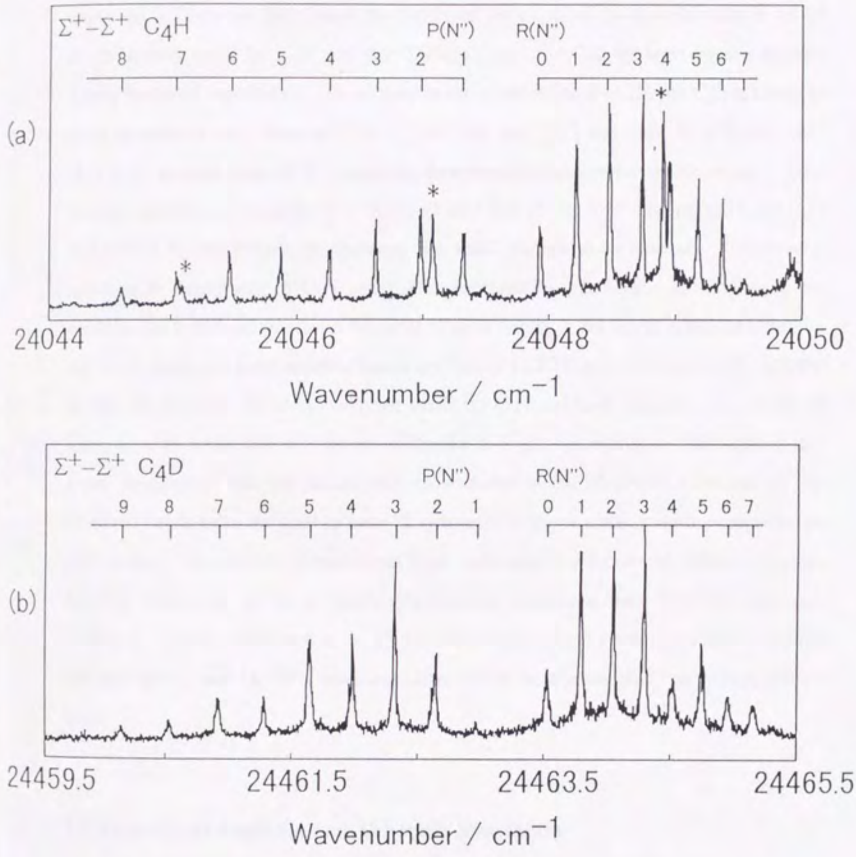

Fig.2.4 High resolution LIF spectra of Σ^{+}-Σ^{+} bands (a) C_4H and (b) C_4D, corresponding to bands [C] and [e] in FIg.2.3..

$^2\Sigma$ state from the combination defferences, they are R(N''-1)−P(N''+1) = B''(4N''+2), on an assumption that spin splittings of the ground state were small enough to be neglected. Thus, we determined the rotational constants of the ground state B" to be 0.158715(64) cm-1 for C_nH and 0.147291(61) cm^{-1} for C_nD by least square fittings. These rotational constants B'' determined in our observation for C_nH and C_nD are both in good agreement with those of C_4H, 0.15873191 cm^{-1} [23] and C_4D, 0.14731691 cm^{-1} [25] in the ground state $\tilde{X}^2\Sigma^+$, precisely determined by microwave spectroscopy. Spin rotation interaction constants γ=-0.0012891 cm^{-1} and -0.0012039 cm^{-1} for C_4H and C_4D determined by microwave spectroscopy are small enough to be ignored. Conversely, referring B'' constants of C_4H and C_4D determined by microwave spectroscopy, we could assign rotational structures for most of other bands. We finally concluded that the carrier of these two band series of bands are C_4H (CCCCH) and C_4D (CCCCD) radicals. So far, we observed 20 and 17 vibronic bands for C_4H and C_4D, respectively. Some of them were so weak that one cannot recognize in Fig.2.3(a) and (b). Throughout this paper we consider that hot bands were not included in our observation because all the observed bands were assigned to have $^2\Sigma$ symmetry as lower states from the combination differences. Observation of transitions from a vibronic $^2\Sigma$ state of v=2, where v is some bending vibrational mode, is improbable because transitions from v=1($^2\Pi$) were not observed. Since the lower state is $^2\Sigma^+$, the observable excited states should be $^2\Sigma$ and $^2\Pi$ vibronic states, and $^2\Delta$, $^2\Phi$... were not observed in the present study as will be shown later.

2.5 Rotational Analysis and Vibronic Symmetry

We have carried out rotational analyses for most of the observed bands, and determined molecular constants of the excited state. The band types were assigned to either $^2\Pi$-$^2\Sigma$, $^2\Sigma^+$-$^2\Sigma^+$ and $^2\Sigma^{(\pm)}_{1/2}-{}^2\Sigma^+$, all of which started from the vibronic ground state, $\tilde{X}^2\Sigma^+$ v=0. The symmetry of the electronic excited state was determined to $^2\Pi_i$ from the rotational analysis of the $^2\Pi$-$^2\Sigma$ band. Therefore, observed $^2\Sigma$ vibronic states accompany excitation of some bending modes. Rotational structures of every type of bands are affected by vibronic interaction including the Renner-Teller effect, and especially for the $^2\Sigma$ -$^2\Sigma$ bands, magnitude of the Renner-Teller effect, which depends on the excited bending modes, are remarkably different for $^2\Sigma^+$ and $^2\Sigma^{(\pm)}_{1/2}$ vibronic states, where $^2\Sigma^+$ and $^2\Sigma^{(\pm)}_{1/2}$ suggest strong and weak Renner-Teller effect, respectively as mentioned in the previous section. This observation of different types of Σ states is characteristic to polyatomic linear molecules containing more than 4 atoms.

2.5.1 $^2\Pi$-$^2\Sigma$ bands

Three $^2\Pi$ bands of C_4H and two of C_4D have been observed and rotational analyses were made as case (a) $^2\Pi$ bands which are the same as that of diatomic molecules. The term values Tv, the rotational constants B' and effective spin-orbit coupling constants A_{eff} were determined by least square fittings as shown in Tables 2.1 and 2.2. An example of high resolution LIF spectrum of $^2\Pi$-$^2\Sigma$ band of C_4H is shown in Fig. 2.5(a) and (b), which was the lowest pair of bands we observed, bands [A] and [B] in Fig.2.3. Both bands consist of four branches, and the rotational assignment was made as shown in Fig.2.5. Since the lowest rotational level in the upper state is $J' = 1.5$ for band [A] and $J'=0.5$ for band [B], they belong to $P = 3/2$ and $P = 1/2$ components of a $^2\Pi$ vibronic state in Hund's case (a), respectively, separated by A_{eff} which is expressed approximately by equation (2.13).

2.5.2 $^2\Sigma$–$^2\Sigma$bands.

$^2\Sigma^+$-$^2\Sigma^+$ bands, where the upper $^2\Sigma^+$ state arise from vibrational excitation of a bending mode accompanying a strong Renner-Teller effect. $^2\Sigma^+$-$^2\Sigma^+$ bands have simple P and R branches as shown in Figs. 2.3(a) and (b). We have observed four $^2\Sigma^+$-$^2\Sigma^+$ bands for C_4H, and eight for C_4D, and determined molecular constants of the upper states, Tv and B', by least square fittings as shown in Tables 2.1 and 2.2. Spin splittings were not resolved in the present resolution. In some case irregular large spin splittings were observed as a result of some local perturbations in $^2\Sigma^+$-$^2\Sigma^+$ bands. Therefore, the spin rotation interaction constant of the upper state γ' was neglected for both the cases.

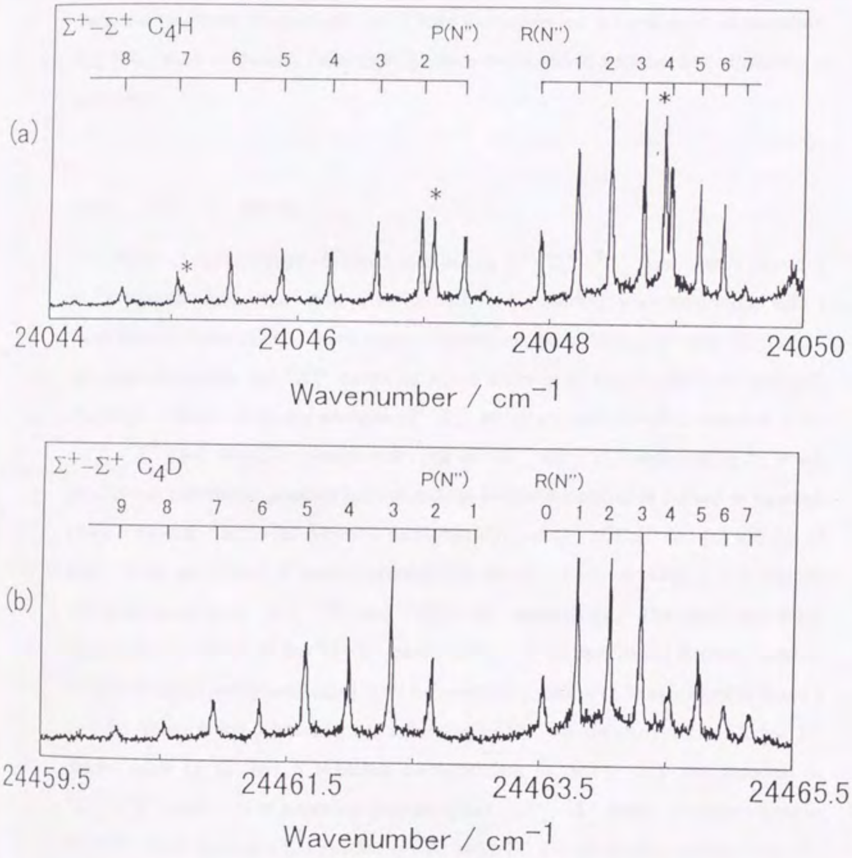

Fig.2.4 High resolution LIF spectra of Σ^+-Σ^+ bands (a) C_4H and (b) C_4D, corresponding to bands [C] and [e] in FIg.2.3..

When an irregular spin splitting are recognized, center frequencies of two spin components were used in the least squares fitting. Centrifugal distortion constants D were also neglected because only low J lines were observed in the present jet condition. The other state of Renner-Teller pair, Σ^-, were not observed because Σ^--Σ^+ transition is forbidden.

2.5.3 ${}^2\Sigma^{(\pm)}_{1/2}-{}^2\Sigma^+$ bands.

Most of the observed vibronic bands belong to ${}^2\Sigma^{(\pm)}_{1/2}-{}^2\Sigma^+$ type, that is transition to ${}^2\Sigma$ vibronic state which arise from excitation of a bending vibrational mode with a weak Renner-Teller effect. In this type of transitions, both ${}^2\Sigma^{(+)}_{1/2}-{}^2\Sigma^+$ and ${}^2\Sigma^{(-)}_{1/2}-{}^2\Sigma^+$ are allowed because the ${}^2\Sigma^{(\pm)}_{1/2}$ states are mixed states of Σ^+ and Σ^-, and both have a Σ^+ character. Since vibrational energies of ${}^2\Sigma^{(\pm)}_{1/2}$ states are represented as equation (2.4), ${}^2\Sigma^{(\pm)}_{1/2}-{}^2\Sigma^+$ band should be observed as a pair of ${}^2\Sigma^{(+)}_{1/2}$ and ${}^2\Sigma^{(-)}_{1/2}$ separated by $2r$, which depends on vibrational quantum number and the Renner parameter as defined in equation (2.6). Typical ${}^2\Sigma^{(\pm)}_{1/2}-{}^2\Sigma^+$ vibronic bands are [D] and [E] of C_4H, and [c] and [d] of C_4D. High resolution LIF spectra of bands [D] and [E] are shown in Figs.2.6 (a) and (b), which are assigned to ${}^2\Sigma^{(+)}_{1/2}-{}^2\Sigma^+$ and ${}^2\Sigma^{(-)}_{1/2}-{}^2\Sigma^+$, respectively. The band features are quite similar to those of the ${}^2\Pi$ -${}^2\Sigma^+$ bands of Fig.2.5, except for the intensity pattern. Rotational assignments are labeled by N following to equation (2.5) expressed in Hund's case (b), where P and R branches corresponding to $\Delta N=\pm 1$ are observed in ${}^2\Sigma^{(+)}_{1/2}-{}^2\Sigma^+$ bands, while O, Q, and S branches corresponding to $\Delta N=0, \pm 2$ are observed in ${}^2\Sigma^{(\pm)}_{1/2}-{}^2\Sigma^+$ bands. The transition diagram of the ${}^2\Sigma^{(\pm)}_{1/2}-{}^2\Sigma^+$ bands are summarized in Fig.2.7. High resolution LIF spectra of C_4D bands [d] and [e] are also shown in Fig.2.8, corresponding to ${}^2\Sigma^{(+)}_{1/2}-{}^2\Sigma^+$ and ${}^2\Sigma^{(-)}_{1/2}-{}^2\Sigma^+$. Band [d] are overlapped with C_3 $\tilde{A}(300)$-$\tilde{X}(300)$[38]. If we compare the relative intensities of ${}^2\Sigma^{(+)}_{1/2}-{}^2\Sigma^+$ and ${}^2\Sigma^{(-)}_{1/2}-{}^2\Sigma^+$, the former is stronger than the latter by a factor 2 in the case of bands [D] and [E] of C_4H, which suggests that ${}^2\Sigma^{(+)}_{1/2}$ has larger ${}^2\Sigma^+$ character than ${}^2\Sigma^{(-)}_{1/2}$. The quantitative discussion will be described in the next section.

Term value Tv, and effective molecular constants $B_{eff}^{(\pm)}$ and $\gamma_{eff}^{(\pm)}$ in equation (2.5) were determined by least square fittings and summarized in Tables 2.1 and 2.2. When a ${}^2\Sigma_{1/2}^{(+)}$ and ${}^2\Sigma_{1/2}^{(-)}$ pair was observed, the splitting parameter r was also determined. However ${}^2\Sigma_{1/2}^{(+)}$ and ${}^2\Sigma_{1/2}^{(-)}$ are indistinguishable with each other when one of the ${}^2\Sigma_{1/2}^{(\pm)}$ pair are not observed by its weak intensity or obscured by other species, because their rotational structure can be expressed as the same formula except the γ_{eff} constant. Namely as understood from Fig.2.7, if γ_{eff} of ${}^2\Sigma_{1/2}^{(+)}$ increases more than the rotational structure, the rotational structure is almost identical to that of ${}^2\Sigma_{1/2}^{(-)}$. In this case we analyzed these bands as ${}^2\Sigma_{1/2}^{(+)}$ because ${}^2\Sigma_{1/2}^{(+)}$ has larger intensity than ${}^2\Sigma_{1/2}^{(-)}$. When the assignment was correct reasonable molecular constants were obtained. But some bands showed considerably large γ_{eff} constant, like $\gamma_{eff}>2B_v$, when analyzed as ${}^2\Sigma_{1/2}^{(+)}$. In such cases, we re-analyzed them as ${}^2\Sigma_{1/2}^{(-)}$, for example 24837.981 cm^{-1} band of C_4H.

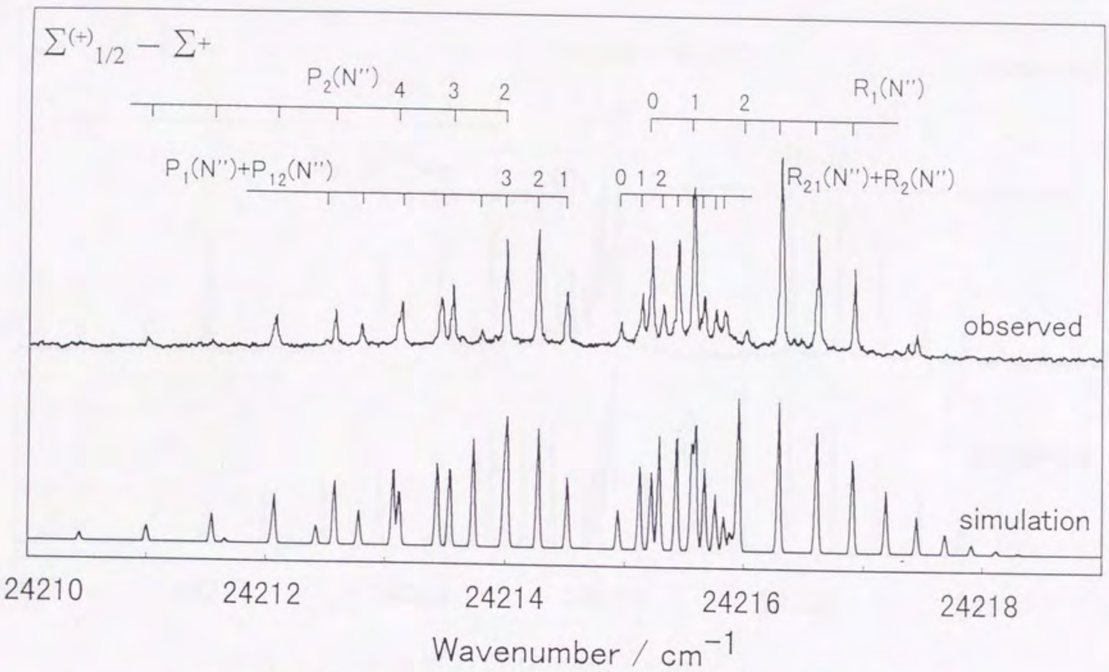

Fig.2.6(a) High resolution LIF spectrum and simulation of C_4H $^2\Sigma^{(+)}_{1/2}-{}^2\Sigma^+$ band. (Band[D] in Fig.2.3).

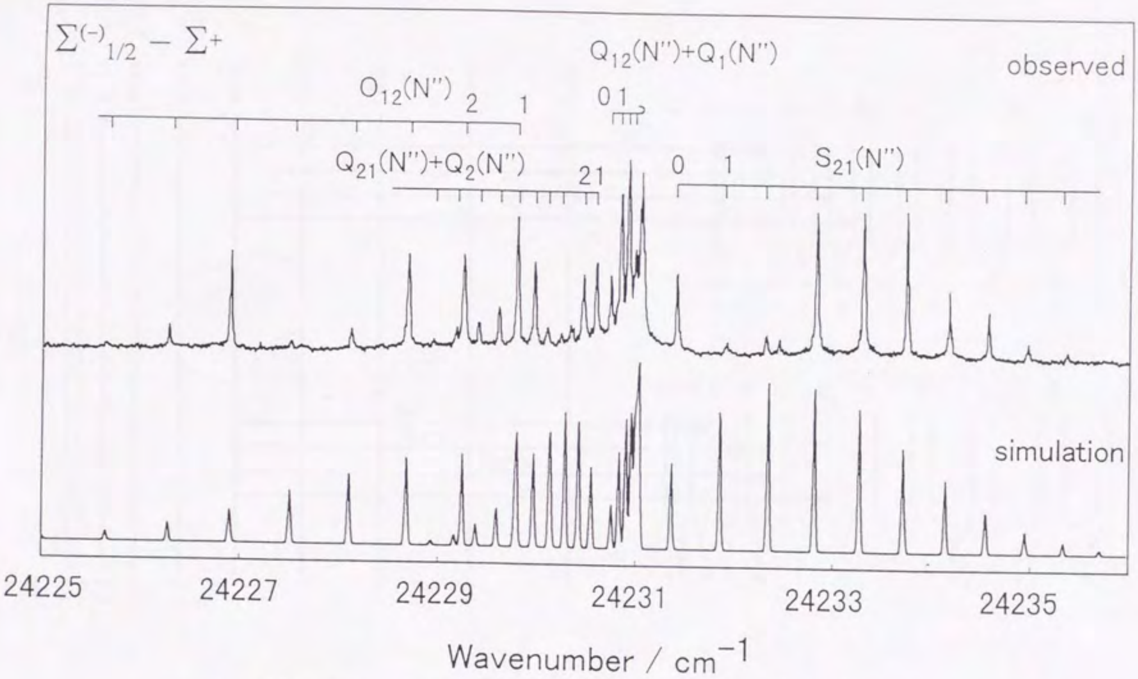

Fig.2.6(b) High resolution LIF spectrum and simulation of C_4H $^2\Sigma^{(-)}_{1/2} - {}^2\Sigma^+$ band.
(Band [E] in Fig.2.3).

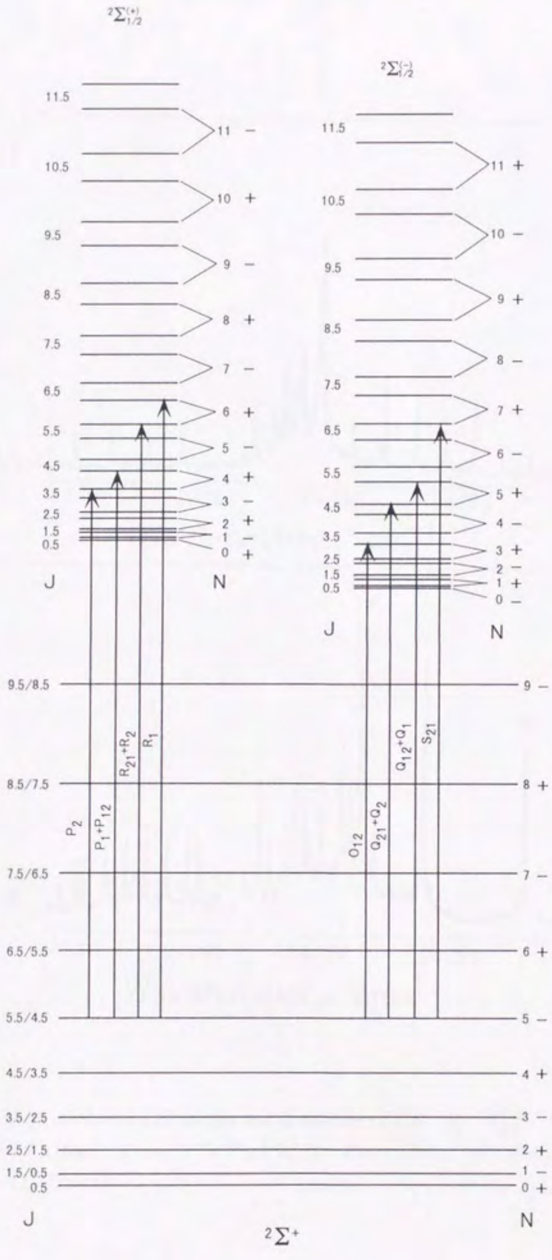
²Σ$_{1/2}^{(+)}$
²Σ$_{1/2}^{(-)}$
J
N
11.5
10.5
9.5
8.5
7.5
6.5
5.5
4.5
3.5
2.5
1.5
0.5
11 −
10 +
9 −
8 +
7 −
6 +
5 −
4 +
3 −
2 +
1 −
0 +
11 +
10 −
9 +
8 −
7 +
6 −
5 +
4 −
3 +
2 −
1 +
0 −
P$_2$
P$_1$+P$_{12}$
R$_{21}$+R$_2$
R$_1$
O$_{12}$
Q$_{21}$+Q$_2$
Q$_{12}$+Q$_1$
S$_{21}$
9.5/8.5
8.5/7.5
7.5/6.5
6.5/5.5
5.5/4.5
4.5/3.5
3.5/2.5
2.5/1.5
1.5/0.5
0.5
9 −
8 +
7 −
6 +
5 −
4 +
3 −
2 +
1 −
0 +
²Σ⁺

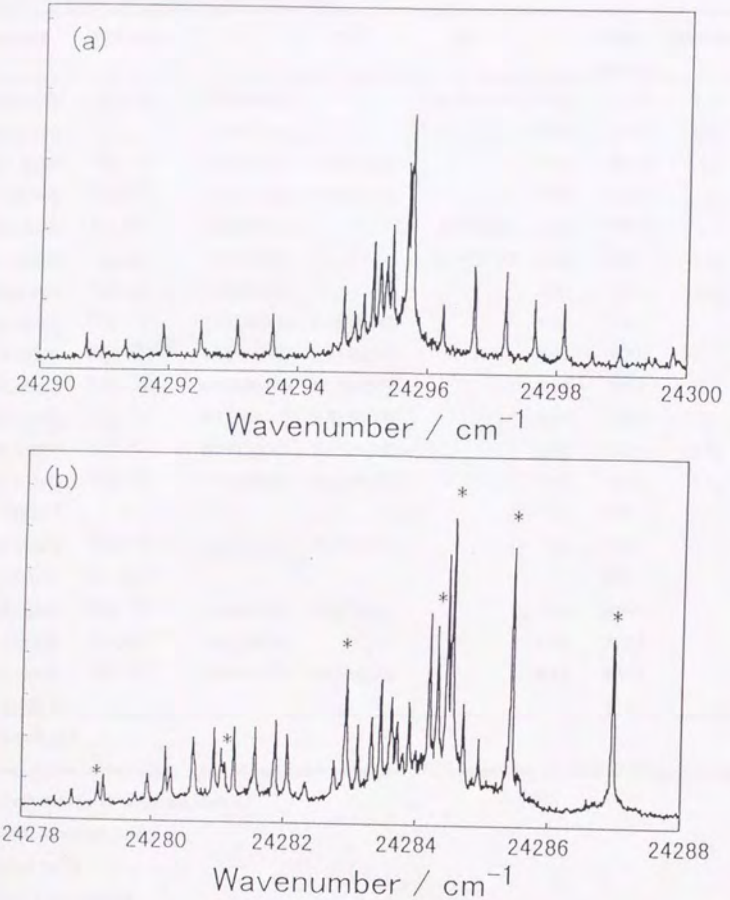

Fig.2.8 High resolution LIF spectra and simulation of C_4D, (a) $^2\Sigma^{(-)}_{1/2}-{}^2\Sigma^+$ and (b) $^2\Sigma^{(+)}_{1/2}-{}^2\Sigma^+$ (Band [d] and [c] in Fig.2.3(b)). Peaks labeled with asterisks are C_3 $\tilde{A}$ (300)- $\tilde{X}$ (300).

Table.2.1 Observed vibronic bands of C_4H.

band origin	band type	B_{eff}'	γ_{eff}[a]	A_{eff}	σ[b]	relative energy	assignment
24033.432(6)	$^2\Pi-^2\Sigma^+$	0.15038(22)		-14.7644(80)	0.02	0.0	0 - 0
24047.631(1)	$^2\Sigma^+-^2\Sigma^+$	0.15005(05)			0.00	14.2	ν_5
24214.735(5)	$^2\Sigma^{(+)}_{1/2}-^2\Sigma^+$	0.14922(15)	0.1885(13)		0.01	181.3	ν_6
24230.660(4)	$^2\Sigma^{(-)}_{1/2}-^2\Sigma^+$	0.15181(10)	0.1942(13)		0.01	197.2	ν_6
24389.339(6)	$^2\Pi-^2\Sigma^+$	0.14870(27)		-5.0431(58)	0.02	355.9	
24417.296(4)	$^2\Pi-^2\Sigma^+$	0.15240(19)		-16.4651(47)	0.01	383.9	$2\nu_6$
24490.806(6)	$^2\Sigma^+-^2\Sigma^+$	0.15076(17)			0.02	457.4	$3\nu_5$
24567.683(3)	$^2\Sigma^{(+)}_{1/2}-^2\Sigma^+$	0.14948(09)	0.1995(04)		0.01	534.3	
24576.432(2)	$^2\Sigma^{(+)}_{1/2}-^2\Sigma^+$	0.14984(08)	0.2146(07)		0.01	543.0	
24580.034(2)	$^2\Sigma^{(-)}_{1/2}-^2\Sigma^+$	0.15233(09)	0.1886(13)		0.01	546.6	
24589.626(2)	$^2\Sigma^{(-)}_{1/2}-^2\Sigma^+$	0.15308(17)	0.2389(13)		0.01	556.2	
24598.830(4)	$^2\Sigma^{(+)}_{1/2}-^2\Sigma^+$	0.15020(13)	0.1529(09)		0.01	565.4	$3\nu_6$
24615.375(4)	$^2\Sigma^{(-)}_{1/2}-^2\Sigma^+$	0.15210(24)	0.1516(17)		0.01	581.9	$3\nu_6$
24823 [c]						790	
24837.981(6)	$^2\Sigma^{(-)}_{1/2}-^2\Sigma^+$	0.15115(33)	0.1598(45)		0.02	804.5	
24847 [d]	$^2\Sigma^+-^2\Sigma^+$?					814	
24849.990(3)	$^2\Sigma^{(+)}_{1/2}-^2\Sigma^+$	0.15391(12)	0.2876(11)		0.01	816.6	
24872.218(9)	$^2\Sigma^+-^2\Sigma^+$	0.15119(51)			0.02	838.8	
24938.123(3)	$^2\Sigma^{(+)}_{1/2}-^2\Sigma^+$	0.15093(13)	0.1554(10)		0.01	904.7	
24948 [d]	?					915	

all in unit of cm^{-1}.

[a] γ' does not show the normal spin-rotation constant but the effective splitting constant of Hougen's expression for $^2\Sigma$ vibronic state in $^2\Pi$ electronic state.

[b] 1σ of least square fitting.

[c] masked by C_3.

[d] heavily perturbed.

Table.2.2 Observed vibronic bands of C_4D.

band origin	band type	B_{eff}'	γ'_{eff}[a]	A_{eff}	σ[b]	relative energy	assignment
24099.191(2)	${}^2\Sigma^+ - {}^2\Sigma^+$	0.14017(05)			0.01	-6.1	ν_6
24105.309(3)	${}^2\Pi - {}^2\Sigma^+$	0.14014(07)		-10.9926(35)	0.01	0.0	0 - 0
24282.545(4)	${}^2\Sigma^{(+)}_{1/2} - {}^2\Sigma^+$	0.13950(10)	0.1335(08)		0.01	177.2	ν_6
24295.521(4)	${}^2\Sigma^{(-)}_{1/2} - {}^2\Sigma^+$	0.14154(08)	0.1360(11)		0.01	190.2	ν_6
24361.705(4)	${}^2\Pi - {}^2\Sigma^+$	0.14043(14)		-13.1172(46)	0.01	256.4	
24463.240(2)	${}^2\Sigma^+ - {}^2\Sigma^+$	0.14107(04)			0.00	357.9	$3\nu_5$
24480.545(4)	${}^2\Sigma^{(+)}_{1/2} - {}^2\Sigma^+$	0.13836(07)	0.1890(08)		0.02	375.2	
24489.19(1)	${}^2\Sigma^{(-)}_{1/2} - {}^2\Sigma^+$	0.14261(53)	0.1928(33)		0.02	383.9	
24550.601(2)	${}^2\Sigma^{(+)}_{1/2} - {}^2\Sigma^+$	0.14209(05)	0.2376(43)		0.01	445.3	
24583.911(5)	${}^2\Sigma^{(+)}_{1/2} - {}^2\Sigma^+$	0.14018(17)	0.2651(14)		0.02	478.6	
24591.76(1)	${}^2\Sigma^+ - {}^2\Sigma^+$	0.14050(31)			0.03	486.5	
24667[c]	?					561.7	
24705.86(1)	${}^2\Sigma^+ - {}^2\Sigma^+$	0.13968(35)			0.03	600.6	
24799.962(6)	${}^2\Sigma^+ - {}^2\Sigma^+$	0.14108(13)			0.02	694.7	
24938.5[c]	${}^2\Sigma^+ - {}^2\Sigma^+$?					833	
24959.0[c]	${}^2\Sigma^+ - {}^2\Sigma^+$?					854	
24962.993(5)	${}^2\Sigma^{(+)}_{1/2} - {}^2\Sigma^+$	0.14390(23)	0.2866(16)		0.01	853.7	
24992.386(4)	${}^2\Sigma^+ - {}^2\Sigma^+$	0.14111(10)			0.01	887.1	

all in unit of cm^{-1}.

[a] γ' does not show the normal spin-rotation constant but the effective splitting constant of Hougen's expression for ${}^2\Sigma$ vibronic state in ${}^2\Pi$ electronic state.

[b] 1σ of least square fitting.

[c] heavily perturbed.

2.6 Vibrational Assignment of the $\tilde{B}\,^2\Pi_i$ state

The stick diagrams and assignments of vibrational structures of C_4H and C_4D in $\tilde{B}\,^2\Pi_i$ are shown in Fig.2.9. $^2\Pi$ vibronic band corresponding to the 0-0 band of C_4H was observed at 24047.631(1) cm^{-1}, which was the lowest vibronic band we observed. ν_5 mode (CCH bending) were observed at 24033.432(6) cm^{-1} and 24490.806(6) cm^{-1} corresponding to the $\nu_5(^2\Sigma^+)$ and $3\nu_5(^2\Sigma^+)$ vibronic states of $\tilde{B}\,^2\Pi_i$. Since vibronic symmetry of ν_5 mode is $^2\Sigma^+$ indicating a large Renner-Teller effect in this bending mode, the vibrational structure of the ν_5 bending mode is quite irregular. In contrast to the ν_5 mode, ν_6 mode (CCC bending) has a regular vibrational structure whose Renner-Teller effect is very small, where $^2\Sigma^{(+)}_{1/2}$ and $^2\Sigma^{(-)}_{1/2}$ pair could be observed. We found the ν_6 progression at 24214.735(5) and 24230.660(4) cm^{-1} for ν_6 ($^2\Sigma^{(\pm)}_{1/2}$), 24417.296(4) cm^{-1} for $2\nu_6$ ($^2\Pi$) and 24598.830(4) and 24615.375(4) cm^{-1} for $3\nu_6$ ($^2\Sigma^{(\pm)}_{1/2}$) with an interval of about 190 cm^{-1}. Some correspondence of vibrational states between C_4H and C_4D are found as drawn by dotted lines in Fig.2.9. The 0-0 band of C_4D is at 24105.309(3) cm^{-1}, and $\nu_5(^2\Sigma^+)$ at 24099.191(2) cm^{-1}, $3\nu_5(^2\Sigma^+)$ at 24463.240(2) cm^{-1} and $\nu_6(^2\Sigma^{(\pm)}_{1/2})$ at 24282.545(4) and 24295.521(4) cm^{-1}, where the vibrational energy of ν_6 is about 183 cm^{-1}. All the determined vibrational frequencies and Renner parameters are summarized in Table 2.3. $\nu_5(^2\Sigma^+)$ vibronic state of C_4D lies below the origin. This fact indicates distortion of the potential surface along the ν_5 normal mode due to a strong vibronic interaction.

In the energy region above 24500 cm^{-1}(relative energy from origin is 400 cm^{-1}) the vibrational structure rapidly loses correspondences between C_4H and C_4D, and many unassigned band remain for both species. This feature must be caused by the complicated vibronic interaction involving three bending modes.

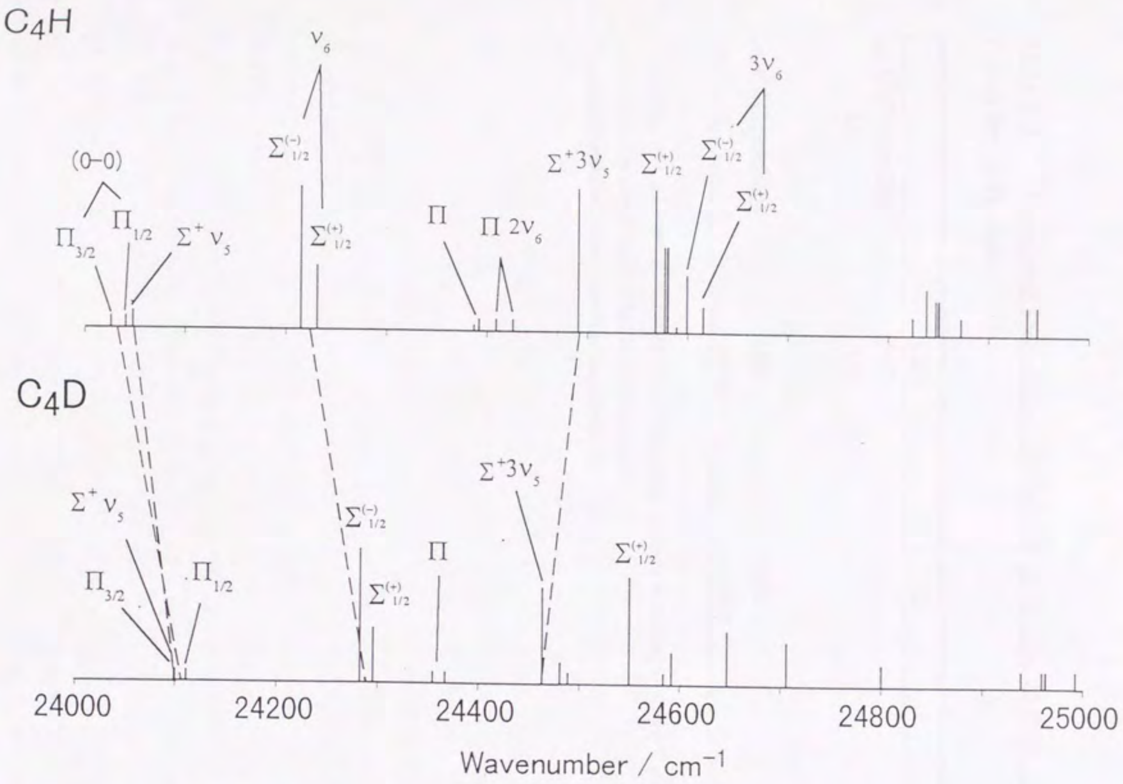

Fig.2.9 Stick diagram of vibrational structures of (a) C_4H and (b) C_4D in $\tilde{B}^2\Pi_i$ electronic state.

Table. 2.2 Vibrational Frequencies and Renner parameters of C_4H and C_4D in the $\widetilde{B}^2\Pi_i$ state.

	C_4H	C_4D
ω_5 (CCH bending)[a)]	563	......
ε_5[a)]	-0.97	....
ω_6(CCC bending)	191	184
ε_6[b)]	-0.015	-0.019

[a)] ω_5 and ε_5 of C_4H were determined from vibrational analysis including v=0, v_5=1 and v_5=3, where Herzberg-Teller effect is not considered.

[b)] ε_6 were determined from rotational analysis of v_6=1 states.

2.7 Results and Discussions

2.7.1 Assignment of the $\tilde{B}^2\Pi_i$ state and the Electron Configuration.

The molecular constants determined in the least square fittings of bands [A] and [B] yielded term energy Tv=24033.432(6) cm^{-1}, B'=0.15038(22) cm^{-1} and A_{eff}=-14.7644(80) cm^{-1}, where the spin-rotation constant γ', parameters for the Λ-type doubling and the centrifugal distortion constants were fixed to be zero, since their effects are undetectable in such low J levels observed in the jet-cooled condition. A_{eff}, an effective spin-orbit interaction constant is not different from conventional A_{so} constants of diatomic molecules without vibronic interaction. Considering that the spin-orbit interaction constant of the carbon atom ζ(2p) is 29 cm^{-1}, it is clear that the excited state have an orbital angular momentum, and so the electronic symmetry is concluded to be $^2\Pi_i$. The label *i* indicates *inverterd*, that is the lowest term is the *P*=3/2 component and $A_{so}< 0$, whose electronic state have a half filled π orbital. Spin-orbit interaction constants of other carbon chain molecules, $C_3H(\tilde{X}^2\Pi_r)$, for example, are a similar values, 14.2 cm^{-1}[41], which confirming our conclusion. For C_4D, bands [a] and [b] belong to the $^2\Pi$-$^2\Sigma$ bands corresponding to $^2\Pi_{3/2}$ and $^2\Pi_{1/2}$, respectively, and molecular constants were determined to Tv=24099.191(2) cm^{-1}, B'=0.14017(05) cm^{-1} and A_{eff}= -10.9926(35) cm^{-1}. A_{eff} of C_4D is also similar to that of $C_3D(\tilde{X}^2\Pi_r)$, 12.53 cm^{-1}[41]. We have observed three $^2\Pi$ -$^2\Sigma$ bands for C_4H and two for C_4D until now, and their molecular constants are summarized in Tables 2.1 and 2.2. The origin of the $^2\Pi$ electronic state must be $^2\Pi$ vibronic state. We have tried to find other $^2\Pi$ bands in the lower region than 24000 cm^{-1} down to 21200 cm^{-1}, but we did not observed any bands of C_4H. Thus, we concluded that the $^2\Pi$ vibronic states at 24033.43 cm^{-1} for C_4H and at 24099.19 cm^{-1} for C_4D are the origin of the $^2\Pi$ electronic state. A characteristic feature observed commonly for all the $^2\Pi$ -$^2\Sigma$ bands is their very weak intensities, about one tenth of the $^2\Sigma$-$^2\Sigma$ bands, although the electronic transition is $^2\Pi$-$^2\Sigma$. The reason will be discussed in section 2.7.4.

According to an *ab initio* calculation (CASPT2/DZVP) by Sobolewski and Adamowicz[29], the second lowest electronic excited state is $2^2\Pi$ and exists at 3.04 eV(24519 cm^{-1}) from the ground state $\tilde{X}^2\Sigma^+$, which shows a good agreement with the observed $^2\Pi_i$ electronic state. Kobluszewski also calculated (MR-CI(+Q)) that the $\tilde{B}^2\Pi$ state lies at 3.24eV(26133.84 cm^{-1})[42], which is slightly larger than our observation but only 8.7%. Since only one electronic state, $2^2\Pi$, is expected around this energy region in their calculations, it is reasonable to consider that the observed transition is $\tilde{B}^2\Pi_i$ - $\tilde{X}^2\Sigma^+$. The main electronic configuration of the ground state and the low lying first excited state are,

$\tilde{A}^2\Pi_i$ ......$(1\pi)^4(2\pi)^3(n\sigma)^2$

$\tilde{X}^2\Sigma^+$ ......$(1\pi)^4(2\pi)^4(n\sigma)^1$,

where 1π and 2π are bonding π molecular orbitals originated from $2p_{x,y}$ atomic orbitals of four carbon atoms, and $n\sigma$ is a non-bonding σ orbital of the terminal carbon atom, which has been expected to lie a little above 2π as shown in Fig.2.10. The second lowest excited state, $^2\Pi_i$ having a half filled π orbital, must have a main configuration as,

$\tilde{B}^2\Pi_i$ ......$(1\pi)^3(2\pi)^4(n\sigma)^2$.

According to Kobluszewski's CI calculation the electronic configuration of $\tilde{B}^2\Pi_i$ state is also 9%$(1\pi)^4(2\pi)^3(n\sigma)^2$ + 60%$(1\pi)^3(2\pi)^4(n\sigma)^2$. $\tilde{B}^2\Pi_i$ - $\tilde{X}^2\Sigma^+$ transition includes $n\sigma$-1π one electron transition. The third excited state, $3^2\Pi$, was calculated to be 4.17eV(33633 cm^{-1}) by Sobolewski and Adamowicz[29]. Its electronic configuration must be,

$\tilde{C}^2\Pi_r$ ......$(1\pi)^4(2\pi)^4(3\pi)^1$.

In 1975, Dismuke *et al.* observed UV absorption spectrum in Ar matrix with its band origin of 33800 cm^{-1}, and assigned tentatively $^2\Pi_r$-$^2\Sigma^+$ transition[30]. Possibly they observed $\tilde{C}^2\Pi_r$ - $\tilde{X}^2\Sigma^+$ transition.

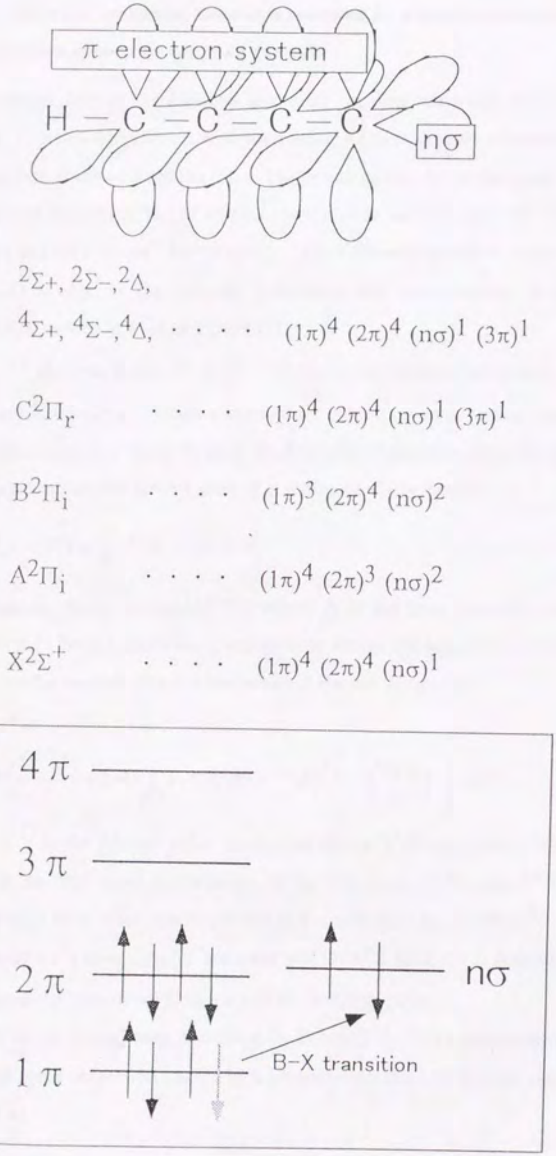

$^2\Sigma+$, $^2\Sigma-$, $^2\Delta$,
$^4\Sigma+$, $^4\Sigma-$, $^4\Delta$, · · · · · $(1\pi)^4\ (2\pi)^4\ (n\sigma)^1\ (3\pi)^1$

$C^2\Pi_r$ · · · · · $(1\pi)^4\ (2\pi)^4\ (n\sigma)^1\ (3\pi)^1$

$B^2\Pi_i$ · · · · $(1\pi)^3\ (2\pi)^4\ (n\sigma)^2$

$A^2\Pi_i$ · · · · $(1\pi)^4\ (2\pi)^3\ (n\sigma)^2$

$X^2\Sigma^+$ · · · · $(1\pi)^4\ (2\pi)^4\ (n\sigma)^1$

Fig.2.10 Molecular orbitals and electronic configurations of C_4H.

2.7.2 Effective molecular constants modified by vibronic interaction: The effective spin-orbit coupling constant

Magnitudes of the effective spin-orbit coupling constants of C_4H and C_4D in the lowest $^2\Pi$ states are different with each other, while in the case of diatomic molecules the A constants obtained from the $^2\Pi_{1/2}$-$^2\Pi_{3/2}$ splittings are almost the same between H and D isotopmers like CH $X^2\Pi_r$ (27.95 cm^{-1} for both CH and CD) and OH $X^2\Pi_i$ (-139.21 cm^{-1} for OH and -139.23 cm^{-1} for OD)[43]. The difference of the A constants between C_4H and C_4D is due to the vibronic interaction and characteristic in polyatomic linear molecules, as well as C_3H and C_3D[41].

$^2\Pi$ vibronic states of $\tilde{B}^2\Pi_i$ v=0 have wavefunction expressed as $|\Lambda=\pm 1$, v=0, l=0> and K=|Λ+l|=1. When a third-order correction term arising from vibronic states with other electronic states through the first term of equation (2.2) the effective spin-orbit coupling constant for K=v+1 state of equation (2.13) is modified as,

$$A_{eff} = A\left[1-\frac{\varepsilon^2}{8}K(K+1)+K\eta\right] \tag{2.14}$$

for triatomic linear molecules[53], where A is the true spin-orbit coupling constant without the vibronic interaction, and must be almost the same for C_4H and C_4D.

ε in the second term is a conventional Renner parameter,

$$\begin{aligned}\varepsilon\omega &= \varepsilon^{(1)}\omega+\varepsilon^{(2)}\omega \\ &= \frac{\langle\xi|V_2e^{\pm 2i\theta}|\xi'\rangle}{hc\gamma}+(-1)\sum_{\xi\subset\Sigma}(-1)^s\left|\langle\xi|V_1e^{\pm i\theta}|\xi'\rangle\right|^2\left[1+\left(\frac{hc\omega}{\Delta E}\right)^2\right]/\Delta E\end{aligned} \tag{2.15}$$

where $\varepsilon^{(1)}$ is the Renner-Teller interaction between vibronic states in the $^2\Pi$ electronic state by the first order perturbation of the first term of H', and $\varepsilon^{(2)}$ is a higher order perturbation from other electronic states ξ' corresponding to either $^2\Sigma^+$ or $^2\Sigma^-$ electronic state, where s is even for a $^2\Sigma^+$ state and odd for a $^2\Sigma^-$ state. γ is defined as $\gamma = 2\pi c\omega / h$ where ω is the vibrational frequency of the bending mode.

η in the second term is derived by Brown[53], which represents a contribution of the third order correction caused by vibronic interactions with other electronic states and defined as

$$\eta = \frac{1}{4\gamma}\sum_{\xi \subset \Sigma,\Delta} \frac{\left|<\xi|V_1 e^{\pm i\theta}|\xi'>\right|^2}{\Delta E^2}\left\{\left[1-(-1)^p\right]\frac{A_{\xi'}}{A_{\xi}}-1\right\} \tag{2.16}$$

ξ' is the $^2\Pi$ electronic state considering and ξ indicates all Σ and Δ electronic states, which can interact with the $^2\Pi$ state through the first order term of the vibronic Hamiltonian, $V_1(Q_+e^{-i\theta}+Q_-e^{i\theta})$, generally called the Herzberg-Teller vibronic coupling. p is an even or an odd integer when ξ' is Σ or Δ, and A_ξ and $A_{\xi'}$ represent the spin-orbit coupling constants of the ξ and ξ' states. ΔE is the energy difference between the ξ and ξ' states. According to equations (2.14)-(2.16), A_{eff} depends on ε and η parameters which are almost the same between C_4H and C_4D except for the CCH bending mode. Vibrational frequencies of CCH is expected to be larger than that of CCD by a factor nearly $\sqrt{2}$, and thus $\gamma^{-1}(C_4H)<\gamma^{-1}(C_4D)$ for the CCH bending mode. Therefore the difference of A_{eff} is caused by the vibronic interaction along the CCH bending mode, ν_5, so we mainly consider the vibronic interaction of ν_5 here, although C_4H has three bending modes.

Generally, the first term of equation (2.15) is much larger than second term and the former indicates a correction of the Renner-Teller effect to A_{eff}, which is different for C_4H and C_4D. However, the observed result, $A_{eff}(C_4H)/A_{eff}(C_4D)=1.343$, cannot be explained by considering only $\varepsilon^{(1)}$. Therefore, we should consider contributions of the Herzberg-Teller vibronic interaction with other electronic states, such as $^2\Sigma^{+/-}$ or $^2\Delta$. When appropriate $^2\Sigma$ and $^2\Delta$ electronic states exist, they interact with $\widetilde{B}^2\Pi_i$ through Herzberg-Teller vibronic coupling along the CCH bending mode, and as a result A_{eff} became different between C_4H and C_4D as explained by equations, (2.14) and (2.16). In the present case, the following electronic states can be considered as candidates of such $^2\Sigma$ and $^2\Delta$ States. The $(1\pi)^4(2\pi)^4(n\sigma)^1$ configuration produces $\widetilde{X}^2\Sigma^+$, which is the only state lying lower than $\widetilde{B}^2\Pi_i$, and the $(1\pi)^4(2\pi)^3(n\sigma)^1(3\pi)^1$ configuration produces $^2\Sigma^+$, $^2\Sigma^-$ and $^2\Delta$, and their quartet states. According to an *ab initio* study [29], $^2\Delta$ state lies about only 10000 cm^{-1} above $\widetilde{B}^2\Pi_i$, while $\widetilde{X}^2\Sigma^+$ is 24000 cm^{-1} below $\widetilde{B}^2\Pi_i$. Thus $^2\Delta$ and $^2\Sigma^+$ derived from the configuration of $(1\pi)^4(2\pi)^3(n\sigma)^1(3\pi)^1$ contribute dominantly to the η constant, and η takes a negative value with $|\eta(C_4H)|<|\eta(C_4D)|$, since $\gamma(C_4H)^{-1}<\gamma(C_4D)^{-1}$ for the CCH bending mode. Consequently, the absolute value of effective spin-orbit coupling constant $|A_{eff}|$ in equation (2.14) of C_4H is observed to be much larger than that of C_4D by a factor 1.343. This conclusion suggests simultaneously that the second order Herzberg-Teller interaction between $\tilde{B}^2\Pi$ and higher $^2\Sigma$ and $^2\Delta$ states expressed as $\left|\left\langle B^2\Pi \middle| V_1 e^{\pm i\theta} \middle| {}^2\Sigma_{or}\, {}^2\Delta \right\rangle\right|$ in not negligible for the vibrational structure, as well as the Renner-Teller vibronic interaction, and occurrence of such an effect is actually confirmed from vibrational structure of the $\tilde{B}^2\Pi_i$ state as will be described in section 2.7.3.

Effective Molecular Constants of $^2\Sigma^{(+)}_{1/2}$ and $^2\Sigma^{(-)}_{1/2}$ vibronic states.

The Renner-Teller effect can be discussed qualitatively from $^2\Sigma^{(+)}_{1/2}$ and $^2\Sigma^{(-)}_{1/2}$, which are separated by the Renner-Teller effect and the spin-orbit coupling, by using equations (2.4)-(2.9). Let us consider the ν_6 vibronic states, bands [D] $^2\Sigma^{(+)}_{1/2}$ and [E] $^2\Sigma^{(-)}_{1/2}$ of C_4H, and [c] $^2\Sigma^{(+)}_{1/2}$ and [d] $^2\Sigma^{(-)}_{1/2}$ of C_4D, corresponding to $^{\mu}\Sigma$ and $^{\kappa}\Sigma$, respectively. We use notation of (+) and (-) instead of μ and κ used in equations (2.4)-(2.9) in the following discussions. According to equation (2.4) the splitting between $^2\Sigma^{(+)}_{1/2}$ and $^2\Sigma^{(-)}_{1/2}$ corresponds to $2r$, which is 15.925 cm^{-1} for ν_6 the vibronic state. Using A_{eff}=-14.7644 cm^{-1} determined from the rotational analysis of the $^2\Pi$ origin band, we obtaine $|\sin 2\beta|$=0.3747, $|\cos 2\beta|$=0.9271 and $|\varepsilon\omega(v+1)|=5.968$. Since ν_6=1 and ω=189 cm^{-1}, the Renner-Teller parameter is derived as ε_6=-0.016, which indicates that the Renner-Teller effect is very small for the ν_6 bending mode. The mixing ratio of Σ^+ and Σ^- is also obtained by replacing $|\sin\beta|$=0.2764 and $|\cos\beta|$=0.9610 to equation (2.9),

$$\begin{aligned} \Sigma^{(+)}_{1/2} &= 0.829\Sigma^{+} + 0.559\Sigma^{-} \\ \Sigma^{(-)}_{1/2} &= 0.559\Sigma^{+} - 0.829\Sigma^{-} \end{aligned} \qquad (\nu_6 \text{ state of } C_4H \text{ in } \tilde{B}^2\Pi_i)$$

Thus, the ratio of the transition intensities should be $\left|\left\langle \Sigma^{(+)}_{1/2} \middle| \mu \middle| \Sigma^{+} \right\rangle\right|^2 / \left|\left\langle \Sigma^{(-)}_{1/2} \middle| \mu \middle| \Sigma^{+} \right\rangle\right|^2 = 2.2$, which is qualitatively consistent with the observation shown in Fig.2.3 where band[D] is about two times stronger than band[E].

The effective constants $B^{(+)}_{eff}$ and $\gamma^{(+)}_{eff}$, $B^{(-)}_{eff}$ and $\gamma^{(-)}_{eff}$ can be calculated by using equations (2.8) and (2.9) from the above $|\sin\beta|$ and $|\cos\beta|$ as, $B^{(+)}_{eff}$=0.1493 cm^{-1},

$\gamma_{eff}^{(+)}$=0.186 cm^{-1}, $B_{eff}^{(-)}$=0.1517 cm^{-1} and $\gamma_{eff}^{(-)}$=0.191 cm^{-1}. These values show in surprisingly good agreement with those of the observed, $B_{eff}^{(+)}$=0.14922 cm^{-1} and $\gamma_{eff}^{(+)}$=0.1885 cm^{-1}, $B_{eff}^{(-)}$=0.15181 cm^{-1} and $\gamma_{eff}^{(-)}$=0.1942 cm^{-1}.

In the similar way, we obtain |sin2β|=0.3747, |cos2β|=0.9271 and $|\varepsilon\omega(\mathrm{v}+1)|$=5.968, and ε_6=-0.019 where ω=183 cm^{-1} for ν_6 state of C_4D (band [c] and [d]). The eigen functions are expressed as,

$$\begin{aligned} \Sigma_{1/2}^{(+)} &\approx 0.875\Sigma^{+} + 0.484\Sigma^{-} \\ \Sigma_{1/2}^{(-)} &\approx 0.484\Sigma^{+} - 0.875\Sigma^{-} \end{aligned} \qquad (\nu_6 \text{ state of } C_4D \text{ in } \tilde{B}\,^2\Pi_i)$$

However estimated intensity ratio from the above eigen functions is $\left|\left\langle\Sigma_{1/2}^{(+)}\middle|\mu\middle|\Sigma^{+}\right\rangle\right|^2 / \left|\left\langle\Sigma_{1/2}^{(-)}\middle|\mu\middle|\Sigma^{+}\right\rangle\right|^2 \approx 3.3$, which is slightly larger than the observed value, ≈ 2.0. (Note that band [c] in Fig.2.3 is overlapped with C_3) The effective constants are $B_{eff}^{(+)}$=0.1394 cm^{-1}, $\gamma_{eff}^{(+)}$=0.130 cm^{-1}, $B_{eff}^{(-)}$=0.1416 cm^{-1} and $\gamma_{eff}^{(-)}$=0.134 cm^{-1} which are in less good agreement with the observed, $B_{eff}^{(+)}$=0.13950 cm^{-1}, $\gamma_{eff}^{(+)}$=0.1335 cm^{-1}, $B_{eff}^{(-)}$=0.14154 cm^{-1} and $\gamma_{eff}^{(-)}$=0.1360 cm^{-1} compared with the case of ν_6 of C_4H. These slight divergence in intensity ratio and the effective molecular constants are probably caused by Herzberg-Teller vibronic interaction, whose effect is different between C_4H and C_4D.

For other $^2\Sigma_{1/2}^{(+)}$ and $^2\Sigma_{1/2}^{(-)}$ bands, above discussions were not applicable, even for $3\nu_6$ of C_4H, due to higher order vibronic interactions, such as the cross vibronic interaction between two $^2\Sigma$ states (the interaction between different bending modes) which were recently considered by Tang *et al.*[44] for the explanation of anomalous γ_{eff} of HCCS in the ground state.

2.7.3 Vibrational structure of $\widetilde{B}\,^2\Pi_i$ state

ν_5 CCH bending mode

Renner-Teller effect is very large in ν_5 mode, thus vibrational structure of ν_5 mode is quite irregular: $\nu_5\,(^2\Sigma^+)$ state is considerably shifted down to 14.2 cm^{-1} above origin and $3\nu_5\,(^2\Sigma^+)$ lies at 457.4 cm^{-1} for C_4H. When Renner-Teller effect is strong, that is the case of $\varepsilon\omega \gg A$, the vibrational energy may be expressed as,

$$T_v = \omega(v+1) - \frac{1}{8}\varepsilon^2\omega K(K+1) \tag{2.17}$$

for K=v+1 state and,

$$\begin{aligned} T_v^+ &= \omega\left(1-\frac{1}{8}\varepsilon^2\right)(v+1) + \frac{1}{2}\varepsilon\omega\sqrt{(v+1)^2-K^2} \pm \frac{\varepsilon AK(K+1)}{8\sqrt{(v+1)^2-K^2}} \\ T_v^- &= \omega\left(1-\frac{1}{8}\varepsilon^2\right)(v+1) - \frac{1}{2}\varepsilon\omega\sqrt{(v+1)^2-K^2} \pm \frac{\varepsilon AK(K+1)}{8\sqrt{(v+1)^2-K^2}} \end{aligned} \tag{2.18}$$

for K<v+1 states, where Herzberg-Teller vibronic interaction between electronic state is not considered and the sign of shoulder is associated to symmetry of refection plane. Using equation (2.17) for $^2\Pi(v=0)$ and equation (2.18) for $^2\Sigma^+(v=1,3)$, we obtained $\varepsilon_5=-0.975$ and bending frequency $\omega_5=562.65$ cm^{-1} for C_4H in $\widetilde{B}\,^2\Pi_i$. On the other hand, for ν_5 CCD bending mode of C_4D, the vibrational energy are $\nu_5=-6.5$ cm^{-1} and $3\nu_5=357.9$ cm^{-1}. It is worth noting that ν_5 state of C_4D lies below origin of $\widetilde{B}\,^2\Pi_i$. This inversion cannot be explained solely by Renner-Teller effect, so we should consider second order perturbation from other electronic states, that is Herzberg-Teller interaction.

The second order contribution to the vibrational energy is expressed as [53],

$$E^{(2)} = \Delta T - (v+1)hc\Delta\omega^{(2)} + g_K hcK\Lambda + \text{higher order term} \tag{2.19}$$

In this equation, ΔT represents a constant correlation to all vibronic levels of Π electronic state given by

$$\Delta T = \frac{h}{4}\sum_{\Delta states}\frac{\left|\left\langle \xi,\Lambda=1\middle|V_{11}e^{-i\theta}\middle|\xi',\Lambda=2\right\rangle\right|^2}{(\Delta E)^2}. \tag{2.20}$$

where ΔE is a energy difference between $\widetilde{B}\,^2\Pi_i$ and other electronic states involved vibronic interaction. The second term involves $\Delta\omega^{(2)}$ which can be described as a second order correlation to the vibrational frequency,

$$\Delta\omega^{(2)} = \frac{1}{4hc\gamma}\sum_{\xi\subset\Sigma,\Delta}\frac{\left|\langle\xi|V_{11}|\xi'\rangle\right|^2}{\Delta E} \tag{2.21}$$

The sign of the correction $\Delta\omega$ depends on the sign of ΔE, and in the present case since we consider that the contribution of $^2\Sigma^+$ and $^2\Delta$ electronic states lying above $\widetilde{B}^2\Pi_i$ is dominant, so $\Delta\omega>0$. The third term g_k is given by

$$g_K = \frac{\omega}{4\gamma}\sum_{\xi\subset\Sigma,\Delta}\frac{(-1)^p\left|\langle\xi|V_{11}|\xi'\rangle\right|^2}{(\Delta E)^2}, \tag{2.22}$$

p is an even integer for Σ states and an odd integer for Δ states. Considering both Renner-Teller and Herzberg-Teller effects the vibrational energy can be rewretten by

$$\begin{aligned}
{}^2\Pi(v=0) &= T_0+\omega-\frac{1}{4}\varepsilon^2\omega+\Delta T-hc\Delta\omega^{(2)}+g_K K\Lambda\\
{}^2\Sigma^+(v=1) &= T_0+2\omega+\varepsilon\omega-\frac{1}{4}\varepsilon^2\omega+\Delta T-2hc\Delta\omega^{(2)}\\
{}^2\Sigma^+(v=3) &= T_0+4\omega+2\varepsilon\omega-\frac{1}{2}\varepsilon^2\omega+\Delta T-4hc\Delta\omega^{(2)}\\
{}^2\Sigma^+(v=5) &= T_0+6\omega+3\varepsilon\omega-\frac{3}{4}\varepsilon^2\omega+\Delta T-6hc\Delta\omega^{(2)}
\end{aligned} \tag{2.23}$$

…………………

Following these expression, $\nu_5(^2\Sigma^+)$ must be shifted down further by Herzberg-Teller interaction in addition to Renner-Teller effect. From equations (2.21) and (2.22), $hc\Delta\omega^{(2)}$ is expected to be larger than g_k because $\Delta E>>\omega$, thus the energy difference is approximately written as,

$$^2\Sigma(\nu_5)-{}^2\Pi(\mathrm{v}=0)\approx(1+\varepsilon)\omega-2hc\Delta\omega^{(2)} \tag{2.24}$$

In the present case of C_4D since Herzberg-Teller interaction is enough large and $1-\varepsilon$ is close to zero, the above energy difference has a negative value, $^2\Sigma(\nu_5)<{}^2\Pi(\mathrm{v}=0)$. Considering a correlation of vibrational energy structure between linear and bent molecules, $\Sigma^+(v=1)$ state correlate to v=0, K=0 level, which is the lowest level in a bent molecule, and $\Pi(v=0)$ correlates to v=0, K=1 level which is the second lowest level. Namely the order of vibrational energy in a linear molecule is inverted in a bent molecule. Therefore vibrational structure of C_4D and also C_4H in $\widetilde{B}^2\Pi_i$ state suggest that $\widetilde{B}^2\Pi_i$

state is in the middle of linear and bent molecule along CCH angle, namely "quasi-linear" molecule, whose vibration averaged geometry is generally linear but potential enery surface is distorted. Qualitative potential curve of $\tilde{B}^2\Pi_i$ state and other electronic states associated in vibronic interaction are described in Fig.2.11.

If $\Delta\omega^{(2)}$ is independent to vibrational levels, then $\Sigma^+(3\nu_3)-\Sigma^+(\nu_3)=\Sigma^+(5\nu_3)-\Sigma^+(3\nu_3)$ from equation (2.23), then vibrational energy of $\Sigma^+(5\nu_3)$ state can be expected as 900.6 and 721.9 $cm^{-1}$for C_4H and C_4D. Σ^+ state at 838.8 cm^{-1} of C_4H and 694.7 cm^{-1} of C_4D are most reliable candidates for $5\nu_5$ state. $^2\Pi$ bands corresponding to $2\nu_5$ or $4\nu_5$ were not also assigned certainly. Anyway such Π states must have a small A_{eff} because Renner-Teller effect is so large that spin-orbit coupling is not important leading to quenching of electron angular momentum. $^2\Pi$ band at 355.9 cm^{-1} of C_4H have a small A_{eff} constant, -5 cm^{-1}, is likely to be $2\nu_5$

ν_6 CCC bending mode

ν_6 CCC bending mode has a harmonic vibrational structure which shows Renner-Teller effect is weak along ν_6 mode. This was confirmed from the rotational structures of $^2\Sigma^{(+)}_{1/2}$ and $^2\Sigma^{(-)}_{1/2}$ vibronic states as described in rotational anlysis. Since the term energies of Σ vibronic states without perturbations for ν_6 mode are expressed as $Tv=[E(^2\Sigma^{(+)}_{1/2})+E(^2\Sigma^{(-)}_{1/2})]/2$, we could obtain ν_6=189.25 cm^{-1}, $2\nu_6$=383.9 cm^{-1} and $3\nu_6$=573.65 cm^{-1}. By averaging these term values we determined the vibrational frequency, ω_6=191 cm^{-1} for C_4H in $\tilde{B}^2\Pi_i$. For C_4D, only ν_6=183.7 cm^{-1} was observed, and so we estimated ω_6=184 cm^{-1}. All determined molecular constants for vibrational structure of the $\tilde{B}^2\Pi_i$ state were summarized in Table 2.3.

In the $2\nu_6$ state, however two $^2\Pi$ state must arise, namely linear combinations of $|\Lambda=\pm1, l=0>$ and $|\Lambda=\pm1, l=\mp2>$, we could observe only one $^2\Pi$ state. It is for this reason that since Renner-Teller effect of ν_6 mode is very weak, vibronic mixing between $|\Lambda=\pm1, l=0>$ and $|\Lambda=\pm1, l=\mp2>$ is also small, and consequently only $^2\Pi$ vibronic states with $|\Lambda=\pm1, l=0>$ was observed by l selection rule.

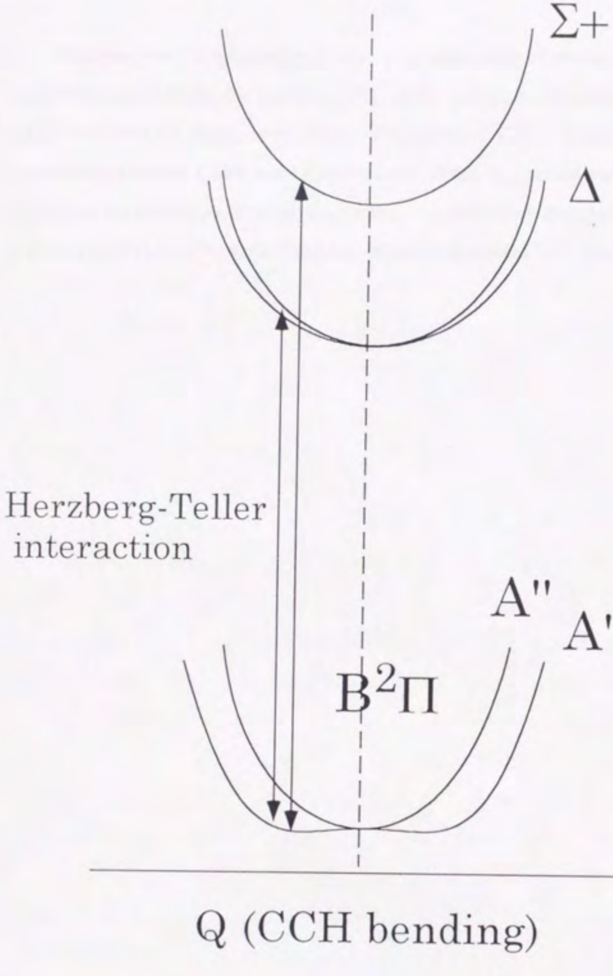

Fig.2.11 Vibronic interaction between $\tilde{B}^2\Pi_i$ and higher lying other electronic states. Potential energy surface of $\tilde{B}^2\Pi_i$ is distorted along CCH bending mode.

There are even many unassigned vibronic states in spite of whose rotational analysis can be completely made, for example, $^2\Sigma^{(\pm)}_{1/2}$ pairs with their term energy of 573.86 and 583.03 cm^{-1} from the origin, a little below of 3ν_6 states of C_4H. Because their rotational structure were those of with weak Renner-Teller effect, it is considered that they do not accompany the excitation of ν_5 bending mode. Possibly they are combination bands of ν_6 and ν_7, such as $2\nu_6+\nu_7$, $\nu_6+2\nu_7$ and $3\nu_7$, where ν_7 is another CCC bending mode.

2.7.4 Vibronic interaction in the ground state.

It is surprising that $^2\Sigma$-$^2\Sigma$ bands were observed very intensively compared with $^2\Pi$–$^2\Sigma$ bands by about ten times as recognized in Fig.2.9. Because the electronic transition $\tilde{B}^2\Pi_i - \tilde{X}^2\Sigma^+$ is induced by a perpendicular transition moment $\mu_{x,y}$, $^2\Pi$–$^2\Sigma$ perpendicular transition is symmetry allowed and thus observable, while $^2\Sigma$-$^2\Sigma$ parallel transition is symmetry forbidden and not observed under Born-Oppenheimer (BO) approximation. Therefore the $\tilde{B}^2\Pi_i - \tilde{X}^2\Sigma^+$ system must involve some perturbations caused by breakdown of BO approximation, and observed intensity pattern of vibronic bands must reflect contribution of this effect. We consider that the main contribution of this observed result is vibronic coupling between $\tilde{X}^2\Sigma^+$ and $\tilde{A}^2\Pi_i$ as schematically described in Fig.2.12.

According to *ab initio* calculation by Sobolewski and Adamowicz[29] oscillator strength f ($\propto|\mu|^2$) of $\tilde{B}$-$\tilde{X}$ transition is 4.6×10^{-4}, on the other hand that of $\tilde{B}$-$\tilde{A}$ transition is 1.3×10^{-2}, about 30 times lager than that of $\tilde{B}$-$\tilde{X}$. From another *ab initio* study by Kolbuszewski, $|\mu|^2$ of $\tilde{B}$-$\tilde{X}$ and $\tilde{B}$-$\tilde{A}$ transitions are 0.0017 and 6.60 respectively, which are different by a factor 400[42]. Since $|\mu|^2$ is directly related to signal intensity, if $\tilde{X}^2\Sigma^+$ v=0 state has a character of $\tilde{B}^2\Pi_i$, then parallel transitions $^2\Sigma$-$^2\Sigma$ or $^2\Pi$-$^2\Pi$ induced by $\tilde{B}$-$\tilde{A}$ parallel transition moment μ_z come out predominant rather than perpendicular transitions, in other words "intensity borrowing" from $\tilde{A}^2\Pi_i$. The first excited electronic state $\tilde{A}^2\Pi_i$ has been predicted to be very close to the ground state, and from recent *ab initio* calculations the energy gap between $\tilde{A}^2\Pi_i$ and $\tilde{X}^2\Sigma^+$ is expected to 565 cm^{-1}[29], 70 cm^{-1}[45] and 150$\pm$100 cm^{-1}[46]. Thus exceptionally strong vibronic coupling can occur between $\tilde{X}^2\Sigma^+$ $|\Lambda=0, v''=0, l=0\rangle$ and $^2\Sigma$ vibronic states of $\tilde{A}^2\Pi_i$, $|\Lambda=\pm1, v', l=\mp1\rangle$ through HT vibronic interaction, the first term of H' in equation (2.2), where same vibronic states($^2\Sigma$) labeled quantum number K=0 are mixed. In this case Λ and l are no longer good quantum numbers and only K($|\Lambda+l|$) is a good quantum number, the wavefunction of the ground state can be expressed as

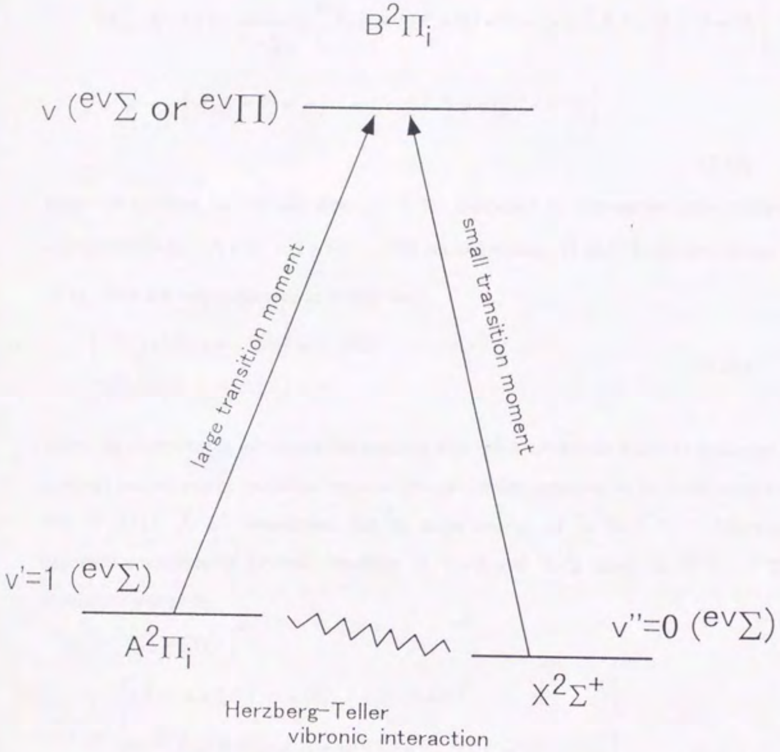

Fig.2.12 Vibronic interaction between $\tilde{X}^2\Sigma^+$ and $\tilde{A}^2\Pi_i$.

$$
\begin{aligned}
\left|\Psi_{GS}^{\Sigma}, K = 0\right\rangle &= \frac{1}{\sqrt{1+\sum_i {c_i}^2}}\left[\left|\widetilde{X}, \Lambda = 0\right\rangle\left|\mathrm{v}'' = 0, l = 0\right\rangle + \sum_i c_i\left|\widetilde{A}, \Lambda = \pm 1\right\rangle\left|\mathrm{v}_i{}', l = \mp 1\right\rangle\right] \\
&\approx \frac{1}{\sqrt{1+c^2}}\left[\left|\widetilde{X}, \Lambda = 0\right\rangle\left|\mathrm{v}'' = 0, l = 0\right\rangle + c\left|\widetilde{A}, \Lambda = \pm 1\right\rangle\left|\mathrm{v}', l = \mp 1\right\rangle\right]
\end{aligned}
\tag{2.25}
$$

where all possible $^2\Sigma$ vibronic state of $\widetilde{A}^2\Pi_i$ expressed by summation were replaced approximately by $\left|\Lambda = \pm 1, \mathrm{v}', l = \mp 1\right\rangle$. The excited states, $^2\Pi$ and $^2\Sigma$ vibronic states of $\widetilde{B}^2\Pi_i$ state are also expressed in similar way,

$$
\begin{aligned}
\left|\Psi_{EX}^{\Pi}\right\rangle &\approx \left|\widetilde{B}, \Lambda = \pm 1\right\rangle\left|\mathrm{v}, l = 0_{or} \mp 2\right\rangle \\
\left|\Psi_{EX}^{\Sigma}\right\rangle &\approx \left|\widetilde{B}, \Lambda = \pm 1\right\rangle\left|\mathrm{v}, l = \mp 1\right\rangle
\end{aligned}
\tag{2.26}
$$

where the contribution of vibronic interaction with other electronic states as discussed in previous section can be excluded because vibronic mixing expected to be small compared that of $\widetilde{A}^2\Pi_i$ - $\widetilde{X}^2\Sigma^+$ interaction due to large energy of $^2\Delta$,$^2\Sigma$- $\widetilde{B}^2\Pi_i$. Therefore transition intensities of vibronic transition of $^2\Pi$-$^2\Sigma$ and $^2\Sigma$-$^2\Sigma$ bands in $\widetilde{B}^2\Pi_i$ - $\widetilde{X}^2\Sigma^+$ system are written by,

$$
\begin{aligned}
I_{\Pi\text{-}\Sigma} &= \left|\left\langle\Psi_{EX}^{\Pi}\right|er\left|\Psi_{GS}^{\Sigma}\right\rangle\right|^2 \\
&= \frac{1}{1+c^2}\left[\begin{array}{l}\left|\left\langle\widetilde{B}, \Lambda = \pm 1\right|\mu\left|\widetilde{X}, \Lambda = 0\right\rangle\left\langle \mathrm{v}, l = 0 | \mathrm{v}', l = 0\right\rangle\right|^2 \\ + c^2\left|\left\langle\widetilde{B}, \Lambda = \pm 1\right|\mu\left|\widetilde{A}, \Lambda = \pm 1\right\rangle\left\langle \mathrm{v}, l = 0_{or} \mp 2 | \mathrm{v}'' = 0, l = \mp 1\right\rangle\right|^2\end{array}\right] \\
&= \frac{1}{1+c^2}\left|\mu_{BX}\right|^2 C'_{FC} \\
&\propto \frac{1}{1+c^2} f_{BX} C'_{FC}
\end{aligned}
\tag{2.27}
$$

and,

$$\begin{aligned}
I_{\Sigma\text{-}\Sigma} &= \left|\left\langle \Psi_{EX}^{\Sigma} \middle| er \middle| \Psi_{GS}^{\Sigma} \right\rangle\right|^2 \\
&= \frac{1}{1+c^2}\left[\begin{array}{l} \left|\left\langle \widetilde{B}, \Lambda = \pm 1 \middle| \mu \middle| \widetilde{X}, \Lambda = 0 \right\rangle \left\langle \mathrm{v}, l = \mp 1 \middle| \mathrm{v}', l = 0 \right\rangle\right|^2 \\ + c^2 \left|\left\langle \widetilde{B}, \Lambda = \pm 1 \middle| \mu \middle| \widetilde{A}, \Lambda = \pm 1 \right\rangle \left\langle \mathrm{v}, l = \mp 1 \middle| \mathrm{v}'' = 0, l = \mp 1 \right\rangle\right|^2 \end{array}\right] \\
&= \frac{c^2}{1+c^2} \left|\mu_{BA}\right|^2 C_{FC} \\
&\propto \frac{c^2}{1+c^2} f_{BA} C_{FC}
\end{aligned} \tag{2.28}$$

μ_{mn} and f_{mn} indicate transition dipole moment and oscillator strength of electronic transition from state m to state n, and C_{FC} is Franck-Condon factor. First and second term in square brackets vanishes because $\Delta l \neq 0$. These formula of transition intensity suggests that $^2\Pi$-$^2\Sigma$ band include $\widetilde{B}^2\Pi_i$ - $\widetilde{X}^2\Sigma^+$ electronic transition while $^2\Sigma$-$^2\Sigma$ band is induced by transition from $\widetilde{A}^2\Pi_i$ character of $\widetilde{X}^2\Sigma^+$ v=0 to $\widetilde{B}^2\Pi_i$. The ratio of $\widetilde{A}^2\Pi_i$ character in $\widetilde{X}^2\Sigma^+$ v=0 can be estimated to about 37% from simulation of relative intensities between $^2\Sigma$ -$^2\Sigma$ and $^2\Pi$ -$^2\Sigma$, where $^2\Sigma$ -$^2\Sigma$ transition is ten times stronger and $f_{AB}/f_{AX} \approx 30$ from ref. 29, and the Frank-Condon factor is same between equations (2.27) and (2.28). The strong vibronic coupling between $\widetilde{X}^2\Sigma^+$ and $\widetilde{A}^2\Pi_i$ states is also suggested based on experimental results obtained by microwave spectroscopy. Chen *et al.*[47] estimated that $\widetilde{X}^2\Sigma^+$ v=0 state contains about 28% of $\widetilde{A}^2\Pi_i$ character from hyperfine coupling constants of ^{13}C. However Chen's and our estimation are based on quite different type of experimental data, both are in good agreement with each other. Yamamoto *et al.* [24] observed rotational structure of vibrationally excited state of $\widetilde{X}^2\Sigma^+$, and mentioned that large spin-orbit coupling constant of $\nu_7(\Pi)$ vibronic state is caused by vibronic interaction from $\widetilde{A}^2\Pi_i$ although it was not v=0 state. Therefore our discussion recomfirmed the dominant opinion that vibronic coupling between $\widetilde{X}^2\Sigma^+$ and $\widetilde{A}^2\Pi_i$ is very strong from phenomenal point of view.

2.7.5 Fluorescence lifetime and relaxation processes of the $\tilde{B}^2\Pi_i$ state.

We have measured fluorescence time profile in order to investigate the relaxation processes. Although fluorescence time profile of C_4H is seemed to be a single exponential decay curve at one view, it consists of two component: a short time component (fast decay) and a long time component (slow decay).

Fig.2.13(a) shows a typical time profile in the decay time of 0-4 μs obtained by P(1) transition of $3\nu_5$ state of C_4H at 24990.499 cm^{-1} (see Fig.2.18), by accumulating of 500 shots with sampling rate of 500MHz. Fig. 2.13(b) is expanded time profile of a short time component in 0-100 ns, where the circles indicate observed decay curve (1 pt./2ns). We analyzed this short time component as a single exponential decay and determined decay time as 11 ns by convolution with laser pulse. Resulting decay curve of fitting were described by a solid line.

Fig.2.14(b) shows long time component of the same timeprofile expanded along vertical axis. One can find that very weak and slow decay signals continue to the region longer than 4 μs. This long time component have a complicated structure on it, which are not noise owing to electronics because base line is flat before laser radiation comes in. Therefore this structure corresponds to "Quantum beat" which reflects the energy structure of the excited states related to non-radiative transition. In order to check the reproducibility and dependence on rotational levels of quantum beat, we compared time profiles of P and R branches both which have the common rotational level in the excited state, as shown in Fig.2.15. The features of quantum beats on the longer decay component are perfectly coincidence between for the common N' levels' leading to that the very weak long time component with quantum beat are real. Although the feature of quantum beats depend on rotational levels, but the decay time is estimated to about 3-4 μm which is common for all rotational levels.

The observation of above two decay component suggest the competition of radiative and non-radiative relaxation processes as mentioned in section 1.4. In the present case, the non-radiative states, "dark states", lying in the same energy region as $\tilde{B}^2\Pi_i$ are considered to be high vibrationally excited states of $\tilde{X}^2\Sigma^+$ and $\tilde{A}^2\Pi_i$ because no other electronic states exist below $\widetilde{B}^2\Pi_i$ considering electronic configuration as discussed in section 2.7.1. Therefore non-radiative transition, $\widetilde{B}^2\Pi_i \rightarrow \widetilde{A}^2\Pi_i$, $\widetilde{X}^2\Sigma^+$, were induced by internal conversion (IC) as schematically shown in Fig.2.16 following zero order model of Feed and Nitzan[52] in which |s> and {|l>} indicate zero order $\widetilde{A}^2\Pi_i$ and { $\widetilde{A}^2\Pi_i$, $\widetilde{X}^2\Sigma^+$ } states, and {|j>} are eigen states produced by IC.

In this model short time component is expressed as,

$$P_s(t) = \exp\left[-\left(\frac{1}{\tau_s}+\Gamma\right)t\right] \tag{2.29}$$

where τ_s is spontaneous emission lifetime of $\widetilde{B}$-$\widetilde{X}$ and $\widetilde{B}$-$\widetilde{A}$ transitions. Γ is relaxation rate constant to non-radiative states (or dephasing rate constant of coherently excites states) and when number of {|l>} states, N, is large (≧10),

$$\Gamma \approx \frac{2\pi}{\hbar}\left|\overline{W}_{sl}\right|^2 \rho_l \quad (\rho_l \propto N) \tag{2.30}$$

where W_{sl} is interaction matrix element and ρ_l is density of states of {|l>}.
Long time component is approximately expressed as,

$$P_s(t) = \frac{1}{N}\exp\left(-\frac{t}{\tau_j}\right) \tag{2.31}$$

where γ_j is lifetime of eigen state |j> which is approximately τ_sN, leading to anomalous long time decay when N is large, generally called "Douglus effect"[51].

The observed short time components have lifetimes about 15 ns, which is an averaged liftime of N'=0-4 of 3ν_5 C_4H, corresponding to $\left(\frac{1}{\tau_s}+\Gamma\right)^{-1}$. Lifetime of spontaneous emission from $\widetilde{A}^2\Pi_i$, τ_s, can be expected from oscillator strength *f* of *ab initio* calculation[29], τ_s =5μs for $\widetilde{B}^2\Pi_i$-$\widetilde{X}^2\Sigma^+$ transition and τ_s=220ns for $\widetilde{B}^2\Pi_i$-$\widetilde{A}^2\Pi_i$ transition. These are much larger than observed lifetime, 15 ns, which suggests that IC is much faster than radiative decay, and thus,

$$\left(\frac{1}{\tau_s}+\Gamma\right)^{-1} \approx \frac{1}{\Gamma} = 15\text{ns}, \text{ and } \tau_s \approx 200\text{ns}.$$

The decay time of long time component is about 3-4 μs, corresponding to $\tau_l \approx \tau_s N$. Thus using τ_s=220 ns, N, number of |l> involving IC process, is expected to 15-20. On the other hand the intensity ratio of short and long time components is ≈ 50 which derive $N \approx 50$. Probably true lifetime of spontaneous emission τ_s is shorter than the theoretical prediction. The quantum beat were observed clearly on the longer component which depend on rotational levels. Therefore in the case of C_4H, although N is expected to be more than 10 which is nearly statistic limit, the interaction between $\tilde{B}^2\Pi_i$ ($|s>$) and $\tilde{A}^2\Pi_i$, $\tilde{X}^2\Sigma^+$ ($\{|l>\}$) remains still "local" character.

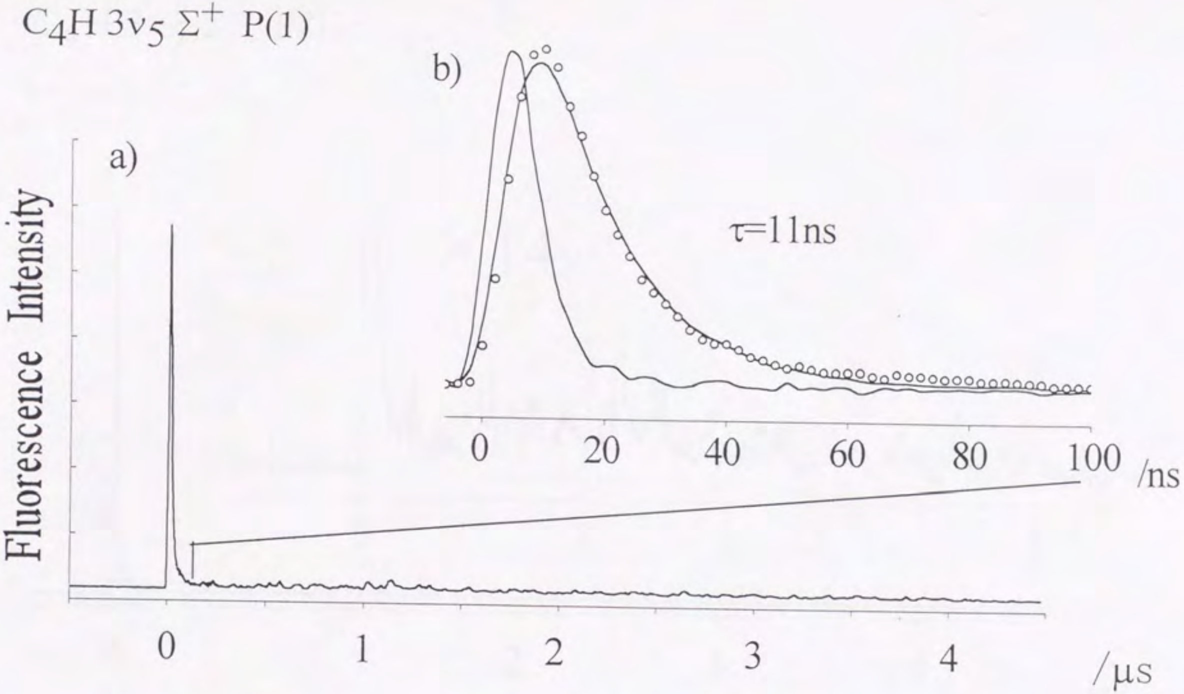

Fig.2.13 Fluorescence time profile of C_4H obtained by excitation of P(1) branch of $\tilde{B}^2\Pi_i\ 3\nu_5$ by accumulation of 500 shots. (a) a long time scale profile (b) an expanded profile of a short time component..

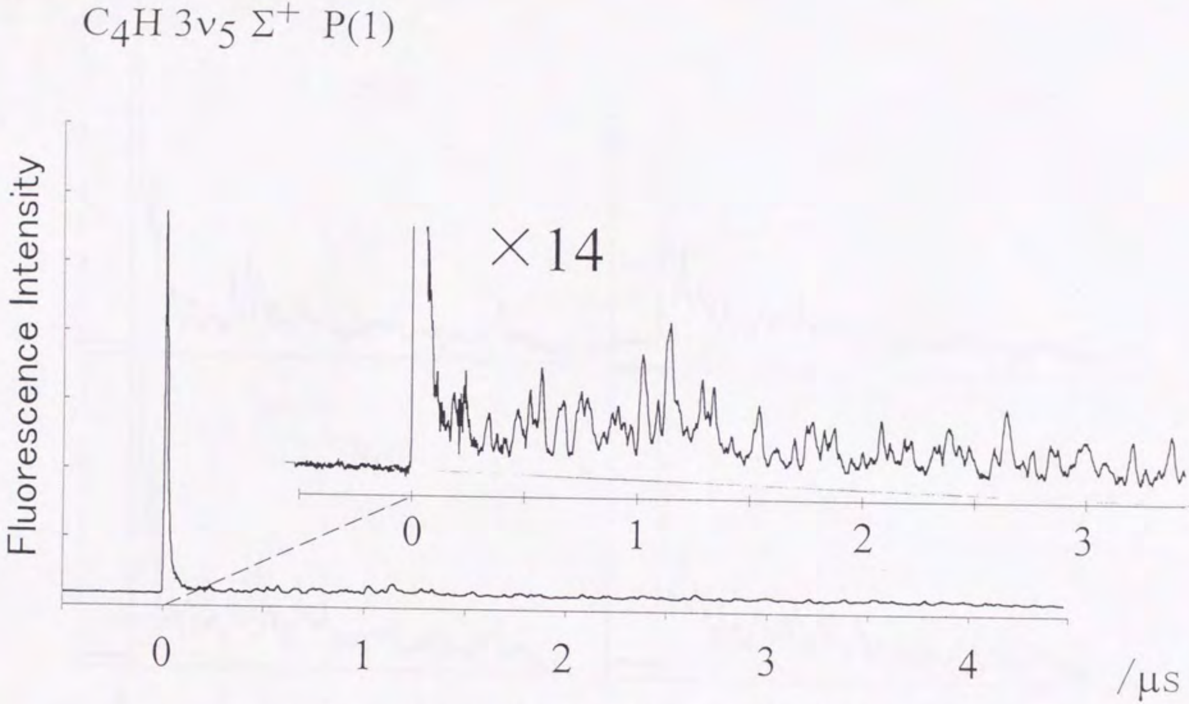

Fig.2.14 Fluorescence time profile of C_4H obtained by excitation of P(1) branch of $\tilde{B}^2\Pi_i\,3\nu_5$ by accumulation of 500 shots. (a) a long time scale profile (b) expanded along vertical axis

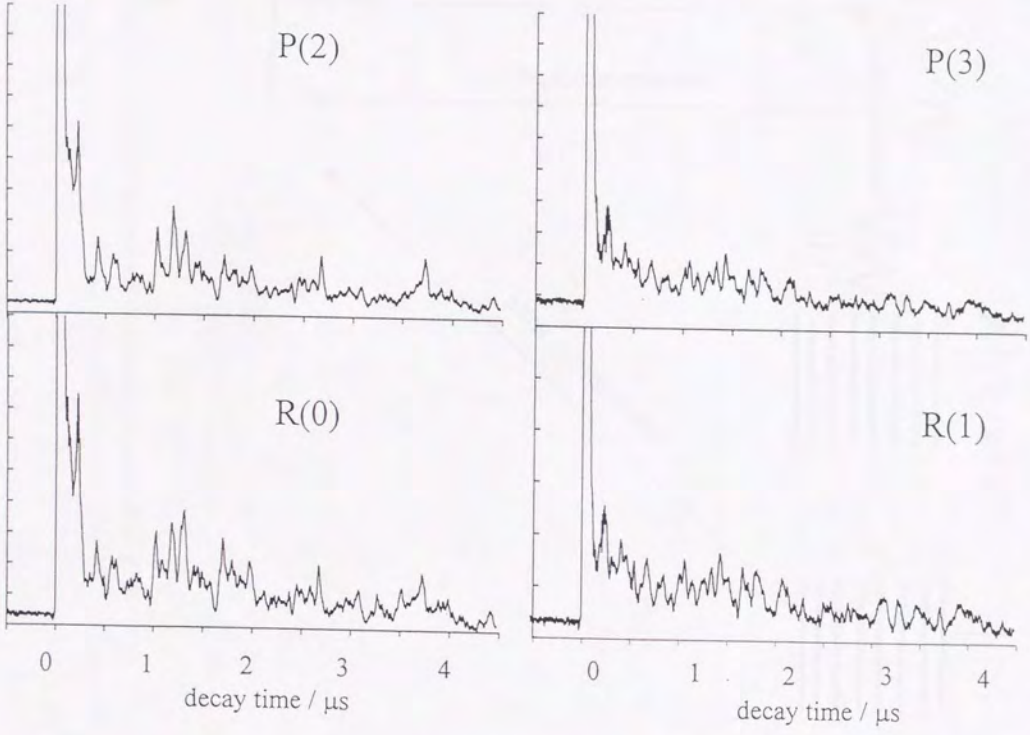

Fig.2.15 Comparison of fluorescence time profiles of C_4H excited by different to different rotational levels in $\tilde{B}^2\Pi_i\,3\nu_5$ obtained by accumulation of 500 shots.

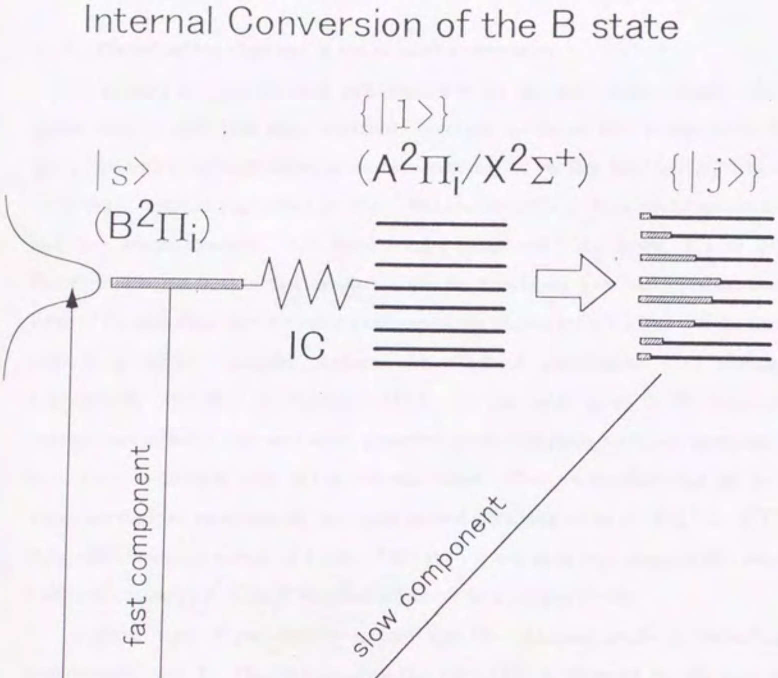

Fig.2.16 Relaxation processes of electronically excited C_4H in $\tilde{B}^2\Pi_i$.

2.7.6 Perturbations observed in the rotational structure.

We found two type of local perturbations in the observed vibronic bands. One typical case is such that some rotational lines are weakened like broken teeth by interaction with some dark states, as we have seen in a $^2\Pi$ vibronic band in Fig.2.5(b) or $^2\Sigma^+$ vibronic bands in Figs.2.4(a) and (b). The characteristic of these perturbations are that they occur randomly, not systematically about rotational levels, J (or N). Therefore it might be said that the dark states have different rotational constant from those of the perturbed vibronic states as schematically shown in Fig.2.17(a). If the dark state have similar rotational constant, the effect of perturbation must changes systematically with J(or N) like Fig.2.17(b). On the other hand, if the rotational constants are different with each other, perturbation can take place in the only particular J level, which is crossing point of two vibronic states. Then we conclude that the dark states, the cause of perturbations, are highly excited vibrational levels of $\tilde{X}^2\Sigma^+$ or $\tilde{A}^2\Pi_i$ state with vibrational energy of 24000-25000 cm^{-1}, which must have considerably small rotational constant due to large vibration amplitude of stretching modes.

Another type of perturbation is such that the rotational levels are perturbed systematically with J. Thus the situation like Fig.2.17(b) is expected for this type of perturbation, where the dark state has a similar rotational constants with the perturbed state. $3\nu_5(^2\Sigma^+)$ state of C_4H is a typical case of this perturbation, as shown in Fig.2.18. in which while spin splitting are not observed for $N' \leqq 3$, suddenly large splitting about 0.04-0.05 cm^{-1} appeared for $N' \geqq 4$. The reduced energy, that is rovibrational energy minus 0.151N(N+1), is shown in Fig. 2.19. One can recognize that level crossing occurs between N'=3 and 4, which causes systematical level shifts about N' levels and anomalous spin splitting. The most probable candidate of the dark state is the other vibronic state of $\tilde{B}^2\Pi_i$. In the case of $3\nu_5$ $^2\Sigma^+$, $^2\Pi$ state is expected to lie in the background as a dark state like Fig.2.20, and interact with $3\nu_5$ $^2\Sigma^+$ through vibration-rotation Hamiltonian*). At the crossing point, F_1 component of N'=4 in $^2\Sigma^+$ interacts with J'=4.5(+), and as a results N'=4 F_1 is shifted up above F_2. For larger N, the similar tendency, $F_1 > F_2$, are expected in fine structure. On the other hand, for lower N', F_1

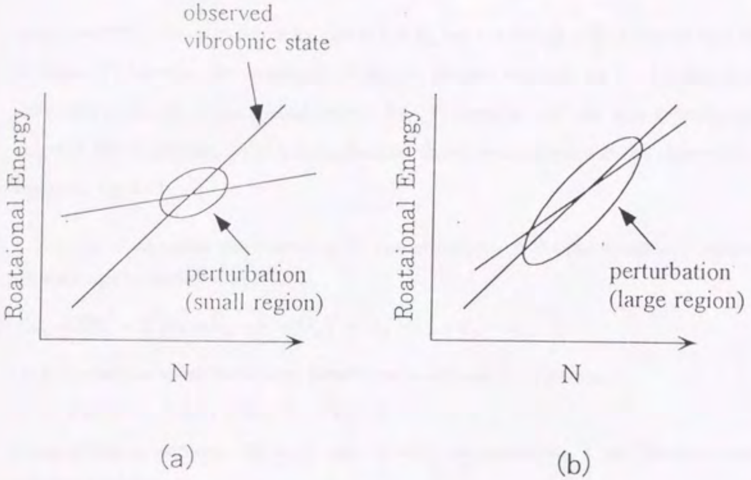

Fig.2.18 Schematic diagram of perturbations: (a) the rotational constant of perturber is much different from those of the observed vibronic state. (b) the rotational constant of perturber is almost the same with those of the observed vibronic state. Perturbations are occurred at particular rotational levels in (a). while systematically in (b).

levels are shifted down to below F_2, that is $F_1 < F_2$, but the energy shift is smaller than that of higher N' because the magnitude of matrix element depends on J. Consequently, since spin sublevels in the ground state is $F_1 < F_2$ because $\gamma<0$, the spin splitting were canceled below crossing point and emphasized above crossing point in the observed LIF spectrum Fig.2.18.

*) This type of interaction was observed in the case of C_3D[R]. A Rotation Hamiltonian including vibratinal angular momentum is,

$$H_{rot} = B\mathrm{R}^2 = B\left[\left(\mathrm{J}_x - \mathrm{L}_x - \mathrm{S}_x - \mathrm{G}_x\right)^2 + \left(\mathrm{J}_y - \mathrm{L}_y - \mathrm{S}_y - \mathrm{G}_y\right)^2\right]$$

and from expansion of this Hamiltonian, perturbation Hamiltonian, H', is obtained as

$$H' = -B\left(J_+G_- + J_-G_+\right) + B\left(S_+G_- + S_-G_+\right).$$

H' have offdiagonal element at $\Delta K = \pm 1$, and $\Delta l = \mp 1$, and thus between $^2\Sigma^+$ and $^2\Pi$ vibronic states with same J and parity.)

Two types of perturbations exist together in the origin band of C_4D where $^2\Pi_{3/2}$ and ν_5 $^2\Sigma^+$ were observed overlapping each other as shown in Fig.2.21. P_{12} and Q_1+R_{12} branches of J'=1.5 and 2.5, and P_1+Q_{12} and R_1 of J'=2.5 were missed or weakened. These line missing are occurred due to the former type of the perturbations. The energy diagram of $^2\Pi_{3/2}$ and $^2\Sigma^+$ calculated from molecular constants of Table 2.2 are described in Fig.2.21. The perturbed levels in LIF spectrum are labeled by asterisks. The perturbed $^2\Pi_{3/2}$ levels can interact with particular levels in $^2\Sigma^+(\nu_5)$ by the latter type of the perturbations. Therefore the effect of perturbation which cause line missing in $^2\Pi_{3/2}$ can act for $^2\Sigma^+$ levels through $^2\Pi_{3/2}$ levels. Actually, both F_1 and F_2 spin sublevels of N'=2 level in $^2\Sigma^+$ can interact with J=2.5 in $^2\Pi_{3/2}$, of which both L components are perturbed by IC, and as a results P(3) and R(1) branches were weakened. On the other hand, N'=3 which were perturbed only in F_2 component, thus in P(4) branch only J'=1.5-J"=2.5 is weakened and J'=2.5-J"=3.5 is not affected by perturbation. Therefore P(4) is not so lost with its intensity.

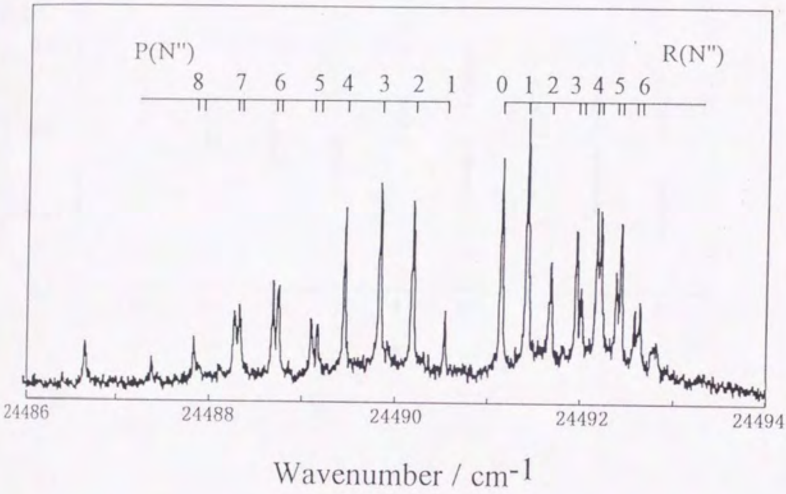

Fig.2.17 High resolution LIF spectrum of C_4H $\tilde{B}^2\Pi_i$ $3\nu_5$ band.

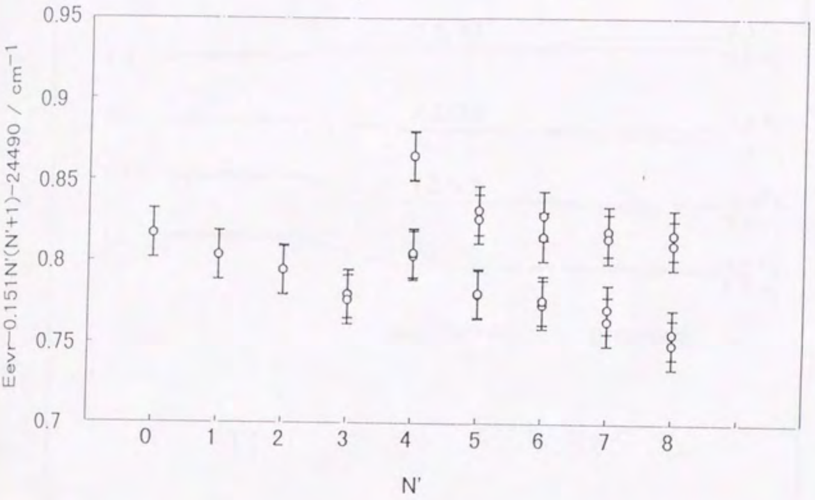

Fig.2.19 Reduced rotational energy of C_4H $\tilde{B}^2\Pi_i$ $3\nu_5$. Error bars indicate laser bandwidth, 0.03 cm^{-1}. Level crossing is found between N'=3 and 4.

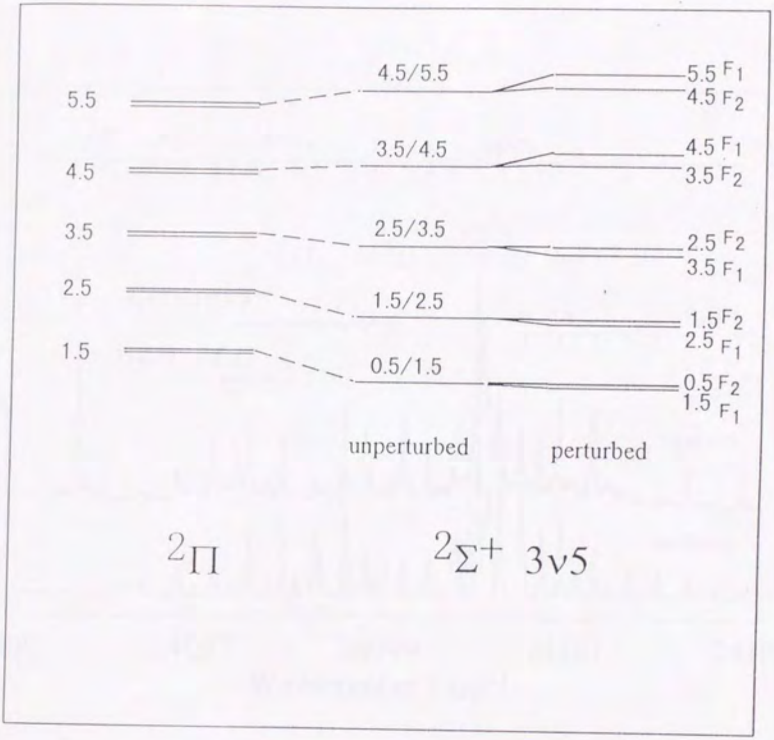

Fig.2.20 Schematic diagram of perturbations for C_4H $\tilde{B}^2\Pi_i$ $3\nu_5$ state.

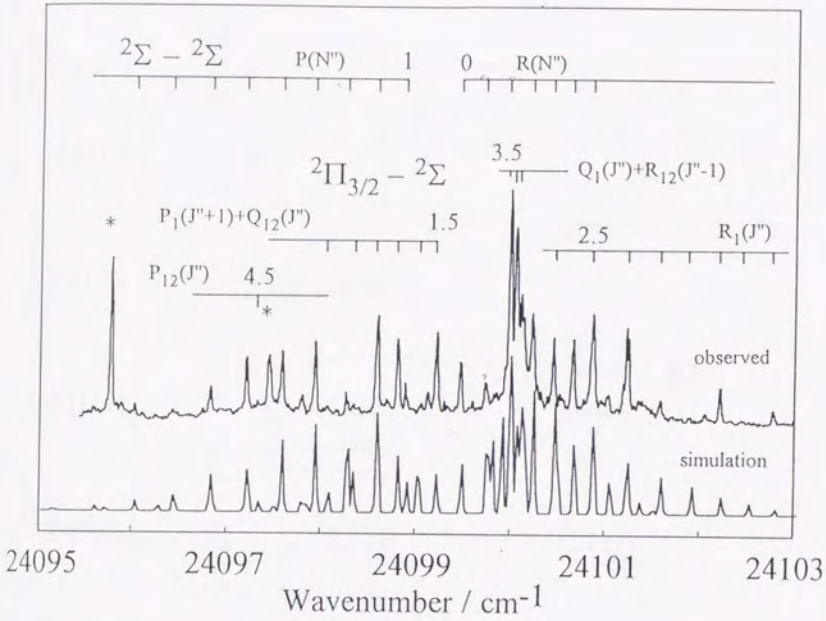

Fig.2.21 High resolution LIF spectrum and simulation of $^2\Pi_{3/2}$ (v = 0) $-{}^2\Sigma^+$ and $^2\Sigma^+(\nu_5)-{}^2\Sigma^+$. Several rotational lines in lower J' or N' are missed or weakened by interaction between $^2\Pi_{3/2}$ and $^2\Sigma^+$. Peaks labeled with asterisks are C_3.

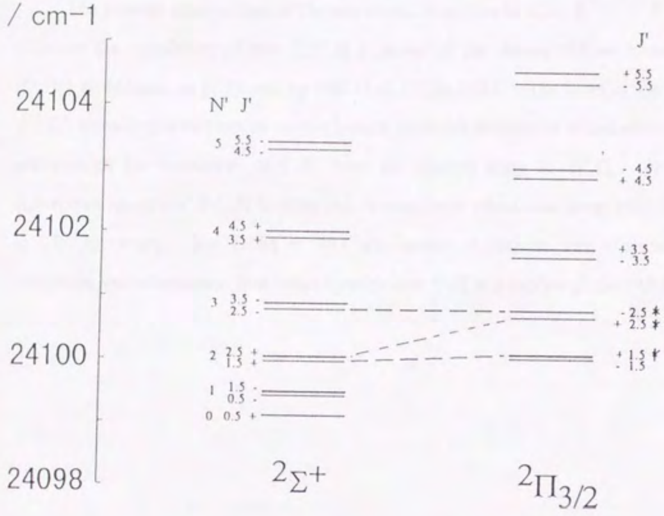

Fig.2.22 Schematic diagram of interaction between ${}^2\Pi_{3/2}$ (v = 0) and ${}^2\Sigma^+$ (ν_5) .

2.7.7 Suggestion for Astronomical Interest

The present observation of the electronic transition of C_4H, $\tilde{B}^2\Pi_i - \tilde{X}^2\Sigma^+$ system, disprove the possibility of that C_4H is a carrier of the strong diffuse interstellar bands (DIBs) at 443 nm, as proposed by Bell *et al.* [3] in 1983. The band origin of $\tilde{B}^2\Pi_i - \tilde{X}^2\Sigma^+$ transition is 416 nm as shown before, thus the absorption of radiation at 443 nm is not enough for excitation of C_4H from the ground state to $\tilde{B}^2\Pi_i$. In addition, if absorption spectrum of C_4H is observed, it must have vibrational progression as observed in LIF spectrum. But DIBs at 443 nm seems to include one vibronic transition. Therefore we recommend that other species than C_4H is a carrire of the 443 nm band.

References

1. K.D. Tucker, M.L. Kutner, and P. Thaddeus, Astrophys. J., **193**, L115 (1974).

2. A. Saddeus. C.A. Gottlieb, A. Hjalmarson, J.E.B. Johason, W.M. Irvine, P. Friberg, and R.A. Linke, Astrophys. J., **294**, L49 (1985).

3. M.B. Bell, P.A. Feldman, and H.E. Matthews, Astrophys. J., **273**, L35 (1983).

4. W.M. Irvine, B. Hoglund, P. Friberg, J. Askne, and J. Ellder, Astrophys. J., **248**, L113 (1981)

5. M.B. Bell, T.J. Sears, and H.E. Matthews. Astrophys. J. **255**, L75 (1982).

6. M. Guelin, P. Friberg, and A. Mezaoui, Astron. Astrophys., **109**, 23 (1982).

7. B.E. Turner, Astrophys. J., **347**, L39 (1989).

8. M. Guelin, and P. Thaddeus, Astron. Astrophys., **212**, L81 (1977).

9. M. Guelin, S. Green, and P. Thaddeus, Astrophys. J., **224,** L27 (1978).

10. S.E. Cummins, M. Morris, and P. Thaddeus, Astrophys. J., **235**, 886 (1980).

11. M. Guelin, J.Cernicharo, S. Navarro, D.R. Woodward, C.A. Gottlieb, and P. Thaddeus, Astron. Astrophys., **182**, L37 (1987),

12. H. Suzuki, M. Ohishi, N. Kaifu, S. Ishikawa, T. Kasuga, S. Saito, and K. Kawaguchi, Pub. Astron. Soc. Jpn., **38**, 911 (1986).

13. P. Thaddeus, C.A. Gottlieb, A. Hjalmarson, J.E.B. Johanson, W.M. Irvine, P. Friberg, and R.A.Linke, Astrophys. J. 294, L49 (1985).

14. M.J. Travers, M.C. McCarthy, C.A. Gottlieb, and P. Thaddeus, Astrophys. J. 465, L77 (1996).

15. J. Cernicharo and M.Guelin, Astron. Astrophys., 309, L27 (1996).

16. M.C. McCarthy, M.J. Travers, A. Kovacs, C.A. Gottlieb, and P. Thaddeus, Astron. Astrophys. 309, L31 (1996).

17. M.C. McCarthy, M.J. Travers, P. Kalmus, C.A. Gottlieb, and P. Thaddeus, Astrophys. J. 467, L125 (1996).

18. M. Guelin and P. Thaddeus, Astrophys. J., 212, L81 (1977).

19. Y. Kasai, Y. Sumiyoshi, Y. Endo. And K. Kwaguchi, submitted to Astrophys. J. Lett.

20. Y. Ohshima and Y. Endo, J. Mol. Spectrosc., 153, 627, (1992).

21. Y. Hirahara, Y. Ohshima, and Y. Endo, Astrophys. J., 408, L115 (1993).

22. Y. Kasai, K. Obi, Y. Ohshima, Y. Hirahara, Y. Endo, K. Kawaguchi, and A. Murakami, Astrophys. J., 410, L45 (1993).

23. C.A. Gottlieb, E.W. Gottlieb, P. Thaddeus, and H. Kawamura, Astrophys. J., **275**, 916 (1983).

24. S. Yamamoto, S. Saito, M. Guelin, H. Suzuki, and M. Ohishi, Astrophys. J., **323**, L149 (1987).

25. D.R. Woodward, J.C. Pearson, C.A. Gottlieb, and P. Thaddeus, Astrophys. J., **333**, L29 (1988).

26. M.E. Jacox, Chem. Phys., 7, 424 (1975).

28. J. Fulara, D. Lessen, P. Freivogel, and J.P. Maier, Nature, **366**, 439 (1993).

29. A.L. Sobolewski and L. Adamowicz, J. Chem. Phys., **102**, 394 (1995).

30. K.I. Dismuke, W.R.M. Graham, and W. Weltner, Jr, J. Mol. Spectrosc., **57**, 127 (1975).

31. L.N.Shen, T.J. Doyle, and W.R.M. Graham, J. Chem. Phys., **93**, 1597 (1990).

32. D. Forney, J. Fulara, P. Freivogel, D. Lessen, and J. P. Maier, J. Chem. Phys., **103**, 48 (1995).

33. P. Freivogel, J. Fulara, M. Jakobi, D. Forney, and J. Maier, J. Chem. Phys., **103**, 54 (1995).

34. Y. Ohshima, Y. Endo, and T. Ogata, J. Chem. Phys., 102, 1493 (1995).

35. T. Ogata, Y. Ohshima, and Y. Endo, J. Am. Chem. Soc., 117, 3593 (1995).

36. H. Kouguchi, Y. Ohshima, and Y. Endo, Chem. Phys. Lett. **254,** 397 (1996).

37. H. Kouguchi, Y. Ohshima, and Y. Endo, accepted to J. Chem. Phys.

38. J. Baker, S.K. Bramblr, and P.A. Hamilton, Chem. Phys. Lett., **213**, 297 (1993).

39. W.J. Balfour, J.Cao, C.V.V. Pasad, and C.X.W. Qian, J. Chem. Phys., **101**, 10343 (1994).

40. M. Izuha and K. Yamanouchi, Chem. Phys. Lett., **242,** 435(1995).

41. S. Yamamoto, S. Saito, M. Ohishi, H. Suzuki, S. Ishikawa, N. Kaifu, and A. Murakami, Astrophys. J. 322, L55 (1987).

42. M. Kolbuszewski, Astrophys. J. 432, L63 (1994)

43. Molecular Spectra and Molecular Structure Ⅳ. Constants of Diatomic Molecules.

44. J. Tang and S. Saito, J. Chem. Phys., 105, 8020 (1996).

45. D.E. Woon, Chem. Phys. Lett., **244**, 45 (1995).

46. M.C. MaCathy. C.A. Gottlieb, P. Thaddeus, M. Horn and P. Botschwina, 103, 7820 (1995).

47. Wei Chen, S.E. Novick, M.C. MaCathy, C.A. Gottlieb, P. Thaddeus, J. Phys. Chem. 103, 7828 (1995).

48. R.T.Renner, Z.Phys. **92**, 172 (1934)

49. J.A. Pople and H.C. Longuet-Higgins, Mole. Phys., **1**, 327 (1958).

50. J.T. Hougen, J. Chem. Phys., 63, 519 (1962).

51. A. E. Douglas, J. Chem. Phys. 45, 1007 (1965).

52. K.F. Freed and A. Nitzan, J. Chem. Phys. 73, 4765 (1980).

53. J. Brown, J. Mol. Spectrosc., 68, 412 (1977).

Appendix 2.1

Matrix elements of the vibronic interaction and the spin-orbit coupling

Herzberg Teller vibronic interaction

$$\left\langle 1, n, K-1, \Sigma \middle| V_1 r \cos(\theta-\phi) \middle| 0, n \pm 1, K, \Sigma \right\rangle = \mp W \sqrt{\left[(n \pm K/2)\right]}$$

$$\left\langle -1, n, K+1, \Sigma \middle| V_1 r \cos(\theta-\phi) \middle| 0, n \pm 1, K, \Sigma \right\rangle = \mp W \sqrt{\left[(n \mp K/2)\right]}$$

$$W \propto \left\langle R_{|\Lambda|=1} \exp(\pm i\theta) \middle| V_1 \exp(\pm i\theta) \middle| R_{\Lambda=0} \right\rangle$$

Renner-Teller vibronic interaction

$$\left\langle 1, n, K-1, \Sigma \middle| V_2 r^2 \cos 2(\theta-\phi) \middle| -1, n, K+1, \Sigma \right\rangle = \frac{\varepsilon\omega}{2} \sqrt{\left(n^2 - K^2\right)}$$

$$\left\langle 1, n, K-1, \Sigma \middle| V_2 r^2 \cos 2(\theta-\phi) \middle| -1, n \pm 2, K+1, \Sigma \right\rangle = \frac{\varepsilon\omega}{4} \sqrt{(n \pm K)\{n \pm (K+2)\}}$$

$$\left\langle -1, n, K+1, \Sigma \middle| V_2 r^2 \cos 2(\theta-\phi) \middle| 1, n \pm 2, K-1, \Sigma \right\rangle = \frac{\varepsilon\omega}{4} \sqrt{(n \mp K)\{n \mp (K-2)\}}$$

$$\varepsilon \propto \left\langle R_{|\Lambda|=1} \exp(\pm i\theta) \middle| V_2 \exp(\pm 2i\theta) \middle| R_{|\Lambda|=1} \exp(\mp i\theta) \right\rangle$$

Spin-orbit coupling

$$\left\langle \pm 1, n, K \mp 1, \Sigma \middle| A L_z S_z \middle| \pm 1, n, K \mp 1, \Sigma \right\rangle = \pm A \Sigma$$

Appendix 2.2 Observed transitions of $\tilde{B}^2\Pi_i$ — $\tilde{X}^2\Sigma^+$ of C_4H.

$^2\Pi_{1/2}$-$^2\Sigma^+$ 24033.4321(58) cm^{-1} band of C_4H.

$^2\Pi_{1/2}$-$^2\Sigma^+$

J''	P_2(J'')	obs.-calc.	P_{21}(J''+1)+Q_2(J'')	obs.-calc.	Q_{21}(J'')+R_2(J''-1)	obs.-calc.	R_{21}(J'')	obs.-calc.
0.5			24040.651	0.004	24040.962	-0.003	24041.098	0.003
1.5			24040.465	-0.003	24041.098	-0.005	24041.855	-0.007
2.5			24040.269	-0.006	24041.216	-0.012	24042.312	0.021
3.5			24040.089	0.021	24041.355	-0.017	24042.695	-0.010
4.5							24043.094	-0.012
5.5							24043.486	-0.007

$^2\Pi_{3/2}$-$^2\Sigma^+$

J''	P_2(J'')	obs.-calc.	P_{21}(J''+1)+Q_2(J'')	obs.-calc.	Q_{21}(J'')+R_2(J''-1)	obs.-calc.	R_{21}(J'')	obs.-calc.
0.5							24026.755	-0.018
1.5			24025.410	0.016	24026.055	0.026	24027.212	0.031
2.5	24024.452	0.011	24025.168	-0.018	24026.132	-0.006	24027.589	0.021
3.5	24023.878	-0.038	24024.972	0.014	24026.181	-0.047	24027.944	0.008
4.5	24023.401	0.030	24024.724	0.013	24026.244	-0.054	24028.324	0.040
5.5			24024.452	0.009	24026.307	-0.042	24028.628	0.015
6.5			24024.185	0.028	24026.358	-0.021	24028.905	-0.017

Σ^+-Σ^+ 24047.6306(13) cm-1 band of C_4H.

N''	P(N'')	obs.-calc.	R(N'')	obs.calc.
0			24047.927	-0.004
1	24047.315	0.002	24048.212	-0.002
2	24046.979	0.001	24048.476	-0.003
3	24046.625	-0.001	24048.734	0.007
4	24046.256	-0.001	24048.955	-0.003
5	24045.874	0.004	24049.174	0.003
6	24045.464	-0.002	24049.367	0.000
7	24045.045	0.001	24049.539	-0.006
8	24044.600	-0.004		

$^2\Sigma^+_{1/2}-{}^2\Sigma^+$ 24214.7351(45) cm^{-1} band of C_4H.

N''	P(N'')				R(N'')			
	$P_2(N'')$	obs.-calc.	$P_1(N'')+P_{12}(N'')$	obs.-calc.	$R_{21}(N'')+R_2(N'')$	obs.-calc.	$R_1(N'')$	obs.-calc.
0					24214.952	0.013	24215.213	-0.009
1			24214.496	-0.017	24215.134	0.011	24215.568	-0.028
2	24213.988	0.003	24214.253	-0.018	24215.314	0.026	24216.007	0.055
3	24213.545	0.011	24213.988	-0.022	24215.437	0.002	24216.296	0.007
4	24213.093	0.028	24213.791	0.060	24215.568	0.006	24216.603	-0.002
5	24212.570	-0.007	24213.449	0.017	24215.656	-0.015	24216.907	0.003
6	24212.067	-0.002	24213.118	0.003	24215.755	-0.005	24217.248	0.065
7	24211.531	-0.012	24212.789	0.011	24215.833	0.003	24217.435	-0.009
8	24210.991	-0.006	24212.798	0.076				

$^2\Sigma^-_{1/2}-{}^2\Sigma^+$ 24230.6604(42) cm^{-1} band of C_4H.

N''	P(N'')				R(N'')			
	$O_{12}(N'')$	obs.-calc.	$Q_{21}(N'')+Q_2(N'')$	obs.-calc.	$Q_{12}(N'')+Q_1(N'')$	obs.-calc.	$S_{21}(N'')$	obs.-calc.
0					24230.725	-0.033	24231.402	0.025
1			24230.577	0.027	24230.826	-0.013	24231.908	0.034
2	24229.780	-0.023	24230.443	0.017	24230.906	-0.002	24232.308	-0.050
3	24229.245	-0.006	24230.325	0.037	24230.977	0.014	24232.816	-0.011
4	24228.682	-0.003	24230.080	-0.056	24231.033	0.029	24233.288	0.006
5	24228.112	0.007	24229.955	-0.016			24233.727	0.004
6	24227.506	-0.005	24229.780	-0.011			24234.158	0.007
7	24226.896	-0.007	24229.601	0.004			24234.560	-0.005
8	24226.282	0.000	24229.395	0.004			24234.961	-0.005
9	24225.641	-0.005	24229.168	-0.002			24235.355	0.003

$^2\Pi$-$^2\Sigma^+$ 24389.3394(58) cm^{-1} band of C_4H.

$^2\Pi_{1/2}$-$^2\Sigma^+$ band.

J''	P_2(J'')	obs.-calc.	P_{21}(J''+1)+Q_2(J'')	obs.-calc.	Q_{21}(J'')+R_2(J''-1)	obs.-calc.	R_{21}(J'')	obs.-calc.
0.5			24391.691	-0.001	24392.020	0.010	24392.504	0.036
1.5	24391.064	0.007	24391.528	0.012	24392.155	0.004	24392.910	-0.005
2.5	24390.572	0.009	24391.334	0.006	24392.288	0.008	24393.357	0.007
3.5	24390.055	-0.002	24391.121	-0.006	24392.403	0.006	24393.786	0.015
4.5	24389.546	0.007	24390.918	0.004	24392.504	0.003	24394.169	-0.011
5.5	24389.022	0.013	24390.669	-0.020	24392.561	-0.033	24394.571	-0.006
6.5			24390.438	-0.012	24392.653	-0.019		
7.5							24395.323	-0.006
8.5							24395.679	-0.006

$^2\Pi_{3/2}$-$^2\Sigma^+$ band.

J''	P_2(J'')	obs.-calc.	P_{21}(J''+1)+Q_2(J'')	obs.-calc.	Q_{21}(J'')+R_2(J''-1)	obs.-calc.	R_{21}(J'')	obs.-calc.
0.5							24387.064	-0.039
1.5			24386.119	-0.031	24386.759	-0.027	24387.476	-0.032
2.5			24385.897	-0.024	24386.853	-0.020	24387.885	-0.001
3.5			24385.676	0.012	24386.944	0.010	24388.283	0.047
4.5			24385.434	0.056	24387.019	0.053		
5.5								
6.5								

$^2\Pi$-$^2\Sigma^+$ **24417.2961(43) cm^{-1} band of C_4H.**

$^2\Pi_{1/2}$-$^2\Sigma^+$ **band.**

J''	$P_2(J'')$	obs.-calc.	$P_{21}(J''+1)+Q_2(J'')$	obs.-calc.	$Q_{21}(J'')+R_2(J''-1)$	obs.-calc.	$R_{21}(J'')$	obs.-calc.
0.5			24425.435	0.071	24425.767	0.086		
1.5	24424.807	0.078					24426.597	0.003
2.5			24425.026	0.019	24425.983	0.024	24427.046	0.011
3.5	24423.727	-0.009	24424.807	-0.007	24426.091	0.008	24427.468	0.001
4.5	24423.214	-0.012	24424.585	-0.025	24426.186	-0.011	24427.899	0.011
5.5	24422.681	-0.024	24424.398	0.001	24426.324	0.023		
6.5	24422.191	0.017	24424.145	-0.029	24426.375	-0.021		
7.5								
8.5								

$^2\Pi_{3/2}$-$^2\Sigma^+$ **band.**

J''	$P_2(J'')$	obs.-calc.	$P_{21}(J''+1)+Q_2(J'')$	obs.-calc.	$Q_{21}(J'')+R_2(J''-1)$	obs.-calc.	$R_{21}(J'')$	obs.-calc.
0.5							24409.361	-0.003
1.5			24408.416	0.005	24409.057	0.010	24409.786	-0.016
2.5			24408.207	-0.008	24409.158	-0.009	24410.220	-0.004
3.5	24406.940	-0.005	24408.009	0.007	24409.266	-0.005	24410.630	-0.001
4.5			24407.773	-0.001	24409.361	-0.000	24411.015	-0.007
5.5	24405.868	-0.001	24407.522	-0.008	24409.460	0.025		
6.5								

Σ^+-Σ^+ 24490.8059(61) cm^{-1} band of C_4H.

N''	P(N'')	obs.- calc	R(N'')	obs.-calc.
0			24491.105	-0.002
1	24490.499	0.011	24491.383	-0.010
2	24490.153	-0.002	24491.635	-0.027
3	24489.795	-0.011	24491.980	0.034
			.920	
4	24489.417	-0.024	24492.183	0.007
			.135	
5	24489.122	0.032	24492.395	-0.001
	.061		.356	
6	24488.689	0.004	24495.603	-0.001
	.642		.560	
7	24488.281	0.005	24495.793	-0.006
	.226		.738	
8	24487.846	-0.002		
	.790			
9	24487.402	-0.006		
	.335			

$^2\Sigma^+_{1/2}-^2\Sigma^+$ **24567.6845(27) cm^{-1} band of C$_4$H.**

N''	$P_2(N'')$	obs.-calc.	$P_1(N'')+P_{12}(N'')$	obs.-calc.	$R_{21}(N'')+R_2(N'')$	obs.-calc.	$R_1(N'')$	obs.-calc.
0					24567.883	0.000	24568.179	-0.003
1			24567.478	0.012	24568.066	0.004	24568.546	-0.017
2	24566.947	0.019	24567.228	-0.002	24568.222	-0.002	24568.933	0.008
3	24566.471	-0.003	24566.947	-0.030	24568.371	0.004	24569.271	0.002
4	24566.002	0.002	24566.712	0.008	24568.491	-0.000	24569.586	-0.009
5	24565.512	0.004	24566.412	-0.001	24568.598	0.001	24569.908	0.007
6	24565.003	0.005	24566.102	-0.001	24568.684	-0.001	24570.193	0.004
7	24564.466	-0.003	24565.776	0.000			24570.408	-0.051
8	24563.913	-0.008	24565.432	0.004			24570.702	-0.008
9			24565.003	-0.060				

$^2\Sigma^+_{1/2}-^2\Sigma^+$ **24576.4316(24) cm^{-1} band of C$_4$H.**

N''	$P_2(N'')$	obs.-calc.	$P_1(N'')+P_{12}(N'')$	obs.-calc.	$R_{21}(N'')+R_2(N'')$	obs.-calc.	$R_1(N'')$	obs.-calc.
0					24576.621	-0.003	24576.946	-0.000
1			24576.215	-0.008	24576.792	-0.006	24577.339	0.003
2	24575.676	0.007	24575.995	0.000	24576.949	-0.005	24577.703	-0.005
3	24575.212	0.003	24575.753	0.003	24577.091	-0.001	24578.043	-0.019
4	24574.734	0.004	24575.489	0.002	24577.207	-0.005	24578.404	0.005
5	24574.247	0.013	24575.212	0.005	24577.307	-0.008	24578.716	-0.002
6	24573.715	-0.004	24574.929	0.021			24579.009	-0.010
7	24573.196	0.010	24574.597	0.005			24579.299	-0.003
8			24574.247	-0.011				
9			24573.917	0.011				

$^2\Sigma^-_{1/2}-{}^2\Sigma^+$ **24580.0336(20) cm^{-1} band of C$_4$H.**

N''	O_{12}(N'')	obs.-calc.	Q_{21}(N'')+Q_2(N'')	obs.-calc.	Q_{12}(N'')+Q_1(N'')	obs.-calc.	S_{21}(N'')	obs.-calc.
0					24580.133	0.005	24580.750	-0.009
1			24579.931	0.004	24580.215	0.007	24581.262	-0.000
2	24579.174	0.001	24579.800	-0.008	24580.271	-0.006	24581.751	-0.001
3	24578.626	0.007	24579.678	0.002	24580.329	-0.002	24582.236	0.007
4	24578.043	-0.010	24579.532	0.001			24582.696	0.003
5	24577.477	0.004	24579.378	0.005			24583.142	-0.003
6			24579.174	-0.028			24583.591	0.007
7			24579.009	-0.011			24584.006	-0.004
8			24578.812	-0.012				
9			24578.626	0.012				

$^2\Sigma^-_{1/2}-{}^2\Sigma^+$ **24589.6256(24) cm^{-1} band of C$_4$H.**

N''	O_{12}(N'')	obs.-calc.	Q_{21}(N'')+Q_2(N'')	obs.-calc.	Q_{12}(N'')+Q_1(N'')	obs.-calc.	S_{21}(N'')	obs.-calc.
0					24589.747	0.002	24590.298	-0.008
1			24589.498	0.002	24589.843	-0.009	24590.787	-0.001
2	24588.791	0.000	24589.361	0.007	24589.957	0.009	24591.260	0.002
3	24588.259	0.007	24589.201	0.000	24590.030	-0.003	24591.705	0.013
4	24587.731	0.000	24589.042	0.005			24592.161	-0.005
5	24587.172	0.005	24588.862	0.000				
6			24588.686	0.011				
7								
8								
9								

$^2\Sigma^-_{1/2}-^2\Sigma^+$ 24615.3748(44) cm^{-1} band of C_4H.

N''	$O_{12}(N'')$	obs.-calc.	$Q_{21}(N'')+Q_2(N'')$	obs.-calc.	$Q_{12}(N'')+Q_1(N'')$	obs.-calc.	$S_{21}(N'')$	obs.-calc.
0					24615.432	-0.019	24616.141	0.006
1			24615.285	-0.001	24615.510	-0.002	24616.660	0.005
2	24614.476	-0.020	24615.191	0.007	24615.557	-0.003	24617.176	0.013
3	24613.936	0.013	24615.083	0.013	24615.605	0.009	24617.638	-0.020
4	24613.334	-0.003	24614.953	0.011			24618.145	0.009
5	24612.743	0.006	24614.774	-0.026				
6	24612.131	0.007	24614.647	0.002				
7	24611.492	-0.006						
8								
9								

$^2\Sigma^-_{1/2}-^2\Sigma^+$ 24837.9810(60) cm^{-1} band of C_4H.

N''	$O_{12}(N'')$	obs.-calc.	$Q_{21}(N'')+Q_2(N'')$	obs.-calc.	$Q_{12}(N'')+Q_1(N'')$	obs.-calc.	$S_{21}(N'')$	obs.-calc.
0					24838.054	-0.007	24838.716	-0.012
1			24837.856	-0.011	24838.161	0.036	24839.229	-0.009
2	24837.103	-0.004	24837.769	-0.008	24838.228	0.055	24839.755	0.022
3	24836.532	-0.004	24837.648	-0.004			24840.252	0.039
4	24835.938	-0.011	24837.528	0.016			24840.642	-0.036
5	24835.347	-0.002	24837.408	0.051			24841.117	-0.010
6							24841.559	-0.003
7							24841.988	0.008
8								
9								

Σ^+-Σ^+ 24847.138(40) cm^{-1} band of C_4H. heavily perturbed

N''	P(N'')	obs.- calc	R(N'')	obs.-calc.
0			24847.478	
1	24846.813		24847.717	
			.554	
2	24846.516		24848.053	
			7.814	
3	24846.120		24848.337	
	5.962		053	
4	24845.826		24848.229	
	588			
5	24845.494		24848.420	
	194			
6	24844.746			
7	24844.316			
8	24843.928			

$^2\Sigma^+_{1/2} - {^2\Sigma^+}$ **24849.9900(31) cm^{-1} band of C$_4$H.**

N''	$P_2(N'')$	obs.-calc.	$P_1(N'')+P_{12}(N'')$	obs.-calc.	$R_{21}(N'')+R_2(N'')$	obs.-calc.	$R_1(N'')$	obs.-calc.
0					24850.153	-0.002	24850.573	-0.012
1			24849.209	0.009	24850.314	0.006	24851.044	0.016
2	24849.848	0.031	24848.732	0.014	24850.438	-0.013	24851.456	-0.005
3	24849.607	-0.027	24848.229	0.002	24850.574	-0.012	24851.888	0.004
4	24849.446	0.004	24847.717	-0.010	24850.723	0.004	24852.306	0.008
5	24849.234	-0.006	24847.222	0.005			24852.711	0.009
6	24849.036	0.007					24853.099	0.002
7	24848.809	0.001					24853.479	-0.002
8	24848.576	-0.000					24853.849	-0.008

Σ^+-Σ^+ **24872.2176(88) cm^{-1} band of C$_4$H.** (cm^{-1})

N''	P(N'')	obs.-calc.	R(N'')	obs.calc.
0			24872.513	-0.007
1	24871.950	0.050	24872.797	-0.010
2	24871.566	-0.002	24873.104	0.025
3	24871.199	-0.021	24873.344	0.007
4	24870.882	0.022	24873.563	-0.016
5	24870.084	-0.003		

${}^2\Sigma^+_{1/2}-{}^2\Sigma^+$ 24938.1226(29) cm^{-1} band of C_4H.

N''	$P_2(N'')$	obs.-calc.	$P_1(N'')+P_{12}(N'')$	obs.-calc.	$R_{21}(N'')+R_2(N'')$	obs.-calc.	$R_1(N'')$	obs.-calc.
0					??		24938.571	-0.009
1			24937.884	0.000	24938.571	0.017	24938.925	-0.020
2	24937.392	-0.000	24937.630	0.001	24938.740	-0.006	24939.298	0.005
3	24936.970	0.004	24937.354	-0.004	24938.925	0.002	24939.624	-0.003
4	24936.524	0.001	24937.088	0.015	24939.086	0.002	24939.936	-0.008
5	24936.062	-0.003	24936.777	0.006			24940.259	0.012
6	24935.581	-0.007	24936.455	0.001			24940.528	-0.006

Appendix 2.3 Observed transitions of $\widetilde{B}^2\Pi_i - \widetilde{X}^2\Sigma^+$ of C_4D.

Σ^+-Σ^+ 24099.1908(20) cm^{-1} band of C_4D.

N''	P(N'')	obs.-calc.	R(N'')	obs.-calc.
0			24099.473	0.002
1	24098.888	-0.008	24099.742	0.005
2	24098.582	-0.006	24099.996	0.007
3	24098.266	0.002	24100.224	-0.003
4	24097.930	0.004	24100.452	0.002
5	24097.574	0.000	24100.653	-0.005
6	24096.822	-0.007	24100.862	0.009
7	24096.434	0.001	24101.037	0.004
8	24096.018	-0.006		

$^2\Pi$-$^2\Sigma^+$ 24105.3088(25) cm^{-1} band of C$_4$D.

$^2\Pi_{1/2}$-$^2\Sigma^+$

J''	P$_2$(J'')	obs.-calc.	P$_{21}$(J''+1)+Q$_2$(J'')	obs.-calc.	Q$_{21}$(J'')+R$_2$(J''-1)	obs.-calc.	R$_{21}$(J'')	obs.-calc.
0.5			24110.653	0.003	24110.947	0.002	24111.385	0.014
1.5	24110.064	0.002	24110.488	0.001	24111.076	0.000	24111.796	0.011
2.5	24109.595	-0.008	24110.318	0.005	24111.202	0.006	24112.176	-0.013
3.5	24109.132	-0.002	24110.116	-0.011	24111.292	-0.013	24112.579	-0.004
4.5			24109.927	-0.003	24111.385	-0.020	24112.987	0.023
5.5			24109.726	0.003	24111.565	0.073	24113.343	0.008
6.5			24109.498	-0.007			24113.702	0.006
7.5			24109.268	-0.008			24114.052	0.008
8.5			24109.036	-0.000				

$^2\Pi_{3/2}$-$^2\Sigma^+$

J''	P$_{12}$(J'')	obs.-calc.	P$_1$(J''+1)+Q$_{12}$(J'')	obs.-calc.	Q$_1$(J'')+R$_{12}$(J''-1)	obs.-calc.	R$_1$(J'')	obs.-calc.
0.5								
1.5								
2.5					24099.975	-0.006	24100.862	-0.003
3.5					24100.047	-0.001	24101.244	0.018
4.5			24098.802	0.000	24100.107	0.010	24101.581	0.011
5.5			24098.582	0.007			24101.879	-0.018
6.5			24098.326	-0.004			24102.208	0.002
7.5								
8.5			24097.779	-0.006				

$^2\Sigma^+_{1/2}-^2\Sigma^+$ 24282.5454(40) cm^{-1} band of C$_4$D.

N''	P$_2$(N'')	obs.-calc.	P$_1$(N'')+P$_{12}$(N'')	obs.-calc.	R$_{21}$(N'')+R$_2$(N'')	obs.-calc.	R$_1$(N'')	obs.-calc.
0					24282.760	0.013	24282.938	-0.020
1			24282.330	0.011	24282.938	-0.015	24283.321	0.032
2	24281.872	-0.000	24282.055	-0.020	24283.118	-0.016	24283.624	0.020
3			24281.872	0.055	24283.321	0.023	24283.891	0.012
4	24281.053	-0.017	24281.563	0.021	24283.460	0.013	24284.187	0.000
5	24280.625	-0.020	24281.244	-0.009	24283.624	0.043	24284.456	0.001
6	24280.207	0.001	24280.943	-0.004	24283.704	0.005	24284.710	0.003
7	24279.761	0.012	24280.625	0.001	24283.793	-0.008	24284.944	-0.001
8	24279.277	-0.001	24280.286	-0.004				
9	24278.788	-0.003	24279.938	0.001				

${}^2\Sigma^-_{1/2}-{}^2\Sigma^+$ 24295.5206(35) cm^{-1} band of C_4D.

N''	$O_{12}(N'')$	obs.-calc.	$Q_{21}(N'')+Q_2(N'')$	obs.-calc.	$Q_{12}(N'')+Q_1(N'')$	obs.-calc.	$S_{21}(N'')$	obs.-calc.
0					head		24296.232	-0.002
1			24295.439	-0.003			24296.717	-0.004
2	24294.707	0.004	24295.356	0.005			24297.205	0.008
3	24294.197	0.028	24295.257	0.008			24297.657	-0.004
4	24293.605	-0.019	24295.147	0.012			24298.109	-0.004
5	24293.061	-0.007	24295.011	0.001			24298.546	-0.009
6	24292.495	-0.005	24294.877	0.004			24298.973	-0.011
7	24291.918	-0.002	24294.707	-0.019			24299.415	0.013
8	24291.333	0.004	24294.563	-0.002			24299.789	-0.019
9	24290.727	0.001					24300.227	0.024

${}^2\Pi$-${}^2\Sigma^+$ 24361.7048(36) cm^{-1} band of C_4D.

${}^2\Pi_{1/2}$-${}^2\Sigma^+$

J''	$P_2(J'')$	obs.-calc.	$P_{21}(J''+1)+Q_2(J'')$	obs.-calc.	$Q_{21}(J'')+R_2(J''-1)$	obs.-calc.	$R_{21}(J'')$	obs.-calc.
0.5			24368.113	0.004	24368.402	-0.002	24368.847	0.017
1.5	24367.522	0.002	24367.954	0.008	24368.532	-0.003	24369.265	0.021
2.5	24367.057	-0.005	24367.787	0.015	24368.671	0.016	24369.645	-0.003
3.5	24366.614	0.021	24367.583	-0.003	24368.758	-0.006	24370.041	-0.000
4.5	24366.103	-0.010	24367.386	-0.004	24368.847	-0.016	24370.409	-0.015
5.5	24365.611	-0.011	24367.170	-0.013	24368.916	-0.034		
6.5	24365.106	-0.014						
7.5								
8.5								

$^2\Pi_{3/2}$-$^2\Sigma^+$

J''	$P_2(J'')$	obs.-calc.	$P_{21}(J''+1)+Q_2(J'')$	obs.-calc.	$Q_{21}(J'')+R_2(J''-1)$	obs.-calc.	$R_{21}(J'')$	obs.-calc.
0.5							24355.407	-0.015
1.5					24355.125	-0.003	24355.834	0.011
2.5	?		24354.521	-0.017	?		24356.168	-0.038
3.5	24353.144	-0.028	24354.350	0.001	24355.271	-0.051	24356.592	0.019
4.5	?		24354.098	-0.046	24355.407	0.013	24356.933	0.010
5.5	24352.166	0.012	24353.936	0.015	24355.458	0.008	24357.270	0.014
6.5	24351.610	-0.010	24353.683	0.001	24355.495	0.006	24357.585	0.012
7.5			24353.426	-0.000			24357.665	-0.201
8.5			24353.144	-0.010			24358.138	-0.019
9.5							24358.523	0.099

Σ^+-Σ^+ 24463.2403(15) cm^{-1} band of C_4D.

N''	P(N'')	obs.- calc	R(N'')	obs.-calc.
0			24463.528	0.006
1	24462.961	0.016	24463.789	-0.003
2	24462.641	0.002	24464.047	-0.002
3	24462.321	0.002	24464.295	0.001
4	24461.988	0.001	24464.519	-0.007
5	24461.643	0.001	24464.744	-0.001
6	24461.282	-0.003	24464.953	-0.000
7	24460.917	0.002	24465.152	0.004
8	24460.528	-0.005		
9	24460.142	0.004		

$^2\Sigma^+_{1/2}-{}^2\Sigma^+$ 24480.5447(35) cm^{-1} band of C_4D.

N''	P$_2$(N'')	obs.-calc.	P$_1$(N'')+P$_{12}$(N'')	obs.-calc.	R$_{21}$(N'')+R$_2$(N'')	obs.-calc.	R$_1$(N'')	obs.-calc.
0					24480.733	0.006	24481.0345	0.023
1			24480.363	0.018	24480.872	-0.018		
2	24479.856	0.015	24480.142	0.015	24481.034	-0.002	24481.676	-0.025
3	24479.414	-0.002			24481.164	0.000	24482.002	-0.017
4	24478.982	0.009	24479.612	-0.027	24481.293	0.019	24482.313	-0.006
5	24478.514	0.003	24479.362	-0.006	24481.365	-0.001	24482.597	-0.004
6	24478.098	0.022			24481.429	-0.011	24482.859	-0.006
7	24477.527	-0.008	24478.771	-0.001			24483.120	0.008
8	24477.010	-0.010	24478.445	-0.002			24483.339	-0.002
9	24476.481	-0.005					24483.556	0.005
10	24475.930	-0.006						

$^2\Sigma^-_{1/2}-{}^2\Sigma^+$ 24489.1885(98) cm^{-1} band of C_4D.

N''	O$_{12}$(N'')	obs.-calc.	Q$_{21}$(N'')+Q$_2$(N'')	obs.-calc.	Q$_{12}$(N'')+Q$_1$(N'')	obs.-calc.	S$_{21}$(N'')	obs.-calc.
0							24489.867	0.015
1					24489.324	-0.047	24490.318	0.001
2			24489.007	0.039	24489.437	-0.010	24490.784	0.012
3	24487.857	-0.039	24488.855	0.011	24489.516	0.001	24491.209	-0.010
4	24487.338	0.004	24488.721	0.009	24489.585	0.012	24491.636	-0.020
5	24486.883	0.021	24488.556	-0.012				
6	24486.342	0.011	24488.418	0.002				
7								
8								
9								

$^2\Sigma^+_{1/2}-^2\Sigma^+$ **24550.6013(19) cm^{-1} band of C$_4$D.**

N''	$P_2(N'')$	obs.-calc.	$P_1(N'')+P_{12}(N'')$	obs.-calc.	$R_{21}(N'')+R_2(N'')$	obs.-calc.	$R_1(N'')$	obs.-calc.
0					24550.767	0.001		
1			24550.415	-0.011	24550.926	0.005		
2	24549.888	0.007	24550.206	-0.035	24551.067	0.002	24551.904	0.005
3	24549.442	-0.004	?		24551.194	-0.004	24552.276	0.005
4	24548.997	-0.003	24549.846	0.009	24551.267	-0.050		
5	24548.534	-0.011	24549.621	0.000	24551.437	0.004	24552.981	-0.003
6					24551.536	0.001	24553.326	0.001
7	24547.603	0.002	24549.151	-0.004	24551.629	0.002		
8	24547.120	0.005	24548.904	-0.003				
9	24546.613	-0.004						

$^2\Sigma^+_{1/2}-^2\Sigma^+$ **24583.9107(55) cm^{-1} band of C$_4$D.**

N''	$P_2(N'')$	obs.-calc.	$P_1(N'')+P_{12}(N'')$	obs.-calc.	$R_{21}(N'')+R_2(N'')$	obs.-calc.	$R_1(N'')$	obs.-calc.
0					24584.028	-0.030	24584.431	-0.025
1			24583.862	0.112	24584.209	0.018	24584.825	-0.031
2	24583.162	-0.011	24583.591	0.017			24585.252	0.011
3	24582.722	0.006	24583.364	-0.019	24584.431	0.017	24585.629	0.018
4			24583.188	0.009	24584.521	0.017	24585.967	-0.000
5	24581.773	0.012	24582.973	0.013	24584.580	0.000	24586.322	0.012
6	24581.264	0.002	24582.722	-0.005	24584.630	-0.011	24586.621	-0.016
7	24580.734	-0.015	24582.501	0.021			24586.930	-0.021
8			24582.231	0.012				

Σ^+-Σ^+ 24591.763(11) cm^{-1} band of C_4D.

N''	P(N'')	obs.- calc	R(N'')	obs.-calc.
0			24592.048	0.004
1	24591.484	0.016	24592.331	0.020
2	24591.165	0.004	24592.654	0.040
			.557	
3	24590.859	0.021	24592.822	-0.024
			.741	
4	24590.582	0.014	24593.064	-0.018
	.452		2.963	
5	24590.170	-0.045	24593.285	-0.019
	.049		.166	
6	24589.817	-0.027	24593.485	-0.026
	.710		.352	
7	24589.454	-0.021	24593. 686	0.057
	.333			
8	24589.260	-0.033		
	8.923			
9	24588.658	0.037		

Center frequencies of spin splitting were used in least square fit.

Σ^+-Σ^+ 24705.863(10) cm^{-1} band of C_4D.

N''	P(N'')	obs.- calc	R(N'')	obs.-calc.
0			24706.152	0.010
1	24705.555	-0.013	24706.433	-0.000
			.380	
2	24705.275	0.016	24706.727	0.027
			.637	
3	24704.972	0.006	24706.887	-0.002
	.906			
4	24704.656	0.019	24707.078	-0.029
	.566			
5	24704.226	-0.011	24707.283	-0.027
6	24703.830	-0.037	24707.533	0.035
7	24703.450	-0.030		
8	24703.114	0.036		

Σ^+-Σ^+ 24799.9620(15) cm^{-1} band of C_4D.

N''	P(N'')	obs.- calc	R(N'')	obs.-calc.
0			24800.235	-0.009
1	24799.658	-0.009	24800.507	-0.007
2	24799.352	-0.008	24800.783	-0.004
			.751	
3	24799.054	-0.002	24801.039	0.006
	.024		.004	
4	24798.727	-0.004	24801.281	0.032
	.682			
5	24798.387	0.004	24801.449	-0.019
	.349			
6	24798.049	0.041	24801.878	0.008
7	24797.653	-0.015	24802.040	-0.013
	3592			
8	24796.870	0.009		
9	24796.445	-0.010		

$^2\Sigma^+_{1/2} - ^2\Sigma^+$ 24962.9928(45) cm^{-1} band of C_4D.

N''	$P_2(N'')$	obs.-calc.	$P_1(N'')+P_{12}(N'')$	obs.-calc.	$R_{21}(N'')+R_2(N'')$	obs.-calc.	$R_1(N'')$	obs.-calc.
0					24963.162	0.025	24963.532	-0.035
1			??		24963.284	0.010	24964.003	0.010
2	24962.256	0.004	24962.667	-0.002	24963.404	0.000	24964.403	-0.007
3	24961.803	0.004	24962.532	0.012	24963.532	0.005	24964.816	-0.006
4	24961.337	-0.004	24962.345	-0.004	24963.629	-0.015	24965.240	0.014
5	24960.875	0.001	24962.169	-0.002			24965.619	-0.005
6			24961.998	0.011			24966.013	-0.001
7								
8								

Σ^+-Σ^+ 24992.3860(38) cm^{-1} band of C_4D.

N''	P(N'')	obs.- calc	R(N'')	obs.-calc.
0			24992.672	0.004
1	24992.083	-0.010	24992.945	0.007
2	24991.789	0.005	24993.201	0.005
3	24991.462	-0.003	24993.449	0.009
4	24991.123	-0.011		
5	24990.779	-0.010	24993.911	0.017
6			24994.109	0.008
7	24990.052	-0.011	24994.304	0.008
8	24989.669	-0.013		
9	24989.281	-0.006		

Chapter 3

Dispersed Fluorescence Spectra of C_4H and C_4D from $\tilde{B}^2\Pi_i$

Abstract

Dispersed fluorescence (DF) spectra of C_4H and C_4D from $\tilde{B}^2\Pi_i$ to the ground state $\tilde{X}^2\Sigma^+$ or low lying $\tilde{A}^2\Pi_i$ were measured in order to clarify vibronic structures of low energy regions of C_4H and C_4D. We have measured DF spectra from several vibronic states of $\tilde{B}^2\Pi_i$ with relatively strong intensities. Based on dependence of the signal intensities in the DF spectra on vibrational modes of the excited state, we have assigned two bending vibrational modes, which belong to different electronic states. One is a progression of the lowest bending mode, $2\nu_7$ and $4\nu_7$ (CCC bending) of $\tilde{X}^2\Sigma^+$ with frequency of ω_7=118 cm^{-1} and 114 cm^{-1} for C_4H and C_4D respectively. The other is the second lowest bending mode (CCC bending), ν_6 and $3\nu_6$ of $\tilde{A}^2\Pi_i$ with frequency of 206 cm^{-1} and 205 cm^{-1} for C_4H and C_4D, respectively. From the observed vibronic states we have also estimated the term value of the $\tilde{A}^2\Pi_i$ strate as 230 cm^{-1} for C_4H and 217 cm^{-1} for C_4D. The term value of C_4H $\tilde{A}^2\Pi_i$ is in good agreement with that determined from photoelectron spectroscopy of C_4H^- , 226 cm^{-1} (T. Taylor and D.M. Neumark, private communication), while is slightly larger compared with the most recent *ab initio* prediction, 100 ± 50 cm^{-1} (*J. Chem. Phys.* **103**, 7820 (1995)).

3.1 Introduction

C_4H has the low lying first excited state $\tilde{A}^2\Pi_i$ about 0-1000 cm^{-1} above the ground state $\tilde{X}^2\Sigma^+$. The term energy of $\tilde{A}^2\Pi_i$ state has not been determined experimentally until now because it has never been observed directly. Such situation of electronic structure like C_4H is quite limited. For linear unstable molecules including five atoms, spectroscopic studies in electronic excited state is few. As discussed in section 2.7.4, a strong vibronic interaction between $\tilde{X}^2\Sigma^+$ and $\tilde{A}^2\Pi_i$ is expected. Thus the effect of the vibronic interaction to the energy structures of $\tilde{X}^2\Sigma^+$ and $\tilde{A}^2\Pi_i$ are of great interest from a spectroscopic point of view. It is also considered that $\tilde{A}^2\Pi_i$ contributes to unique behaviors of C_4H in astronomical chemistry, in which C_4H is exceptionally vibrationally excited in a carbon star envelope[1]. Thus where the $\tilde{A}^2\Pi_i$ state lies is also of great interest from the spectroscopic point of view.

Experimental investigations of vibronic states of $\tilde{X}^2\Sigma^+$ are quite limited. In 1987, Yamamato *et al.* observed rotational spectra of vibrationally excited state of $\tilde{X}^2\Sigma^+$, $\nu_7(\Pi)$ and $2\nu_7$ (Σ,Δ), and suggested that the large spin splitting constant $(A \approx -3\,\mathrm{cm}^{-1})$ in the $\nu_7(\Pi)$ state is caused by a large vibronic interaction between $\tilde{X}^2\Sigma^+$ and $\tilde{A}^2\Pi_i$ [1]. In 1990 Graham's group reported IR absorption spectra in Ar matrix, and determined vibrational frequencies as ω_1=3307.4 cm^{-1}, ω_2=2083.9 cm^{-1} and ω_3=2060.6 cm^{-1}[2]. But results other than mentioned above in the gas phase experiment has never been published until now.

A number of theoretical studies have been performed, particularly on the excitation energy of the $\tilde{A}^2\Pi_i$ state. In 1994 Kolbuszewski[3] calculated the term value of $\tilde{A}^2\Pi_i$ as 0.01eV (81 cm^{-1}). There were four publications in 1995, with higher calculation levels, where term value of $\tilde{A}^2\Pi_i$ was predicted to 565 cm^{-1} by Sobolowski and Adamowicz (CASPT2/DZVP)[4], 70 cm^{-1} by Woon (RCCSD(T)/cc-pVQZ, est CBS limit) [5] and 100 ± 50 cm^{-1} by McCarhty *et al.*(RSCCSD(T)/cc-pVQZ)[6], however Natterer and Koch[7] were confident that the ground state is not $^2\Sigma^+$ but also $^2\Pi$, where the energy gap between $^2\Pi$ and $^2\Sigma^+$ is calculated to 244-1154 cm^{-1} by ACPF/[432/321]ANO to CCSDT(T)/[432/321]ANO. Although the order of $^2\Pi$ and $^2\Sigma^+$

is very close and seems to be sensitive, we believe that the ground state is $^2\Sigma^+$ because the lowest vibronic state is $^2\Sigma^+$.

In this chapter we present the first direct observation of vibronic structures of the ground state $\tilde{X}^2\Sigma^+$ and the first excited state $\tilde{A}^2\Pi_i$ of C_4H and C_4D by DF spectra from several vibronic states of $\tilde{B}^2\Pi_i$. Vibrational assignment was made for the lower excitation region from the $\tilde{X}^2\Sigma^+$ v=0. We estimated the origin of $\tilde{A}^2\Pi_i$ to be about 230 cm^{-1}, which was comparable with that obtained from photoelectron spectroscopy of C_4H^-, 226 cm^{-1} (private communucation from T.Taylor and D.M. Neumark).

3.2 Experimental

As for production of C_4H and C_4D, and the excitation laser system are the same as those of chapter 2, experimental procedures for the DF spectra is described here.

Dispersed fluorescence spectra were measured using a 50 cm monochromater (SPEX500M, 500nm Braze, 1200 Grooves/mm) and photomultiplier (Hamamatsu R928). The monochromater scanning was synchronized with laser pulses and was typically operated with a 0.04 nm /step. The spectral resolution was about 20 cm^{-1} at 400 nm, and the accuracy of relative frequency was estimated to be $< 3cm^{-1}$ by referring to the Hg atomic lines. In order to get a good signal to noise ratio it was necessary to accumulate 50-80 shots of laser pulses at a point, since the fluorescence signal of C_4H is not so strong and has a short life time, 10-20 ns. When an excitation line overlaps with other species such as C_3, the signal were integrated with a dual gate set up, where one gate is set at 0-40 ns and the other at 50-90 ns, and peaks which have long lifetime, > 50 ns were excluded in the analysis.

3.3 Results and Discussions

3.3.1 Observed DF spectra

We measured DF spectra from several typical vibronic states of $\tilde{B}^2\Pi_i$, one is $3\nu_5(\Sigma^+)$ (CCH bending) which is affected by a large Renner-Teller effect, and the others are ν_6 ($\Sigma^{(\pm)}$) and an unassigned other $\Sigma^{(\pm)}$ vibronic states with weak Renner-Teller effects. The characteristic feature common to all of the DF spectra is that the sharp signals were observed in the lower energy region <1000 cm^{-1}. On the other hand, above 1000 cm^{-1} continuous fluorescence was observed, and it is impossible to distinguish each bands. For example, Fig.3.1 (a) and (b) show DF spectra from $\tilde{B}^2\Pi_i$ $\nu_6({}^2\Sigma^{(+)}_{1/2})$ and $\nu_6({}^2\Sigma^{(-)}_{1/2})$ of C_4H in a wide relative energy region from the vibronic ground state $\tilde{X}^2\Sigma^+(v = 0)$, 0-3500 cm^{-1}. This drastic change from sparse (<1000 cm^{-1}) to complicated (>1000 cm^{-1}) structure is due to the unique structure of the quantum states in the vicinity of the low energy region of C_4H, that is there are "three" bending vibrational modes of which "two" closely lying electronic states. Therefore we will concentrate to the region of 0-1000 cm^{-1} for vibrational analysis.

3.3.2 Vibronic assignments of DF spectra and vibronic structure of the $\tilde{X}^2\Sigma^+$ and $\tilde{A}^2\Pi_i$ states

3.3.2(a) Assignment to vibrational states of ν_7(CCC) bending mode of $\tilde{X}^2\Sigma^+$

Fig.3.2 compares the DF spectra from several vibronic states of C_4H in $\tilde{B}^2\Pi_i$: (a) $3\nu_5({}^2\Sigma^+)$, (b) ν_6 (${}^2\Sigma^{(+)}_{1/2}$), (c) ν_6 (${}^2\Sigma^{(-)}_{1/2}$), and (d) an unassigned band at 24567.683 cm^{-1} (${}^2\Sigma^{(+)}_{1/2}$) in the relative energy of 0 - 2000 cm^{-1}. In Fig.3.2(a) a progression starting from the vibronic ground state was clearly observed, that is 0, 234, 474 cm^{-1} with the intervals of 234 cm^{-1} and 240 cm^{-1}. We assigned this progression to that of ν_7 CCC bending mode of the ground state, $2\nu_7({}^2\Sigma^+)$ and $4\nu_7({}^2\Sigma^+)$. The vibrational frequency was estimated to be ω_7=118 cm^{-1}. Similarly, for C_4D the DF spectra from $\tilde{B}^2\Pi_i$ were shown in Fig.3.3, (a) $3\nu_5({}^2\Sigma^+)$, (b) ν_6 (${}^2\Sigma^{(-)}_{1/2}$), and (c) an unassigned band at 24550.601

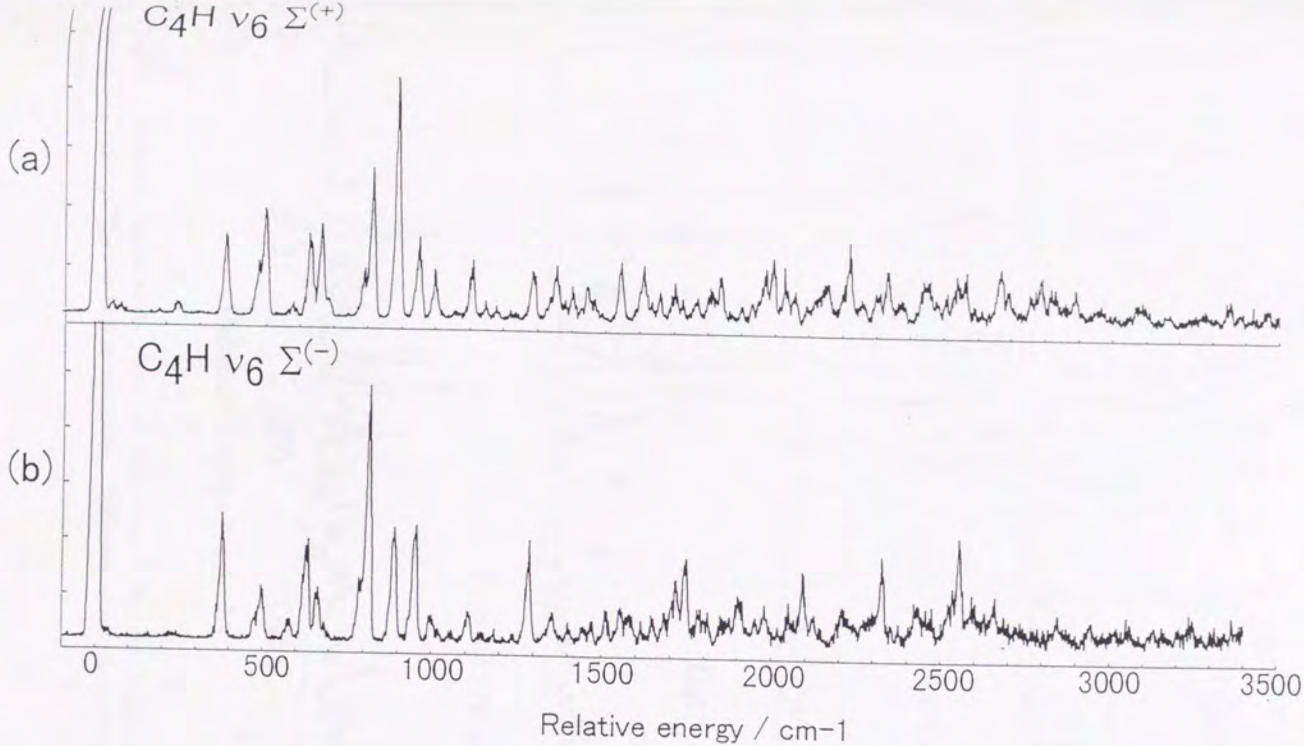

Fig.3.1 Dispersed fluorescence spectra of C_4H from $\tilde{B}^2\Pi_i$, (a) $\nu_6(^2\Sigma^{(+)}_{1/2})$ and (b) $\nu_6(^2\Sigma^{(-)}_{1/2})$ in the relative energy 0-3500 cm^{-1}.

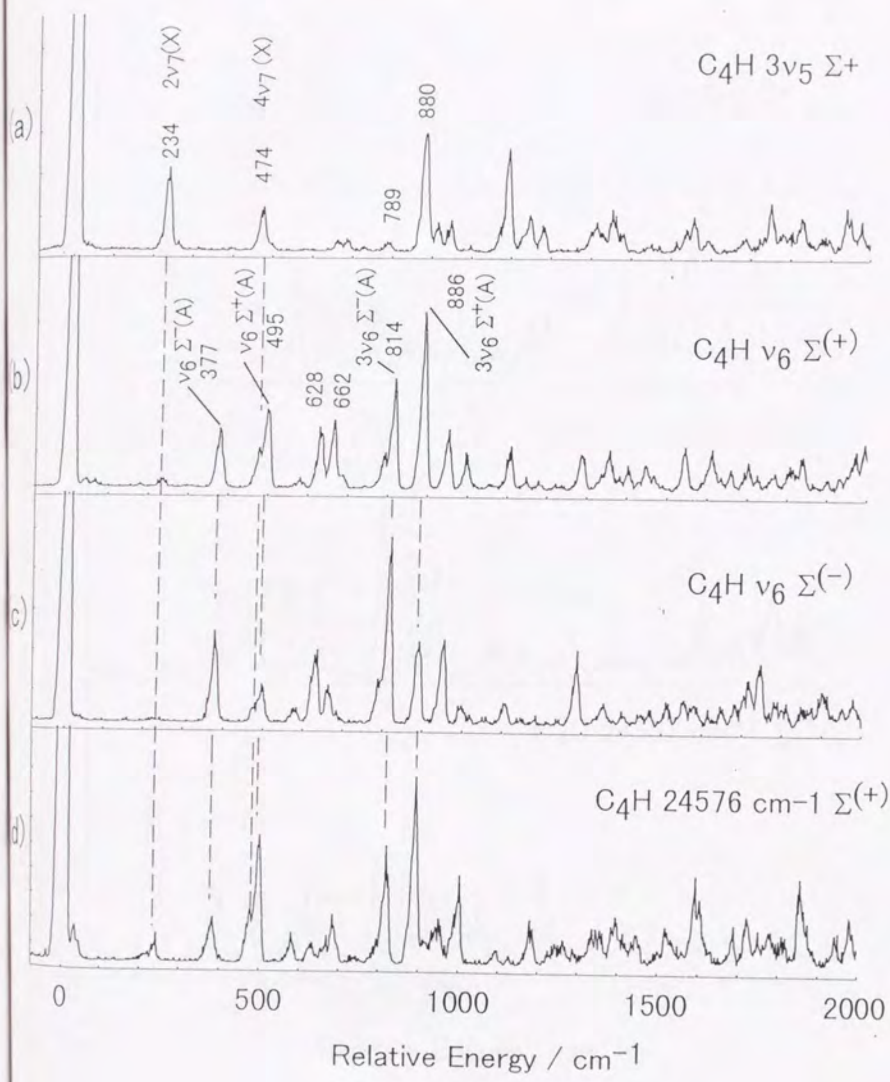

Fig.3.2 Dispersed fluorescence spectra of C_4H from $\tilde{B}^2\Pi_i$, (a) $3\nu_5(^2\Sigma^+)$, (b) $\nu_6(^2\Sigma^{(+)}_{1/2})$, (c) $\nu_6(^2\Sigma^{(-)}_{1/2})$ and (d) an unassigned $^2\Sigma^{(+)}_{1/2}$ state, in the relative energy 0-3500 cm^{-1}.

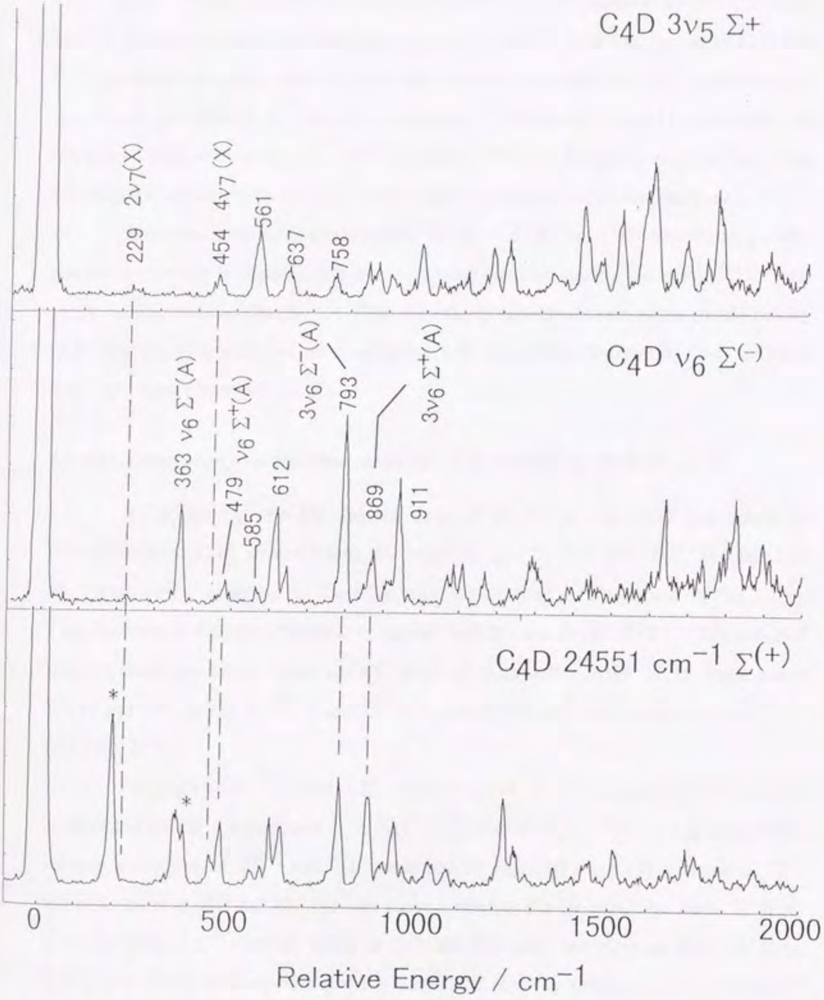

Fig.3.3 Dispersed fluorescence spectra of C_4D from $\tilde{B}^2\Pi_i$, (a) $3\nu_5(^2\Sigma^+)$, (b) $\nu_6(^2\Sigma^{(-)}_{1/2})$ and (c) an unassigned $^2\Sigma^{(-)}_{1/2}$, in the relative energy 0-3500 cm^{-1}.

cm^{-1} ($^2\Sigma^{(+)}_{1/2}$). Peaks appeared at 229 and 454 cm^{-1} are also assigned to $2\nu_7(^2\Sigma^+)$ and $4\nu_7(^2\Sigma^+)$ with the vibrational frequency of ω_7=114 cm^{-1}. The frequencies of C_4H and C_4D are almost the same, which indicate that ν_7 mode is actually the CCC bending mode, and is not so affected by isotope substitution. Yamamoto *et al.*[1] predicted the vibrational frequency of ν_7 in $\widetilde{X}^2\Sigma^+$ to about 131 cm^{-1} from the data on the *l*-type doubling q constant of the $2\nu_7(^2\Sigma^+)$ state, which is slightly larger than our result.

Since the present DF spectra show $\widetilde{B}^2\Pi_i \rightarrow \widetilde{X}^2\Sigma^+$ or $\widetilde{A}^2\Pi_i$ transitions, parallel transition moment is predominant due to strong vibronic mixing between $\widetilde{X}^2\Sigma^+$ and $\widetilde{A}^2\Pi_i$ as discussed in Chapter 2. Therefore the observed vibronic states should belong to Σ^+ vibronic symmetry, which is consistent with the present results that $2\nu_7(^2\Sigma^+)$ and $4\nu_7(^2\Sigma^+)$ were observed.

3.3.3(b) Assignment to vibrational states of ν_6(CCC) bending mode of $\widetilde{A}^2\Pi_i$

By comparing the DF spectra from $\widetilde{B}^2\Pi_i\,3\nu_5$ in Fig.3.2(a) and others in Fig.3.2(b)-(d) of C_4H, several bands, for example, at 377, 495, 628, 662, 814 and 886 cm^{-1} were newly observed in Fig.3.2(b)-(d), which were not observed in Fig.3.2(a). They have much stronger intensities compared with $2\nu_7$ and $4\nu_7$ in $\widetilde{X}^2\Sigma^+$. We assigned some of these new bands to the ν_6(CCC bending) progression of the $\widetilde{A}^2\Pi_i$ state: peaks at 377 and 495 cm^{-1} to $\nu_6(^2\Sigma^-)$ and $\nu_6(^2\Sigma^+)$, and at 814 cm^{-1} and 886 cm^{-1} to $3\nu_6(^2\Sigma^-)$ and $3\nu_6(^2\Sigma^+)$.

Although both $^2\Sigma^+$ and $^2\Sigma^-$ vibronic states of $\widetilde{A}^2\Pi_i\,\nu_6$ and $\widetilde{A}^2\Pi_i\,3\nu_6$ were observed in the DF spectra from $\widetilde{B}^2\Pi_i\,\nu_6\,(^2\Sigma^{(+)}_{1/2})$ and $\widetilde{B}^2\Pi_i\,\nu_6\,(^2\Sigma^{(-)}_{1/2})$, it is notable that relative intensities of $^2\Sigma^+$ and $^2\Sigma^-$ alternate in Fig.3.2(b) and (c). Namely, $^2\Sigma^+$ vibronic states at 495 and 886 cm^{-1} are more intense in the DF spectrum from $\widetilde{B}^2\Pi_i\,\nu_6$ $(^2\Sigma^{(+)}_{1/2})$, while $^2\Sigma^-$ vibronic states at 377 and 814 cm^{-1} are stronger from $\widetilde{B}^2\Pi_i\,\nu_6$ $(^2\Sigma^{(-)}_{1/2})$, as found in comparison of Fig.3.2(b) and (c). In addition to this, in the DF spectrum from an unassigned vibronic state of $\widetilde{B}^2\Pi_i$ in Fig.3.2(d), whose symmetry of the excited state is $^2\Sigma^{(+)}_{1/2}$, this tendency of intensity alternation is still seen, and the intensity pattern is the same as that from $\widetilde{B}^2\Pi_i\,\nu_6\,(^2\Sigma^{(+)}_{1/2})$ in Fig.3.2(b).

The ${}^2\Sigma^{(+)}_{1/2}$ and ${}^2\Sigma^{(-)}_{1/2}$ states are produced from linear combinations of ${}^2\Sigma^+$ and ${}^2\Sigma^-$. For $\tilde{B}^2\Pi_i$ $\nu_6({}^2\Sigma^{(\pm)}_{1/2})$ of C_4H, they are written as,

$$\Sigma^{(+)}_{1/2} = 0.829\Sigma^+ + 0.559\Sigma^-$$
$$\Sigma^{(-)}_{1/2} = 0.559\Sigma^+ - 0.829\Sigma^-$$

as have been given in Chapter 2. Therefore, it was reasonable that in the case of where the excited state is $\tilde{B}^2\Pi_i$ ${}^2\Sigma^{(+)}_{1/2}$, the fluorescence to $\tilde{A}^2\Pi_i$ ${}^2\Sigma^+$ is stronger than ${}^2\Sigma^-$, and weaker in the case where the excited state is ${}^2\Sigma^{(-)}_{1/2}$. ${}^2\Sigma^+$ and ${}^2\Sigma^-$ vibronic states in $\tilde{A}^2\Pi_i$ were separated largely by 118 and 72 cm^{-1} for ν_6 and $3\nu_6$, respectively, due to the Renner-Teller effect and the Herzberg-Teller effect. Similarly, for C_4D, we assigned peaks at 363 and 479 cm^{-1} to $\nu_6({}^2\Sigma^+)$ and $\nu_6({}^2\Sigma^-)$, and 793 and 869 cm^{-1} to $3\nu_6({}^2\Sigma^+)$ and $3\nu_6({}^2\Sigma^-)$ of $\tilde{A}^2\Pi_i$ in Fig.3.3 (b) and (c), in which intensity alternations were observed between the DF spectra from $\tilde{B}^2\Pi_i$ ${}^2\Sigma^{(+)}_{1/2}$ and ${}^2\Sigma^{(-)}_{1/2}$.

The energy diagram of the assigned vibronic states is shown in Fig.3.4. From this diagram, we have reconstructed the vibronic structure of the ν_6 vibrational states in $\tilde{A}^2\Pi_i$ as shown in Fig.3.4 by dotted lines, and determined vibrational frequencies of the ν_6 mode as ω_6=206 cm^{-1} for C_4H, and 205 cm^{-1} for C_4D.

It is reasonable that the fluorescence from the ν_6 vibronic states of $\tilde{B}^2\Pi_i$ to the ν_6 or $3\nu_6$ states of $\tilde{A}^2\Pi_i$ is observed with strong intensity, because this type of transitions satisfies two conditions: 1) they have a parallel transition dipole moment ($\tilde{B}^2\Pi_i$ (${}^{ev}\Sigma$) - $\tilde{A}^2\Pi_i$(${}^{ev}\Sigma$)) which is predominant in the present case, and 2) they have large Franck-Condon factors, as they are Δl=0 transitions, that is $l_6=\pm1$ to $l_6=\pm1$.

The ${}^2\Sigma^+$-${}^2\Sigma^-$ splitting of the ν_6 vibrational mode of $\tilde{A}^2\Pi_i$ is inconsistent with the theory of Renner-Teller effect[8], where ${}^2\Sigma^+$-${}^2\Sigma^-$ splitting increases as vibrational level increases. This is explained by considering that a Herzberg-Teller vibronic mixing between $\tilde{X}^2\Sigma^+$ v=0 $({}^2\Sigma^+)|\Lambda = 0, l = 0\rangle$ and $\tilde{A}^2\Pi_i$ ν_6 $({}^2\Sigma^+)|\Lambda = \pm1, l_6 = \mp1\rangle$, which shifts up the ν_6 (${}^2\Sigma^+$) vibronic state of $\tilde{A}^2\Pi_i$ considerably. Therefore $\tilde{X}^2\Sigma^+$ v=0 ($|\Lambda = 0, l = 0\rangle$) has larger character of $\tilde{A}^2\Pi_i$ ν_6 ($|\Lambda = \pm1, l_6 = \mp1\rangle$), leading to observation of ν_6 progression in LIF spectra of the $\tilde{B}^2\Pi_i \leftarrow \tilde{X}^2\Sigma^+$ v=0 system.

Energies of the observed vibronic states, assignments and vibrational frequencies of $\widetilde{X}^2\Sigma^+$ and $\widetilde{A}^2\Pi_i$ are summarized in Tables 3.1 and 3.2.

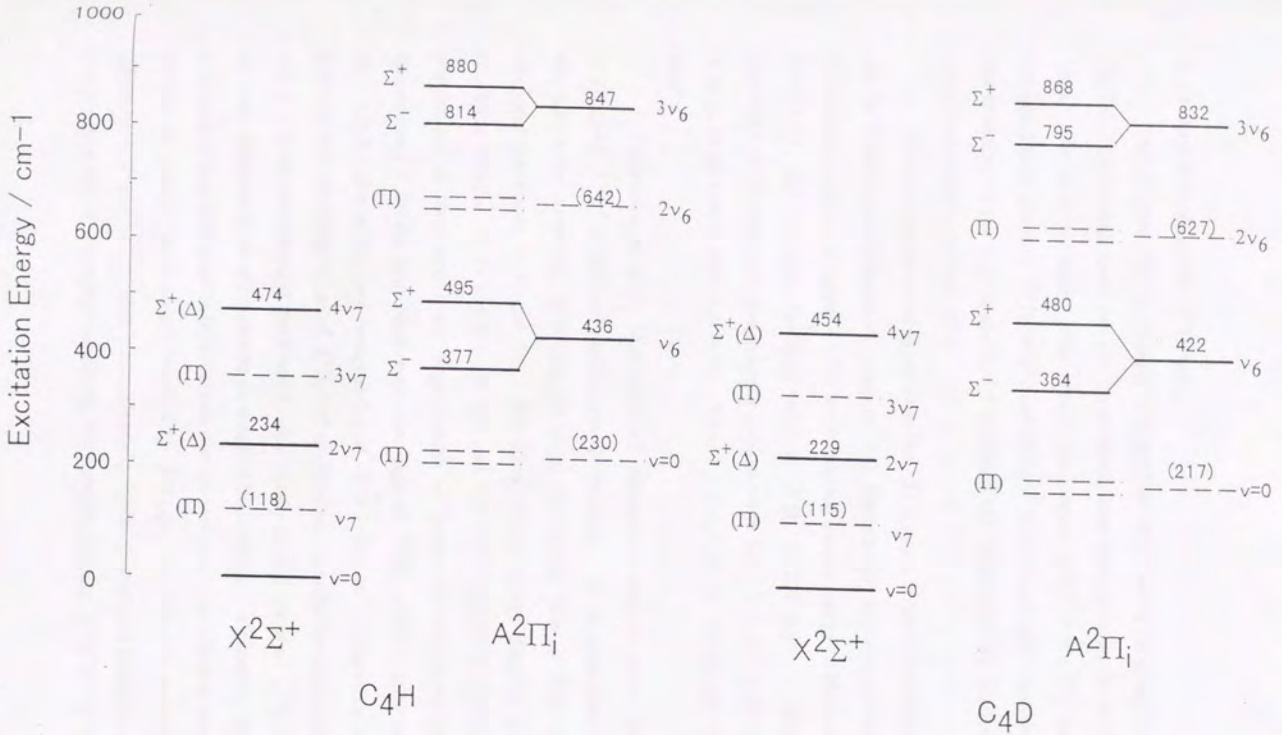

Fig.3.4 Energy diagram of the $\tilde{X}^2\Sigma^+$ and $\tilde{A}^2\Pi_i$ states. Solid lines indicate the observed vibronic states and dotted lines are predicted levels.

3.3.3 Term Energy of the $\tilde{A}^2\Pi_i$ state.

All assigned vibronic states of C_4H and C_4D are shown in the energy diagram of Fig.3.4. Undetected states can also be predicted from these states as shown by dotted lines. The most noticeable state here is the origin, $\tilde{A}^2\Pi_i$ v=0 ($^2\Pi$), band. We estimated term values of $\tilde{A}^2\Pi_i$ to 230 and 217 cm^{-1} for C_4H and C_4D, respectively, from extrapolations of the ν_6 progression. Therefore it can be said that the origin of $\tilde{A}^2\Pi_i$ state is very close to $2\nu_7$ of $\tilde{X}^2\Sigma^+$.

The only experimental approach to the $\tilde{A}^2\Pi_i$ state besides our study is carried out by Taylor *et al.* (Neumark's group of U.C. Berkeley)[9] by using photoelectoron spectroscopy, now in progress. They are measuring kinetic energy of photoelectorons from C_4H^-, and estimated the term value of $\tilde{A}^2\Pi_i$ to 226 cm^{-1}. Although the resolution of photoelectron spectroscopy is expected to be $\sim$100 cm^{-1}, their estimation is in good agreement with our work. Table 3.3 compares our results and theoretical studies.

Yamamoto *et al.*[1] have observed vibrationally excited states, $\nu_7(\Pi)$ and $2\nu_7(\Delta,\Sigma)$ of $\tilde{X}^2\Sigma^+$ in laboratory microwave spectroscopy. At the same time, based on this laboratory detection, they assigned some unidentified lines in IRC+10216 to rotational transitions in ν_7 and $2\nu_7$. According to our energy diagram in Fig.3.4, excitation energies of ν_7 and $2\nu_7$ are 118 and 234 cm^{-1} respectively, indicating the populations of these states are large enough to detect by microwave absorption spectroscopy. On the other hand origin, the origin of $\tilde{A}^2\Pi_i$, v=0(Π), state lies at 230 cm^{-1}, which is almost the same energy as $2\nu_7$ of $\tilde{X}^2\Sigma^+$, 234 cm^{-1}. Therefore, there is a hope that microwave spectrum of $\tilde{A}^2\Pi_i$ v=0 can be observed under the same condition of Ref. 1. In the astronomical observation, vibrationally excited states of $\tilde{X}^2\Sigma^+$, ν_7 and $2\nu_7$ were observed in the circumsteller envelope of IRC+10216. A pumping mechanism is considered that C_4H absorbs IR radiations with its peak at 10 μm, which is described in section 1.2, and is "electronically" excited to $\tilde{A}^2\Pi_i$(v), and after the excitation they radiate to ν_7, $2\nu_7$ of $\tilde{X}^2\Sigma^+$ also "electronically". Because electronic transition moment is larger than that of vibrational transitions, this pumping process $\tilde{X}^2\Sigma^+(\text{v=0}) \rightarrow \tilde{A}^2\Pi_i$

$\rightarrow \widetilde{X}^2\Sigma^+(\nu_7, 2\nu_7)$ is fast, while relaxation from ν_7, $2\nu_7$ to lower states is slow. I think that our results of excitation energy of the vibrational states of $\widetilde{A}^2\Pi_i$ is very suitable for IR absoption.

Thus $\widetilde{X}^2\Sigma^+(\nu_7, 2\nu_7)$ states are much populated. According to this mechanism, $\widetilde{A}^2\Pi_i$ v=0 is not so populated in circumsteller envelopes, because transitions from initially excited $\widetilde{A}^2\Pi_i(\mathrm{v})$ to $\widetilde{A}^2\Pi_i$ v=0 are "vibrational" transitions, being much weaker than electronic transitions generally by a factor of 10^{-4}, and moreover since direct pumping process $\widetilde{A}^2\Pi_i(\mathrm{v}=0) \rightarrow \widetilde{X}^2\Sigma^+$ is fast, the relaxation process $\widetilde{A}^2\Pi_i(\mathrm{v}=0) \rightarrow \widetilde{X}^2\Sigma^+$ is also expected to be fast.

Table.3.1(a) Observed vibronic state in Dispersed Fluorescence Spectra of C_4H.

Relative Energy	Assignment	
0	$\tilde{X}^2\Sigma^+ v=0\ (\Sigma^+)$	
234	$\tilde{X}^2\Sigma^+ 2\nu_7\ (\Sigma^+)$	
377**		$\tilde{A}^2\Sigma^+ \nu_6\ (\Sigma^-)$
474	$\tilde{X}^2\Sigma^+ 4\nu_7\ (\Sigma^+)$	
495**		$\tilde{A}^2\Sigma^+ \nu_6\ (\Sigma^+)$
577**		
628**		
662		
683		
789		
814**		$\tilde{A}^2\Sigma^+ 3\nu_6\ (\Sigma^-)$
880**		$\tilde{A}^2\Sigma^+ 3\nu_6\ (\Sigma^+)$
886		
912*		
947		
996**		
1090*		

* observed only in DF spectrum from $3\nu_5\ (\Sigma^+)$.

** observed only in DF spectrum from $\Sigma^{(\pm)}_{1/2}$

all in unit of cm^{-1}.

Table.4.1(a) Observed vibronic state in Dispersed Fluorescence Spectra of C_4D.

Relative Energy	Assignment	
0	$\tilde{X}^2\Sigma^+ v=0\ (\Sigma^+)$	
229*	$\tilde{X}^2\Sigma^+ 2\nu_7\ (\Sigma^+)$	
363**		$\tilde{A}^2\Sigma^+ \nu_6\ (\Sigma^-)$
454*	$\tilde{X}^2\Sigma^+ 4\nu_7\ (\Sigma^+)$	
479**		$\tilde{A}^2\Sigma^+ \nu_6\ (\Sigma^+)$
561*		
585**		
612**		
637		
758*		
793**		$\tilde{A}^2\Sigma^+ 3\nu_6\ (\Sigma^-)$
848		
869**		$\tilde{A}^2\Sigma^+ 3\nu_6\ (\Sigma^+)$
911		
939*		
986		

Table 3.2 Vibratiobnal Frequency of $\widetilde{X}^2\Sigma^+$ and $\widetilde{A}^2\Pi_i$

	$X^2\Sigma^+$ ν_7 (CCC bending)	$A^2\Pi_i$ ν_6 (CCC bending)
C_4H	118	206
C_4D	114	205

all in unit of cm^{-1}.

Table 3.3 Term energy of $A^2\Pi_i$ state.

	ab initio					experimental		
	MR-CI[+Q][1]	CASPT2 /DZVPVP[2]	RCCSD(T) /cc-pVQZ[3]	RSCCSD(T)/ cc-pVQZ[4]	CCSDT(T)/ [432/321]ANO[5]	photoelectron sp. of C_4H^-[6]	this work DF spectra	
$A^2\Pi_i$	81	565	72	100±50	…	226	230	217 (C_4D)
$X^2\Sigma^+$	…	…	…	…	244-1154	…	…	…

1) M.Kolbuszewski, Astrophys. J. 432, L63 (1994). (ref.3)

2) A. L. Sobolewski and L. Adamowicz, J. Chem. Phys., 102, 394 (1995). (ref.4)

3) D.E. Woon, Chem. Phys. Lett. 244, 45 (1995). (ref.5)

4) M.C.McCarthy, C.A.Gottlieb, P.Thaddeus, M.Horn and P.Botschwina, J. Chem. Phys., 103, 7820 (1995). (ref.7)

5) J. Natterere and W. Koch, Mol. Phys. 84, No.4 691 (1995). (ref.6)

6) T. Taylor and D. Neumark, private communucation.

References

1. S. Yamamoto, S. Saito, M. Guelin, H. Suzuki, and M. Ohishi, Astrophys. J., **323**, L149 (1987).
2. L.N. Shen, T.J. Doyle, and W.R.M. Graham, J. Chem. Phys., 93, 1597 (1990).
3. M. Kolbuszewski, Astrophys. J. 432, L63 (1994)
4. A.L. Sobolewski and L. Adamowicz, J. Chem. Phys., **102**, 394 (1995).
5. D.E. Woon, Chem. Phys. Lett., **244**, 45 (1995).
6. M.C. MaCathy. C.A. Gottlieb, P. Thaddeus, M. Horn and P. Botschwina, 103, 7820 (1995).
7. J. Natterer and W. Koch, Mol. Phys., 84, 691 (1995).
8. For example, "Molecular Spectra and Molecular Structure III. Electronic Spectra and Electronic Strauctures of Polyatonic Molecules" G. Herzberg.
9. private communication, T. Taylor, D. Neumark (1996)

Chapter 4

Laser Induced Fluorescence Spectroscopy of the C_3N radical

Abstract

Laser induced fluorescence spectrum of the C_3N radical, which is an isoelectronic molecule of C_4H, have been observed in a super sonic free expansion. C_3N was generated by a discharge of a mixture of 0.2% HC_3N/HC_5N diluted in Ar by using a pulsed discharge nozzle. One $^2\Pi$-$^2\Sigma$ and five $^2\Sigma$ -$^2\Sigma$ vibronic bands were observed in the region of 28600-29200 $\mathrm{cm^{-1}}$, and the electronic excited state was determined to $\tilde{B}^2\Pi_i$ from rotational analyses of these bands. The origin of $\tilde{B}^2\Pi_i$ was tentatively determined to 28799.6380(14) $\mathrm{cm^{-1}}$. Fluorescence decay curves from single rotational levels in most of the bands consisted of short and long time decay components, where quantum beats were recognized on the latter, leading to a conclusion that two relaxation processes, fluorescence and internal conversion to $\tilde{X}^2\Sigma^+$ and $\tilde{A}^2\Pi_i$, occur competitively. Dispersed fluorescence spectra from several vibronic states in $\tilde{B}^2\Pi_i$ were also measured. We assigned weak band structures, starting from the excitation laser wavelength, to the fluorescence to the ground state $\tilde{X}^2\Sigma^+$, and strong band structures, suddenly appeared above 1800 $\mathrm{cm^{-1}}$, to the fluorescence to the low lying first excited state, $\tilde{A}^2\Pi_i$. The origin of the $\tilde{A}^2\Pi_i$ state was estimated to be 1846 ± 5 $\mathrm{cm^{-1}}$.

4.1 Introduction

The C_3N radical is one of the C_nX (X=H, N, O, S) carbon chain series, which are well known as interstellar molecules. The C_3N radical were found at first in an interstellar medium, IRC+10216, in 1977 by a radio telescope[1], together with C_4H[1,2]. At the same time, theoretical study of C_3N was performed to confirm astronomical identification, and the ground state was determined to $\tilde{X}^2\Sigma^+$[3]. This astronomical observation of C_3N and C_4H was the earliest discovery of C_nX ($n \geqq 3$) carbon chain molecules in the gas phase, which suggests C_3N and C_4H are abundant in interstellar media and very important species for interstellar chemistry. Laboratory detection of C_3N was first carried out by Gottlieb *et al.*[4] by millimeter-wave absorption in a discharge flow of HC_3N and N_2. In 1989, the vibrationally excited state, ν_5 ($^2\Pi$), was observed in laboratory by millimeter wave absorption by Yamamoto *et al.*[5], which is the only report for C_3N other than the vibronic ground state reported until now.

In spite of the early detection of C_3N in 1977, the electronic excited state of this molecule have not been observed. Kolos *et al.*[8] tried to observe a LIF spectrum of C_3N generated by 193 nm photolysis of C_4H_2, but they did not succeeded in detecting any spectrum in the regions of 377-408 nm and 480-580 nm. C_3N has been considered to have a similar electronic configuration with C_4H, since C_4H and C_3N are isoelectronic molecules with each other. Their ground state is $^2\Sigma^+$, with electronic configuration of ....$(1\pi)^4(2\pi)^4(n\sigma)^1$. A low lying first excited electronic state $\tilde{A}^2\Pi_i$ is predicted with its configuration ...$(1\pi)^4(2\pi)^3(n\sigma)^2$, where the splitting between $\tilde{X}^2\Sigma^+$ and $\tilde{A}^2\Pi_i$ of C_3N is considered to be larger than C_4H. According to a recent *ab inio* calculation by Botschwina and co-workers[6] at RCCSD(T)/cc-pVTZ level, the exciteation energy of $\tilde{A}^2\Pi_i \leftarrow \tilde{X}^2\Sigma^+$ is predicted to be 2400 ± 50 cm^{-1}. Sadlej and Roos[9] calculated three vertical excitation energies of low lying electronic excited states including $\tilde{A}^2\Pi_i$ at CASSCF-MRCI/ANO level, and predicted that transition energies were 0.5eV(4033 cm^{-1}) for $\tilde{A}^2\Pi_i$ - $\tilde{X}^2\Sigma^+$, 3.93eV(31670 cm^{-1}) for $\tilde{B}^2\Pi_i$ - $\tilde{X}^2\Sigma^+$ and 5.71 eV(46057 cm^{-1}) for $\tilde{C}^2\Sigma^+$ - $\tilde{X}^2\Sigma^+$. We also made a preliminary calculation of the excitation energy of $\tilde{B}^2\Pi_i \leftarrow \tilde{X}^2\Sigma^+$ transition by CASSCF/6-311G** level, in which we obtained the transition energy ratio of C_3N to C_4H is 1.185. Thus, we estimated $\tilde{B}^2\Pi_i \leftarrow \tilde{X}^2\Sigma^+$ transition energy to be 28480 cm^{-1} from the calculated ratio and 24033 cm^{-1}, which is the exact $\tilde{B}^2\Pi_i \leftarrow \tilde{X}^2\Sigma^+$ transition energy of C_4H determined in Chapter 2.

In this work, we present the first observation of electronic transition of C_3N in the UV region, around 29000cm^{-1}(343-347 nm), by laser induced fluorescence spectroscopy. The relaxation processes of $\tilde{B}^2\Pi_i$ is also discussed based on the fluorescence time profiles. This discovery of the radiative electronic excited state was allowed us to carry out dispersed fluorescence spectroscopy in order to observe the vibronic structure of the ground state, $\tilde{X}^2\Sigma^+$, and the low lying first excited electronic state, $\tilde{A}^2\Pi_i$. Most of the results obtained could be compared with those of the isoelectronic molecule, C_4H.

4.2 Experimental

4.2.1. Production of C_3N.

The C_3N radicals were produced in a supersonic jet condition by using pulsed discharge nozzle (PDN) same as that mentioned in Chapter 2. The precursor we used was a gas mixture of 0.2-0.5 % of cyanoacetylene (HC_3N) and cynodiacetylene (HC_5N) diluted in Ar. The stagnation pressure was kept at 3 atm and the typical background pressure in the vacuum chamber was about $3\text{-}4\times10^{-5}$ Torr. These conditions were the same as C_4H. HC_3N and HC_5N were synthesized by following two methods. The first method is a DC discharge of $(CN)_2/C_2H_2/Ar$ mixture in a flow cell by monitoring the microwave absorption of HC_5N[10]. The second method is dehydration of plopiolic amide ($CH\equiv CCONH_2$) by diphosphorus pentaoxide (P_2O_5)[10]. We also tried a discharge of other two gas mixtures, 0.5% of aclyironitoryl ($CH_2{=}CHCN$) or acetonitryl (CH_3CN) diluted in Ar. The signal intensities of C_3N is about 1/6 in a discharge of $CH_2{=}CHCN/Ar$ and <1/10 in a discharge of CH_3CN/Ar, compared with that of HC_3N and HC_5N mixture. Therefore, we used mainly $HC_3N/HC_5N/Ar$ mixture throughout the present study.

4.2.2. Laser Induced Fluorescence Spectra.

The LIF system is almost the same as those mentioned in C_4H. The excitation beam was obtained by a frequency doubling of the output of a pulsed dye laser(Lambda Physik Scanmate) pumped by the 2nd harmonics of a Q-switched Nd^{3+}:YAG laser (Quanta-Ray GCR-3, 10Hz) by a KDP crystal. The resulting resolution was about 0.03 cm^{-1}. The laser dye used was Pyridine 1.

Laser-induced fluorescence was collected at right angle of the laser propagation by two planoconvex lenses (f=90 and f=120) focused onto an iris put on a quartz window, and detected by a photomultiplier (PMT, Hamamatsu R928) through a low-pass glass filter(HOYA UV-36). The PMT signal was then preamplified (×25), fed to a digital oscilloscope (Lecroy 9350A) at a sampling rate of 1 GHz, and finally converted to digital signals (1pt./ns), that was transferred to a personal computer with a repetition rate of 10Hz. We summed up the time profile over a region of 0-150 ns, and stored in PC. In the measurement of fluorescence time profiles for the discussion of relaxation processes, full digital signals were accumulated for 500 shots, where we used a fast preamplifier (×10, 250MHz).

Calibration of the laser wavenumber was made by measuring an LIF spectrum of I_2 (B-X transition) vapor (200 ℃) using the fundamental dye laser output. The relative uncertainty of the frequency measurement was less than 0.006 cm^{-1}. Etalon fringes (FSR=1.1cm^{-1}) were also monitored simultaneously to ensure of the frequency scan linearity.

4.2.3 Dispersed Fluorescence Spectra.

Dispersed fluorescence spectra were measured using a 50 cm monochromater (SPEX500M, 500nm Blaze, 1200 Grooves/mm) and a photomultiplier (Hamamatsu R928). The monochromater scanning was synchronized to laser pulses, and was typically operated at a 0.04 nm step. Signals for 40-50 pulses were accumulated at each point. The spectral resolution was about 20 cm^{-1} at 400 nm, and an accuracy of relative frequency was estimated to be < 3 cm^{-1} by referring to the Hg atomic lines.

4.3 Laser Induced Fluorescence Spectroscopy

4.3.1 Analysis of the LIF spectra of C_3N.

Figure.4.1 shows the low resolution LIF spectra obtained in a $HC_3N/HC_5N/Ar$ discharge in the region of 28600-29200 cm^{-1}. Strong CN B-X bands were observed at 28910 and 29180 cm^{-1} with lifetimes of 50-100 ns, and CCN $\tilde{C}-\tilde{X}$ system[11] have also observed very weakly with a lifetime of ~250 ns. In the same region, we found a new band series with a lifetime about 100-120 ns, which was not detected in the C_2H_2/Ar discharge. We have determined these bands to the $\tilde{B}^2\Pi_i - \tilde{X}^2\Sigma^+$ system of the linear carbon chain C_3N(CCCN) radical, based on rotational analyses of the observed vibronic bands. Seven vibronic bands of C_3N were observed in this region until now as indicated in Fig.4.1. Two vibronic bands at 28788 and 28811 cm^{-1} were assigned to a pair of a $^2\Pi$-$^2\Sigma^+$ band, each corresponding to $P(=\Lambda+\Sigma+l)=3/2$ and $P=1/2$ components, respectively. Other five vibronic bands belong to two types of $\Sigma-\Sigma$ bands: $^2\Sigma^{(+)}_{1/2}-{}^2\Sigma^+$ or $^2\Sigma^+-{}^2\Sigma^+$, which suggests existence of two bending modes with different vibronic interactions including the Renner-Teller effect, like ν_5 and ν_6 vibronic states of C_4H in $\tilde{B}^2\Pi_i$.

4.3.2 $^2\Pi$-$^2\Sigma$ band.

Figures 4.2(a) and (b) show high resolution LIF spectra of the $^2\Pi$-$^2\Sigma^+$ bands corresponding to $P=3/2$ and $P=1/2$ components. One more vibronic band observed at a little above $^2\Pi_{3/2}$ is a $^2\Sigma^{(+)}_{1/2}-{}^2\Sigma^+$ band. Although $^2\Pi_{1/2}$ band were partly overlapped with CN B-X transition at $P_1(5.5)+Q_{12}(4.5)$ and $R_1(5.5)$, most of the lines in the branches were assigned as single rotational lines. Molecular constants were determined by a least square fitting as T_v=28799.6380(14) cm^{-1}, B_{eff}=0.155219(32) cm^{-1}, and A_{eff}=-23.7772(20) cm^{-1}, where molecular constants of the ground state $\tilde{X}^2\Sigma^+$ were fixed to those determined by microwave spectroscopy[4], B"=0.16503511 cm^{-1}. p' constant associated with the Λ-type doubling and the centrifugal distortion constant could not be determined in the fitting, and so neglected. A_{eff} is an effective spin-orbit coupling constant modified by the vibronic interaction expressed in equation (2.14) if this Π

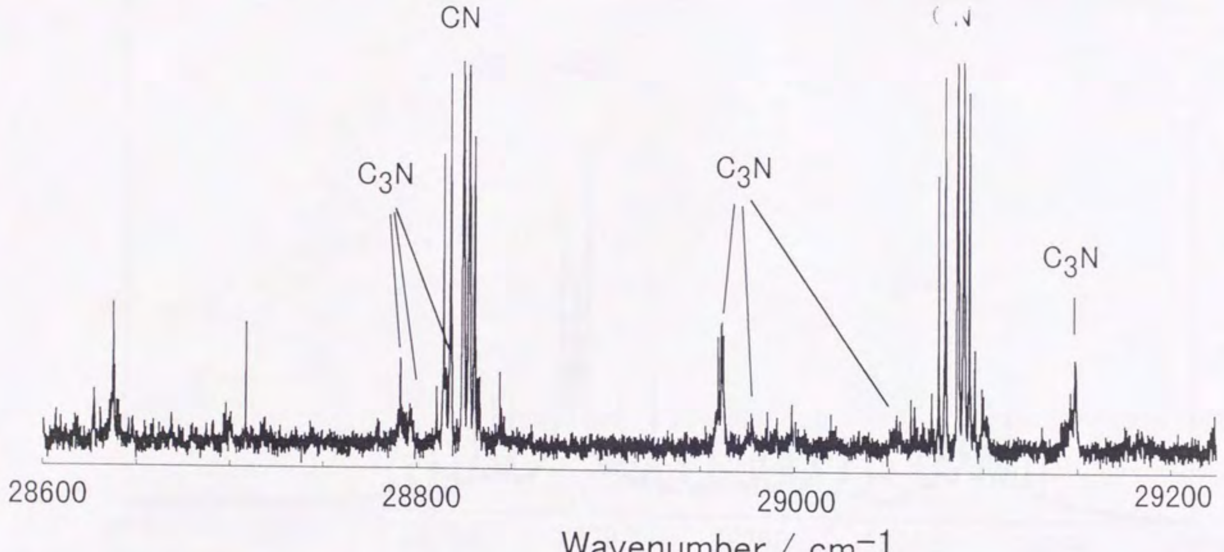

Fig. 4.1 LIF spectrum obtained in a $HC_3N/HC_5N/Ar$ discharge.

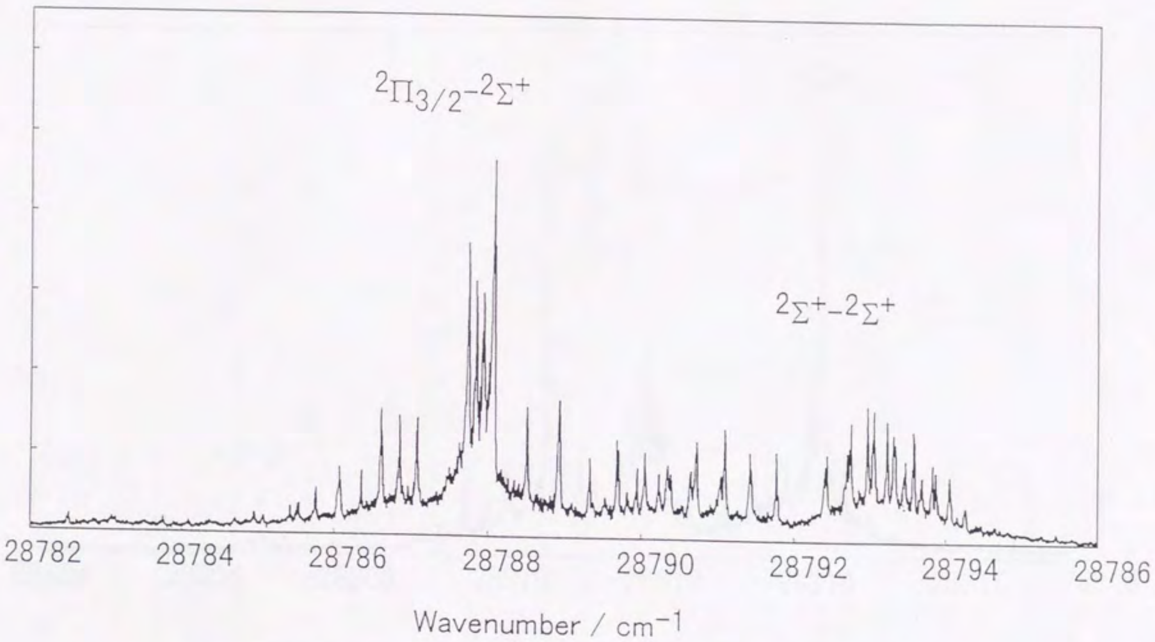

Fig. 4.2(a) High resolution LIF spectrum of C_3N, $^2\Pi_{3/2}$-$^2\Sigma^+$ band. $^2\Sigma^+$-$^2\Sigma^+$ band is also observed in the neighborhood.

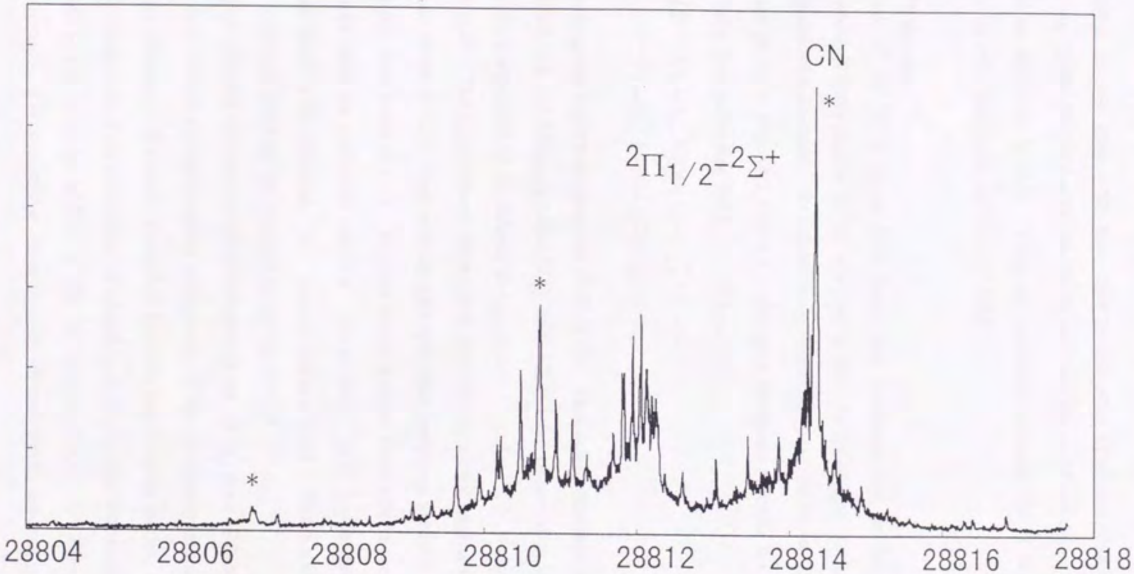

Fig. 4.2(b) High resolution LIF spectrum of C_3N, $^2\Pi_{1/2}$-$^2\Sigma^+$ band. Peaks labeled with asterisks are CN B-X transitions.

vibronic band is the v=0 state. We have tried to find other Π vibronic bands in lower energy regions, 25800-27300 and 28300-28600 cm^{-1}, but we could not detect any bands which could be attributed to C_3N. Thus, we tentatively assigned the Π bands to the origin of the $^2\Pi$ electronic state, namely v=0 state.

4.3.3 $^2\Sigma$-$^2\Sigma$ bands

Most of the $^2\Sigma$-$^2\Sigma$ bands have large spin splittings due to the spin-orbit interaction which is characteristic of the "vibronic $^2\Sigma$ state" in degenerate electronic states of linear polyatomic molecules. Rotational assignment of typical spectra of $^2\Sigma^+$-$^2\Sigma^+$ and $^2\Sigma^{(+)}_{1/2}$-$^2\Sigma^+$ are given in Figs. 4.3 and 4.4. We used Hougen's formula for rotational analyses as have been performed for C_4H in Chapter 2,

$$\begin{aligned} F_1(\Sigma^{\kappa/\mu},N) &= B_{eff}^{\kappa/\mu} N(N+1) + \tfrac{1}{2}\gamma_{eff}^{\kappa/\mu}(N+1) \\ F_2(\Sigma^{\kappa/\mu},N) &= B_{eff}^{\kappa/\mu} N(N+1) - \tfrac{1}{2}\gamma_{eff}^{\kappa/\mu} N \end{aligned} \tag{4.1}$$

where B_{eff} and γ_{eff} are defined in equations (2.6)-(2.8). Molecular constants determined are listed in Table.4.1. Although both $^2\Sigma^{(+)}_{1/2}$ and $^2\Sigma^{(-)}_{1/2}$ were observed in the case of C_4H, which were separated by $2r$ defined in equation (2.6), only $^2\Sigma^{(+)}_{1/2}$ states could be detected for C_3N. The γ_{eff} constants determined from the rotational analyses are small compared with those of C_4H, which indicate that spin-orbit couplings between Σ^+ and Σ^- of C_3N is smaller than those of C_4H. In other words Renner-Teller effects are relatively large compared with the spin-orbit coupling. As a result, $^2\Sigma^{(-)}_{1/2}$ bands have less Σ^+ character than those of the observed $^2\Sigma^{(-)}_{1/2}$ vibronic states of C_4H. This is a reason why $^2\Sigma^{(-)}_{1/2} - \Sigma^+$ transitions could not be detected in our experiment.

A stick diagram of observed vibronic bands of the $\tilde{B}^2\Pi_i$ state of C_3N is shown in Fig.4.5. It is difficult to make definite assignments of the vibrational structures from the data so far obtained. However, since C_3N has only two bending modes, ν_4 and ν_5, and the six Σ states arise from excitations of ν_4 and ν_5, it can be said that Renner-Teller effects of both ν_4 and ν_5 modes of C_3N $\tilde{B}^2\Pi_i$ are relatively large. In order to assign vibrational structures, it is necessary to observe more vibronic bands, especially $^2\Sigma^{(-)}_{1/2}$.

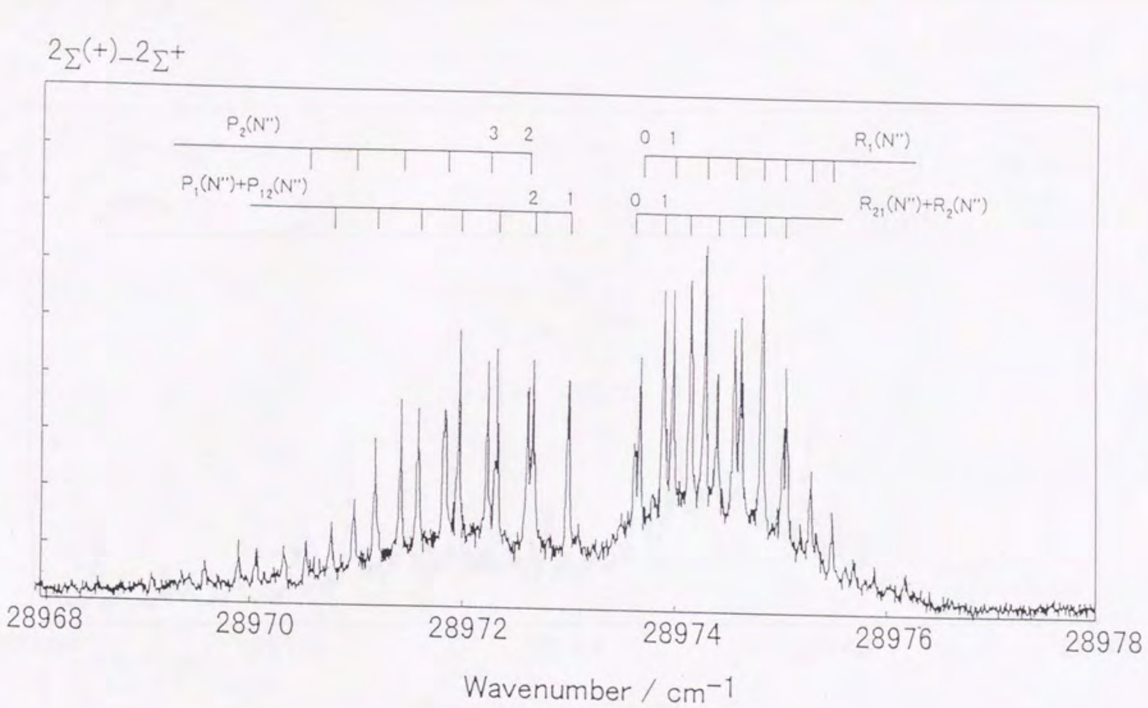

Fig. 4.3 High resolution LIF spectrum of C_3N, $^2\Sigma^+$-$^2\Sigma^+$ band (γ_{eff} = 0.1255).

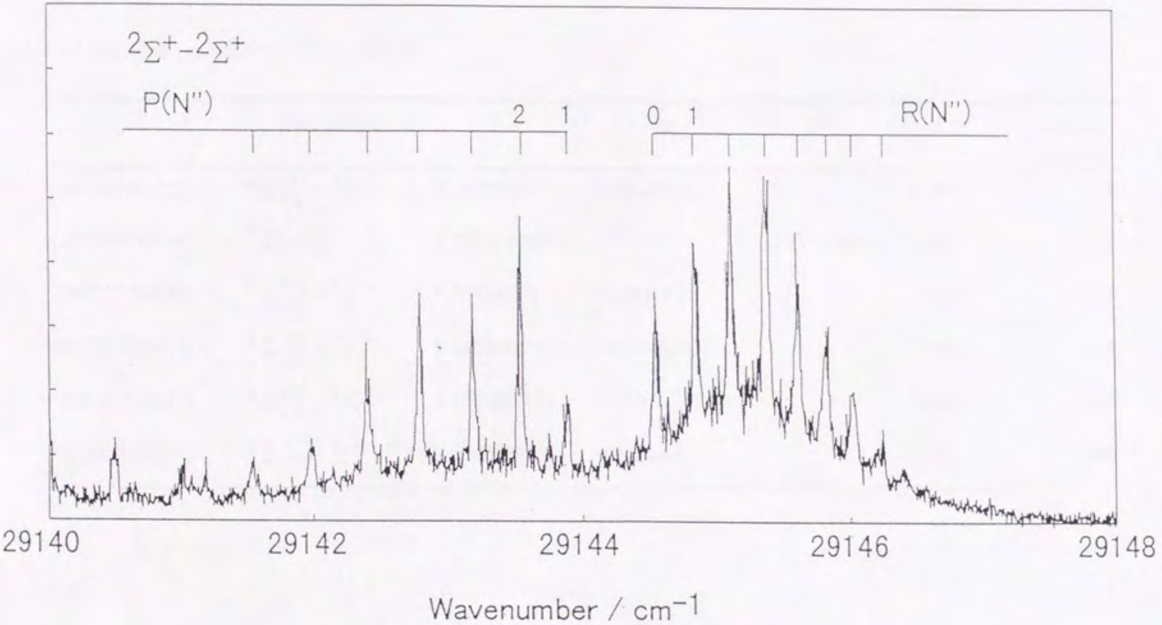

Fig. 4.4 High resolution LIF spectrum of C_3N, ${}^2\Sigma^+$-${}^2\Sigma^+$ band (γ_{eff}= 0).

Table.4.1. Molecular constants of $\tilde{B}^2\Pi_i$ of C_3N

T_v	Band type	B_{eff}	γ_{eff}	A_{eff}	σ	Relative Energy
28792.1016(22)	$^2\Sigma^{(+)}_{1/2} - {}^2\Sigma^+$	0.157021(76)	0.02327(52)		0.006	-8
28799.6380(14)	$^2\Pi - {}^2\Sigma^+$	0.155219(32)		-23.7772(20)	0.007	0.0
28957.2768(38)	$^2\Sigma^{(+)}_{1/2} - {}^2\Sigma^+$	0.15524(11)	0.1225(11)		0.013	158
28973.3218(12)	$^2\Sigma^{(+)}_{1/2} - {}^2\Sigma^+$	0.156494(24)	0.03705(24)		0.004	174
29049.0926(15)	$^2\Sigma^{(+)}_{1/2} - {}^2\Sigma^+$	0.156220(44)	0.05362(37)		0.005	249
29144.2216(34)	$^2\Sigma^+ - {}^2\Sigma^+$	0.156087(63)	0.0 (fixed)		0.007	345

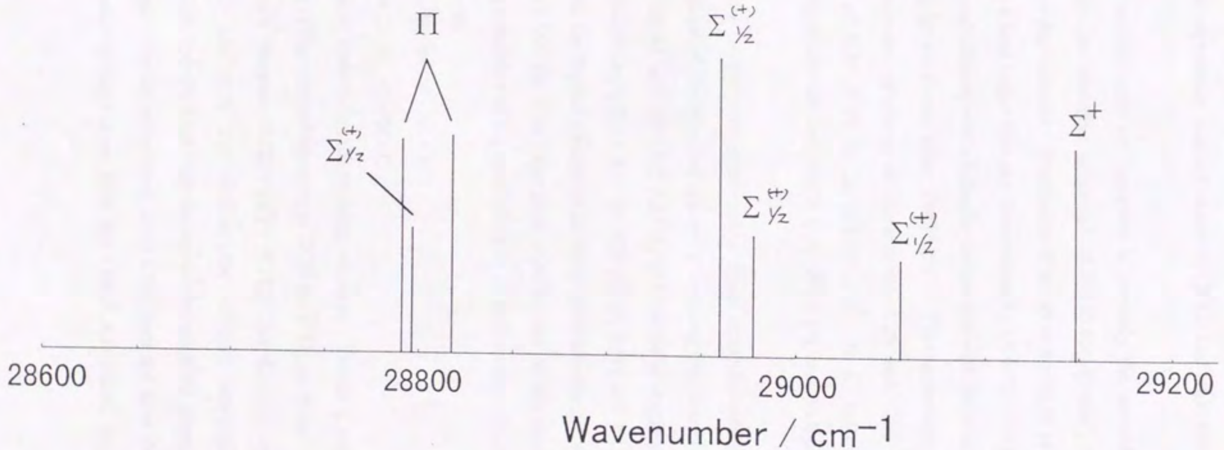

Fig. 4.5 Stick diagram of the observed vibrational levels of C_3N $\tilde{B}^2\Pi_i$.

4.3.4 Determination of electronic excited state to $B^2\Pi_I$ and the effective spin splitting constant.

The electronic excited state we observed is certainly the second electronic excited state $\tilde{B}^2\Pi_i$ with the tentative origin of 28799.6380(14) cm^{-1}, which was confirmed by the negative A_{eff} constant. Prediction of an *ab initio* study by Sadlej and Roos[9] at 31670 cm^{-1} is a little larger than our observation by 13.44%. Our prediction by a lower level *ab initio* calculation, which includes comparison with the exact excitation energy of $\tilde{B}^2\Pi_i$ of C_4H, gave a closer value, 28480 cm^{-1}. This agreement emphasizes the similarity of the electronic structures of isoelectronic C_3N and C_4H. The main electronic configuration of C_3N $\tilde{B}^2\Pi_i$ is $...(1\pi)^3(2\pi)^4(n\sigma)^2$. In CI calcuration 72% of $...(1\pi)^3(2\pi)^4(n\sigma)^2$ configuration are included in C_3N $\tilde{B}^2\Pi_i$ [9], and on the other hand 60% in C_4H $\tilde{B}^2\Pi_i$ [12].

If we compare the results with other carbon chain molecules which contain a nitrogen atom, the magnitude of the effective spin-orbit coupling constant of C_3N, A_{eff} - 23.77 cm^{-1}, is similar to 26.41 cm^{-1} of CNC ($\tilde{X}^2\Pi_g$)[13] while is about a half times smaller than other C_nN molecules, -52.64 cm^{-1} for CN ($\tilde{B}^2\Pi_i$)[15] and 40.37 cm^{-1} for CCN ($\tilde{X}^2\Pi_r$)[14]. Since the Renner parameter of these molecules are not so different, ε=+0.44 for CCN and +0.549 for CNC, the main contribution of this discrepancy is difference in distribution probability of unpaired electron on each atom. CCN and CNC have resonance structures as,

$$\cdot C - C = N: \Leftrightarrow :C = C = N\cdot$$

$$\cdot C - N = C: \Leftrightarrow :C = N - C\cdot$$

where CCN has the unpaired electron on the terminal nitrogen. Ohshima and Endo[16] estimated the spin density of the terminal nitrogen of CCN in $\tilde{X}^2\Pi_r$ as about 30%, which is a reasonable estimation because $0.3\zeta(N{:}2p^3)+ 0.7\zeta(C{:}2p)=42$ cm^{-1} is in good agreement with $A \sim 42$ cm^{-1} [19, 20] without the vibronic interaction, where $\zeta(N{:}2p^3)=73.3$ cm^{-1} and $\zeta(C{:}2p)=29.0$ cm^{-1} are the spin-orbit coupling constants of the nitrogen and carbon atoms. On the other hand, since CNC does not have the unpaired electron density on the center nitrogen atom, CNC has a small A constant, approximately

$0.5\zeta(C{:}2p)+0.5\zeta(C{:}2p)=29.0\ cm^{-1}$, which is similar to the observed value, $26.41\ cm^{-1}$. In the similar sense, C_3N has a resonance electronic structure as,

$$\cdot C\equiv C-C\equiv N{:}\ \Leftrightarrow\ {:}C=\dot{C}-C\equiv N{:}\ \Leftrightarrow\ {:}C=C=C=\dot{N}{:}$$

Because the third structure has the unpaired electron density on the terminal nitrogen atom, A_{eff} constant of C_3N is expected to be larger than CNC. However the observed A_{eff} constant was smaller than that of CNC. The reason is that Renner-Teller effects for the two bending modes are expected to be larger as mentioned at the end of the previous section. As a result, the A_{eff} constant of C_3N were reduced further

4.3.5 Vibronic interactions in the ground state.

As shown in Fig.4.5, the $^2\Pi$-$^2\Sigma^+$ and $^2\Sigma$-$^2\Sigma$ bands have almost the same intensities. Since the $^2\Sigma$-$^2\Sigma$ transition is symmetry forbidden for the present $\tilde{B}^2\Pi_i$-$\tilde{X}^2\Sigma^+$ electronic transition, the observed $^2\Sigma$-$^2\Sigma$ bands are considered to be intensity borrowing transitions from the low lying $\tilde{A}^2\Pi_i$ through the Herzberg-Teller vibronic mixing, like the case of C_4H. Comparing with the case of C_4H, where vibronically induced $^2\Sigma$-$^2\Sigma$ bands were about ten times stronger than allowed $^2\Pi$-$^2\Sigma$, the decrease in intensity of the vibronically induced $^2\Sigma$-$^2\Sigma$ bands of C_3N is caused by the decrease of the magnitude of the vibronic mixing. As shown in section 2.7.4, when eigen wavefunctions are expressed as,

$$\left|\Psi^{\Sigma}_{GS},K=0\right\rangle=\frac{1}{\sqrt{1+c^2}}\left[\left|\tilde{X},\Lambda=0\right\rangle\left|v''=0,l=0\right\rangle+c\left|\tilde{A},\Lambda=\pm1\right\rangle\left|v',l=\mp1\right\rangle\right], \tag{4.2}$$

the transition intensities are written by,

$$I_{\Pi\text{-}\Sigma}\propto\frac{1}{1+c^2}f_{BX}C'_{FC} \tag{4.3}$$

$$I_{\Sigma\text{-}\Sigma}\propto\frac{c^2}{1+c^2}f_{BA}C_{FC} \tag{4.4}$$

The mixing constant c can be replaced by using the second order perturbation theory as,

$$c=\frac{\left\langle\tilde{A},\Lambda=\pm1\left|V_1e^{\pm i\theta}\right|\tilde{X},\Lambda=0\right\rangle}{\Delta E} \tag{4.5}$$

where the denominator is a matrix element of the Herzberg-Teller vibronic coupling and ΔE indicates an energy gap between vibronic states, approximately the $\tilde{A}^2\Pi_i$ - $\tilde{X}^2\Sigma^+$ splitting. As predicted from the *ab initio* calculation, and the results I will present in section 4.4, the energy splitting of $\tilde{A}^2\Pi_i$ and $\tilde{X}^2\Sigma^+$ of C_3N is larger than C_4H, leading to a smaller vibronic mixing for C_3N. Consequently, the $^2\Sigma$-$^2\Sigma$ bands in C_3N were relatively weaker. Assuming that the transition moment of $\tilde{B}$ - $\tilde{X}$ is 30 times larger than that of $\tilde{B}$ - $\tilde{A}$, as those predicted for C_4H by *ab initio* study[21], the $\tilde{X}^2\Sigma^+$ v=0 state of C_3N has about 15% of the $\tilde{A}^2\Pi_i$ character.

4.3.6 Fluorescence Lifetime of $\tilde{B}^2\Pi_i$

Fluorescence time profiles of C_3N $\tilde{B}^2\Pi_i$ does not show a single exponential decay in most of the bands, but consist of fast and slow decay components. For example, time profiles of the rotational levels, N'=0-3 in the $^2\Sigma$-$^2\Sigma$ band at 29144 cm^{-1} are shown in Fig.4.6. Although features of time profiles vary in individual rotational lines, considerable changes depending on the vibronic bands were not recognized. The decay time of the fast component was typically 100-150 ns, and the slow was 2-3 μs. This fluorescence time profile indicates a competition between the radiative decay by fluorescence and non-radiative processes, that is IC, similar to those of isoelectronic C_4H. If the number of non-radiative levels (N) is large, short and long time decays are approximately represented by equations (2.29) and (2.31),

$$I(t) = I_0 \exp\left\{-\left(\frac{1}{\tau_{rad}^0} + W\right)t\right\}, \tag{4.6}$$

$$I(t) = \frac{1}{N}\exp\left(-\frac{t}{\tau_i}\right). \tag{4.7}$$

Thus, the short time component is a dephasing time due to IC, whose relaxation rate is proportional to W, thus to N, and the long time component shows decay of the eigen states, whose intensity is proportional to the inverse of N. (See Fig.2.16) Fig.4.7 shows a comparison of fluorescence decay curves of C_3N and C_4H. A noticeable point here is that in C_3N the short time decay is slower (100-150 ns) and the long time decay is

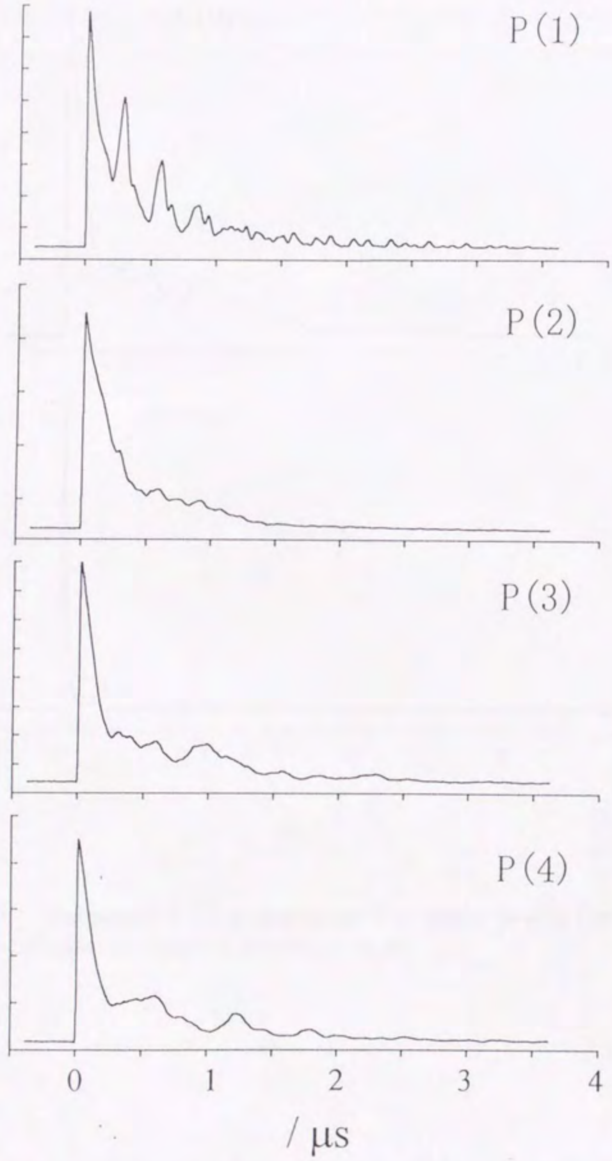

Fig. 4.6 Fluorescence time profile of single rotational levels of C_3N 29144 cm^{-1} band. (Fig. 4.4)

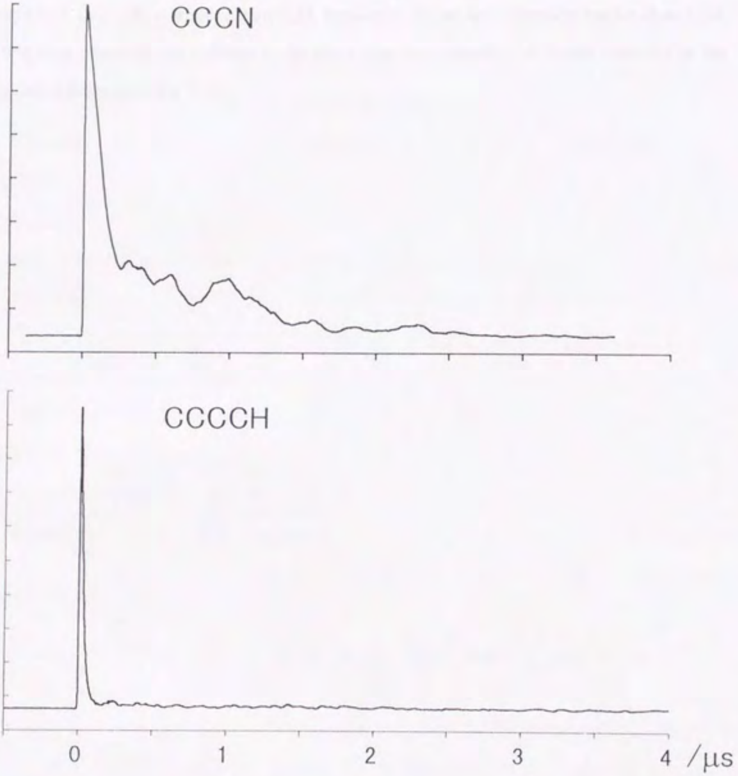

Fig. 4.7 Comparison of typical fluorescence time profiles between C_3N(N'=2 of 29144 cm^{-1} band) and C_4H(N'=1 of 24490 cm^{-1} band).

relatively stronger than those of C_4H. This results reflect the fact that the density of states ($\propto N$) of C_3N is smaller than C_4H, because C_3N has less vibration modes than C_4H, leading to a relatively slow decay in the short time component, and strong intensity in the long time component for C_3N.

4.4 Dispersed Fluorescence Spectra from C_3N $\tilde{B}^2\Pi_i$.

We measured dispersed fluorescence spectra from three vibronic states of $\tilde{B}^2\Pi_i$, as shown in Fig.4.8, 4.9 and 4.10 where the excited states are the $^2\Pi_{3/2}$, $^2\Pi_{1/2}$ and $^2\Sigma$ at 29144 cm^{-1}, respectively. The horizontal axis indicates the relative energy to the excitation laser in wavenumber unit, which corresponds to the excitation energy from $\tilde{X}^2\Sigma^+$ v=0. The structures of the DF spectra can be divided into two regions: they are regions with excitation energy of 0-1800 cm^{-1} and >1800 cm^{-1}. In the former region, weak band structures of $\tilde{X}^2\Sigma^+$ were observed, and in the latter strong band features including a clear vibrational progression begin at around 1800 cm^{-1}, which is considered to be that of the electronic excited state, $\tilde{A}^2\Pi_i$. It is hard to assign the vibrational structures above 1800 cm^{-1} as a vibrational progression of the ground state, because the vibrational structure is completely different between the two regions, 0-1800 cm^{-1} and >1800 cm^{-1}. Therefore, we concluded that strong signals started around 1800 cm^{-1} in the DF spectra correspond to the fluorescence to the low lying first electronic excited state $\tilde{A}^2\Pi_i$ as described in Fig.5.10. The relative intensity of $\tilde{B}^2\Pi_i \rightarrow \tilde{A}^2\Pi_i$ is larger in comparison with that of $\tilde{B}^2\Pi_i \rightarrow \tilde{X}^2\Sigma^+$, which is reasonable considering the transition dipole moment $\mu_{BA} >> \mu_{BX}$.

Fig.4.11 shows the DF spectra in the lower energy region, 0-1800 cm^{-1}, corresponding to the vibrational structures of the ground state. Peak positions and partial assignments are summarized in Table 4.2. The progression of the lowest bending mode, ν_5, was observed in Fig.4.11(a)-(c). Its vibrational frequency estimated from the progression is ω_5=134 cm^{-1}. The most recent *ab initio* study reported by McCarthy *et al.*[17] predicted ω_5=147.2 cm^{-1} which is slightly larger than our result.

Figs. 4.12(a)-(c) show the DF spectra in the higher energy region, >1500 cm^{-1}, corresponding to the vibrational structures of $\tilde{A}^2\Pi_i$. Here some vibronic bands in $\tilde{X}^2\Sigma^+$ may be included with small intensity. In the DF spectra from the $^2\Pi_{3/2}$ and $^2\Pi_{1/2}$ vibronic states, the vibrational progression of the ν_5 bending mode of the $\tilde{A}^2\Pi_i$ electronic state clearly appeared with intervals of about 205-235 cm^{-1}. Peak positions of this progression are summarized in Table.4.3. Since the present $\tilde{A}^2\Pi_i$ - $\tilde{B}^2\Pi_i$ electronic transition is induced by the parallel transition moment, parallel type vibronic transitions, such as $^2\Sigma$-$^2\Sigma$ or $^2\Pi$-$^2\Pi$, are dominant. Thus, strong peaks must belong to $^2\Pi_{3/2}\rightarrow{}^2\Pi_{3/2}$ and $^2\Pi_{1/2}\rightarrow{}^2\Pi_{1/2}$ vibronic transitions in the DF spectra in Figs.4.12(a) and (b) respectively[1)]. Peak positions of $^2\Pi_{3/2}$ are lower than those of $^2\Pi_{1/2}$ by the magnitude of the effective spin splitting constant $2r$[2)](see below)' as discussed in Chapter 2. In the present case, since $\tilde{X}^2\Sigma^+$ lies very close to $\tilde{A}^2\Pi_i$, the effective spin orbit coupling constant decreases to $\approx 1\,\mathrm{cm}^{-1}$(refer to equation 2.14), while it is 23 cm^{-1} for $\tilde{B}^2\Pi_i$, due to the strong vibronic interaction. We assigned the lowest peaks of $^2\Pi_{3/2}$ at 1845 cm^{-1} and $^2\Pi_{1/2}$ at 1846 cm^{-1} to $\tilde{A}^2\Pi_i$ $v=0$. Thus the band origin of $\tilde{A}^2\Pi_i$ was determined to be 1845.5 cm^{-1}. Next, we assigned first few lines to be $2\nu_5$, $4\nu_5$, $6\nu_5$ ... with the bending frequency of about $\omega_5=117$ cm^{-1}. However the long progression observed in Fig.4.12(a) and (b) seems to be attributed to not only the ν_5 mode, because $\tilde{B}$-$\tilde{A}$ transition is a linear-linear transition without considerable geometry change such as linear-bent transitions. In addition to this, the intensity pattern of Figs.4.12(a) has two maxima at 2314 cm^{-1} and 3166 cm^{-1}, while in general the Franck-Condon factor for the linear-linear transition has one maximum. We tentatively consider those to be combination bands including the ν_3 mode, C-C stretching. We assigned the 2726 cm^{-1} band to be $\nu_3=1$ $\nu_5=0$ ($^2\Pi$). The $^2\Pi_{3/2}$ - $^2\Pi_{1/2}$ splitting is almost zero, which is reasonable for the $\nu_5=0$ state, as it is similar to the band origin of $\tilde{A}^2\Pi_i$. Vibrational frequency of ν_3 is thus 2726-1846=880 cm^{-1}, which is close to an *ab initio* prediction of ω_3 in the ground state, 885 cm^{-1}, by McCarthy *et al.* [17]. The electron configuration of $\tilde{A}^2\Pi_i$ is such that a 2π electron is removed to the $n\sigma$ orbital in the $\tilde{X}^2\Sigma^+$ configuration. Since the 2π orbital has a node at a C-C bond, the frequency of C-C stretching, ω_3, is expected to not so change between $\tilde{X}^2\Sigma^+$ and $\tilde{A}^2\Pi_i$.

In contrast, in the DF spectrum from the $^2\Sigma$ band at 29144 cm^{-1} in Fig.4.12(c), ν_5 progression was not observed and a large number of irregular peaks appeared. In order to analyze this band structure, it is necessary to compare the DF spectrum with those from other $^2\Sigma$ states, and to clarify the rotational structures by high resolution techniques such as SEP spectroscopy.

[1] There are two $^2\Pi_{3/2,1/2}$ vibronic states by excitation of particular bending mode, $v \geqq 2$, in $^2\Pi$ electronic state, $|\Lambda = \pm 1, l = 0, \Sigma\rangle and |\Lambda = \mp 1, l = \pm 2, \Sigma\rangle$,and they can interact by Renner-Teller effect. Since the excited $^2\Pi$ states are considered to have a wavefunction of $|\Lambda = \pm 1, l = 0, \Sigma\rangle$, only $|\Lambda = \pm 1, l = 0, \Sigma\rangle$ in $\tilde{A}^2\Pi_i$ is observable without effective Renner-Teller effect considering l selection rule.

[2] ν_5 progression have a regular vibrational structure, indicating a small Renner-Teller effect. In such a case, the magnitude of $^2\Pi_{3/2}$ - $^2\Pi_{1/2}$ splitting depend on vibrational levels. According to Hougen's theory[18], $^2\Pi_{3/2}$ - $^2\Pi_{1/2}$ splitting are expressed by using r (as shown in chapter.3),

$$2r = \sqrt{A_{eff}{}^2 + [(v+1)^2 - K^2]\varepsilon^2\omega^2}$$

In the case of C_3N in $\tilde{A}^2\Pi_i$, A_{eff} is almost zero due to vibronic interaction, and $2r$ increases as vibrational quantum number v.

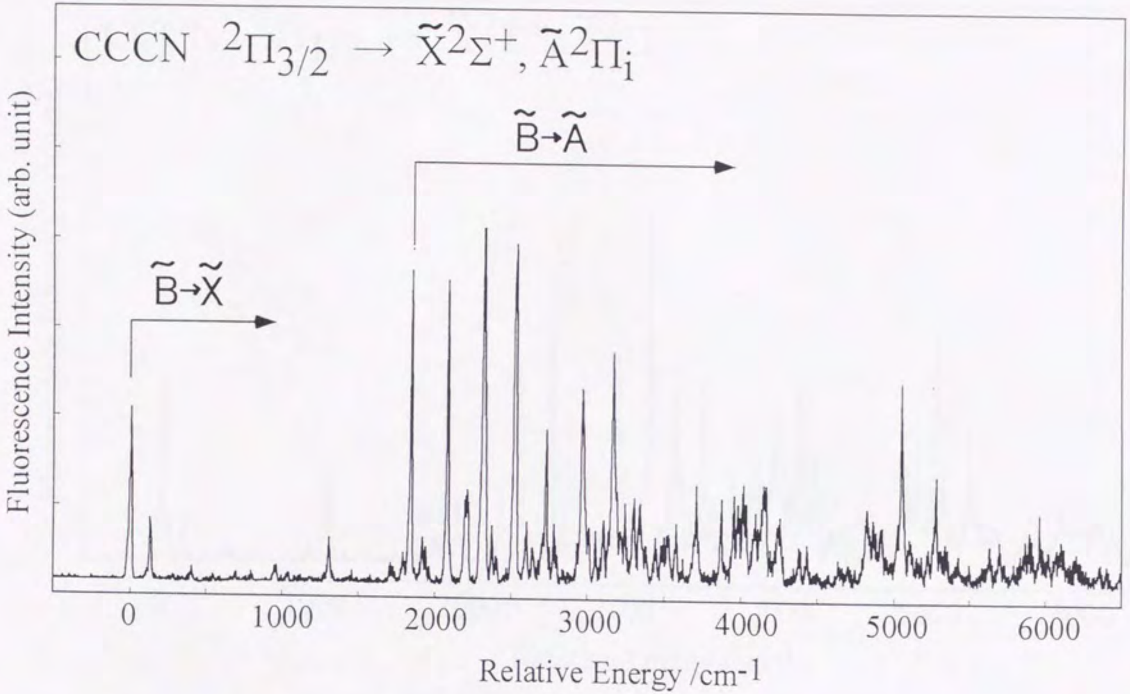

Fig.4.8 Dispersed Fluorescence Spectrum of C_3N from $^2\Pi_{3/2}$ vibronic state excited by Q head at 28788.063 cm^{-1}.

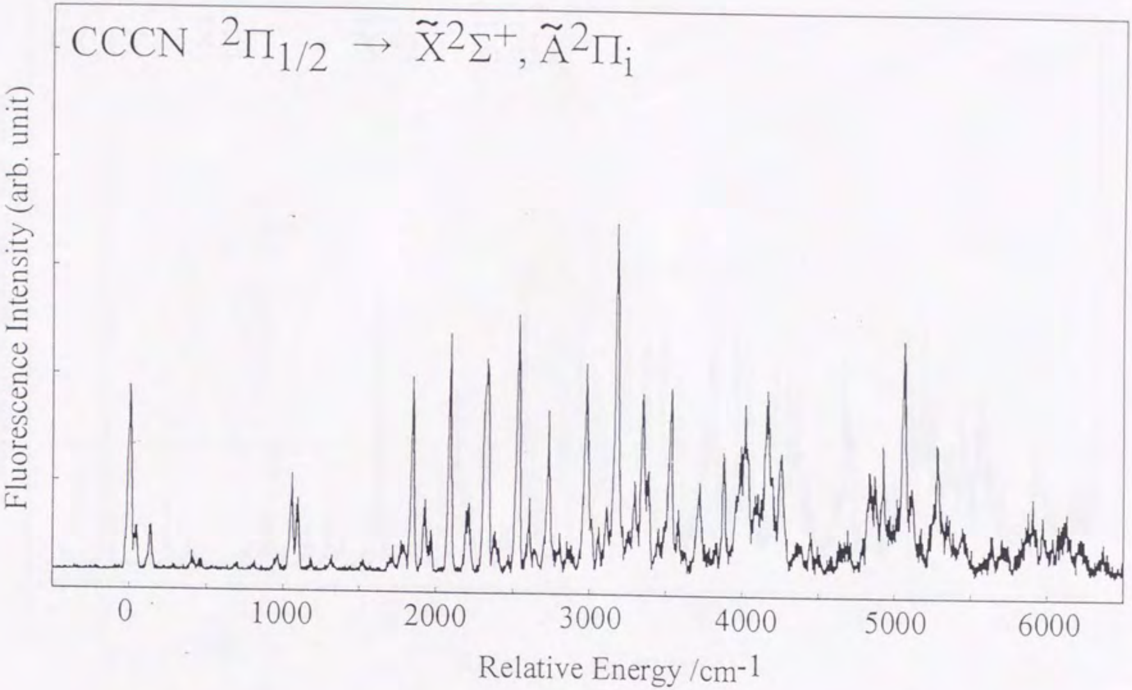

Fig.4.9 Dispersed Fluorescence Spectrum of C_3N from $^2\Pi_{1/2}$ vibronic state excited by $Q_{12}(2.5)+R_2(1.5)$ at 28811.940 cm^{-1}.

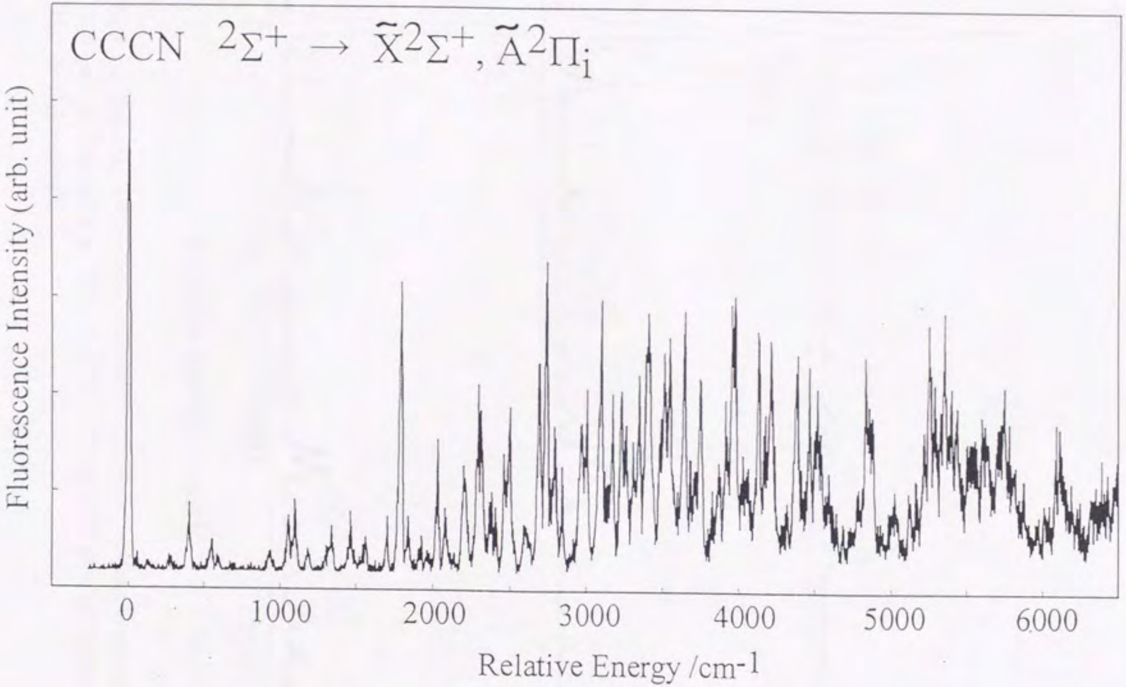

Fig.4.10 Dispersed Fluorescence Spectrum of C_3N from $^2\Sigma^+$ vibronic band excited by R(2) at 29145.098 cm^{-1}.

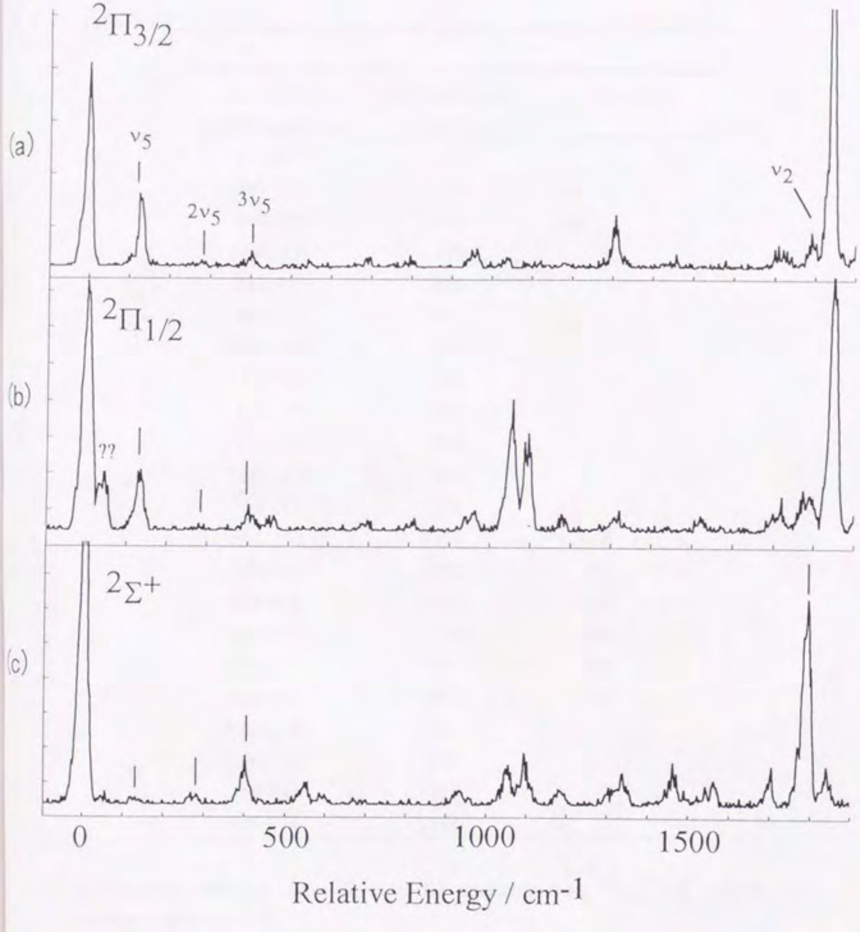

Fig.4.11 Dispersed Fluorescence Spectrum of C_3N in the relative energy region 0-1800 cm^{-1}, corresponding to $\tilde{B}^2\Pi_i \rightarrow \tilde{X}^2\Sigma^+$. The excited vibronic states are (a) $^2\Pi_{3/2}$, (b)$^2\Pi_{1/2}$, and (c)$^2\Sigma^+$.

Table 4.2 Observed vibronic bands in DF spectra in the region of 0-1800 cm^{-1}.

Transition Wavelength/ nm	Relative Energy / cm^{-1}	Remarks
347.077	0	
347.570	41	ν_5
348.700	130	$2\nu_5$
*346.336	271	$3\nu_5$
352.030	400	
352.721	461	
*349.638	544	
*350.205	590	
355.610	691	
357.110	810	
*354.436	931	
359.027	956	
360.250	1051	ν_3? 0
360.757	1092	41
361.895	1180	129
363.646	1310	259
*361.213	1460	409
366.425	1521	470
*362.530	1561	
*364.329	1697	
369.023	1713	
369.979	1786	ν_2

a) Transition energies show those of DF spectrum from $^2\Pi_{1/2}$, and marked with asterisks are those of $^2\Sigma^+$.

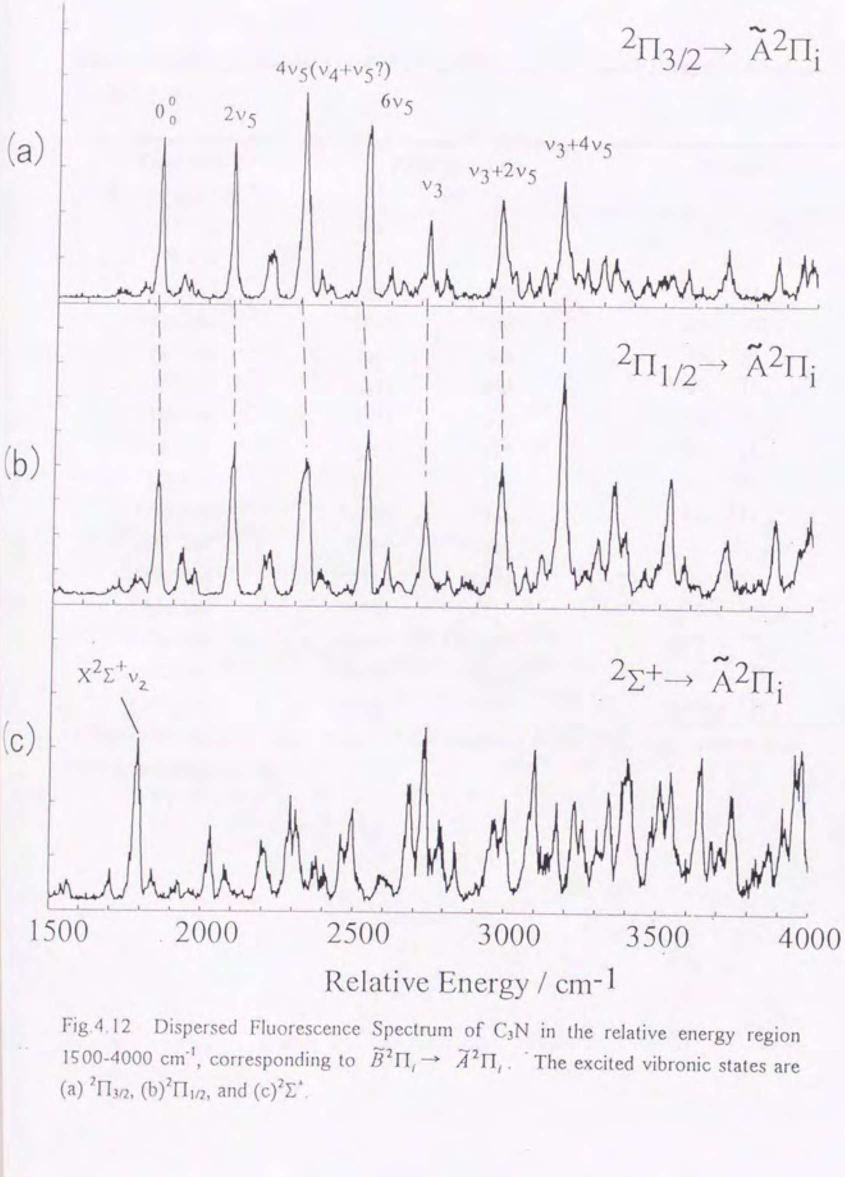

Fig.4.12 Dispersed Fluorescence Spectrum of C_3N in the relative energy region 1500-4000 cm^{-1}, corresponding to $\tilde{B}^2\Pi_i \rightarrow \tilde{A}^2\Pi_i$. The excited vibronic states are (a) $^2\Pi_{3/2}$, (b)$^2\Pi_{1/2}$, and (c)$^2\Sigma^+$.

Table 4.3 Observed vibronic bands in DF spectra from $^2\Pi$ vibronic states in the region of 1800-3500 cm^{-1}.

Transition Wavelength/ nm $^{a)}$	Relative Energy / cm^{-1} $^{a)}$		Remarks
371.148	1845	0	$\tilde{A}\,^2\Pi_i$, v = 0 $^2\Pi_{3/2}$
*370.838	*1846	*1	$^2\Pi_{1/2}$
374.417	2080	235	$2\nu_5$ $^2\Pi_{3/2}$
*374.234	*2091	*246	$2\nu_5$ $^2\Pi_{1/2}$
377.728	2314	469	$4\nu_5$ $^2\Pi_{3/2}$
*377.574	*2327	*482	$4\nu_5$ $^2\Pi_{1/2}$
380.708	2521	676	$6\nu_5$ $^2\Pi_{3/2}$
*380.518	*2532	*687	$6\nu_5$ $^2\Pi_{1/2}$
383.693	2726	881	$8\nu_5$ $^2\Pi_{3/2}$
*383.352	*2726	*881	$8\nu_5$ $^2\Pi_{1/2}$
387.249	2965	1120	ν_3 $^2\Pi_{3/2}$
*387.026	*2974	*1129	ν_3 $^2\Pi_{1/2}$
390.286	3166	1321	$\nu_3+2\nu_5$ $^2\Pi_{3/2}$
*390.049	*3174	*1329	$\nu_3+2\nu_5$ $^2\Pi_{1/2}$
*392.686	*3346	*1501	$\nu_3+4\nu_5$ $^2\Pi_{1/2}$
*395.503	*3528	*1737	$\nu_3+4\nu_5$ $^2\Pi_{1/2}$

a) Transition energies show those of DF spectrum from $^2\Pi_{3/2}$, and marked with asterisks are those of $^2\Pi_{1/2}$.

References

1.M.Guelin and P.Thaddeus, Astrophys. J. Lett., 212, L81(1977).

2.M.Guelin, S.Green, and P.Thaddeus, Astrophys. J. Lett., 224, L27(1978).

3.S.Wilson and S.Green, Astrophys. J. Lett. 212, L87(1977).

4.C.A.Gottlieb, E.W.Gottlieb, P.Thaddus, and H.Kawamura, Astrophys. J. 275,916(1983).

5.H.Mikami, S.Yamamoto, S.Saito, and M.Guelin, Astron. Astrophys., 217, L5(1989).

Calc.

6.P. Botschwina, M. Horn, J. Flugge, and S. Seeger, J. Chem. Soc. Faradae Trans., 89, 2219 (1993).

7.M. C. McCarthy, C.A. Gottlieb, P. Thaddeus, M. Horn, and P. Botschwina, J. Chem. Phys.103, 7820 (1995).

8. Kolos, Z.Zielinski, and Z.R. Grabowski, Chem. Phys. Lett., 180, 73 (1991).

9. Sadlej, and B. O. Roos, Chem. Phys. Lett., 180, 81 (1991).

10. Synthesis of HC_3N/HC_5N by discharge flow cell were carried out in Nobeyama Radio Observatory(NRO). Precursor of dehydration were also synthesized at NRO. I would very much appreciate to Prof. Kentaro Kawaguchi providing these compounds.

11. H. Kohguchi, Y. Ohshima, and Y. Endo, J. Chem. Phys., accepted.

12. M. Kolbuszewski, Astrophys. J. 432,L63, (1994).

13. A.J. Merer and D.N. Travis, Can. J. Phys. 44, 3536 (1966).

14. M. Kakimoto and T. kasuya, J. Mol. Spectrosc. 94, 380 (1982).

15. K.P. Huber and G. Herzberg Constants of diatomic molecules, Van Nostrand Reinhold Company Inc. (1979)

16. Y. Ohshima and Y. Endo, J. Mol. Spectrosc., 172, 225 (1995).

17. M.C. MaCathy. C.A. Gottlieb, P. Thaddeus, M. Horn and P. Botschwina, 103, 7820 (1995).

18. J.T. Hougen, J. Chem. Phys., 36, 519 (1962).

19. C.R. Brazier, L.C. O'Brien, and P.F. Bernath, J. Chem. Phys., 86, 3078 (1987).

20. H. Kohguchi, Y. Ohshima, and Y. Endo, accepted to J. Chem. Phys.

21. A.L. Sobolewski and L Adamowicz, J. Chem. Phys., 102, 394 (1995).

Appendix 4.1

$^2\Sigma^{(+)}_{1/2} - {}^2\Sigma^+$ **28792.1016(22) cm^{-1} band of C_3N.**

	P(N")				R(N")			
N''	P_2(N'')	obs.-calc.	P_1(N'')+P_{12}(N'')	obs.-calc.	R_{21}(N'')+R_2(N'')	obs.-calc.	R_1(N'')	obs.-calc.
0					28792.405	0.013	…	
1			28791.762	-0.010	28792.681	0.001	28792.730	-0.007
2	…		28791.419	0.015	28792.953	0.003	28793.033	0.003
3	28791.026	-0.003	28791.082	-0.003	28793.212	0.008	28793.309	0.001
4	28790.640	0.000	28790.717	-0.001	28793.449	0.006	28793.570	0.001
5	28790.229	-0.006	28790.339	0.003	28793.674	0.008	28793.815	0.001
6	28789.806	-0.007	28789.932	-0.005	28793.868	-0.005	28794.048	0.006
7	28789.369	-0.007	28789.520	-0.002				
8								

$^2\Pi_{1/2}$-$^2\Sigma^+$ 28792.1016(22) cm^{-1} band of C_3N

$^2\Pi_{1/2}$-$^2\Sigma^+$ band.

J''	P_2(J'')	obs.-calc.	P_{21}(J''+1)+Q_2(J'')	obs.-calc.	Q_{21}(J'')+R_2(J''-1)	obs.-calc.	R_{21}(J'')	obs.-calc.
0.5			28811.353	0.001	28811.692	0.010	28812.128	-0.022
1.5	28810.724	0.032	28811.160	-0.001	28811.816	-0.004	28812.593	-0.009
2.5	28810.170	0.000	28810.941	-0.010	28811.940	-0.001	28813.032	-0.003
3.5	28809.638	0.007	28810.724	-0.001	28812.047	0.002	28813.443	-0.008
4.5	28809.072	-0.003	28810.475	-0.005	28812.128	-0.002	28813.853	0.004
5.5	28808.501	0.001	28810.218	0.000	28812.196	-0.002	28814.236	0.007
6.5	28807.916	0.008	28809.943	0.004	28812.251	0.002	28814.583	-0.009
7.5	28807.300	0.002	28809.638	-0.003			28814.942	0.005
8.5	28806.688	0.017	28809.320	-0.006			28815.272	0.007
9.5	28806.023	-0.001	28808.990	-0.004			28815.568	-0.007

$^2\Pi_{3/2}$-$^2\Sigma^+$ band.

J''	P_{12}(J'')	obs.-calc.	P_1(J''+1)+Q_{12}(J'')	obs.-calc.	Q_1(J'')+R_{12}(J''-1)	obs.-calc.	R_1(J'')	obs.-calc.
0.5							28788.063	0.006
1.5	28786.062	-0.015	28787.068	0.002	28787.729	0.002	28788.502	0.004
2.5	28785.525	-0.003	28786.846	-0.002	28787.836	-0.002	28788.921	0.004
3.5	28784.952	-0.005	28786.604	-0.003	28787.932	0.005	28789.342	0.027
4.5	28784.360	-0.004	28786.348	0.003			28789.683	-0.008
5.5	28783.744	-0.006	28786.062	0.002			28790.041	-0.005
6.5			28785.754	-0.001			28790.378	-0.001
7.5			28785.419	-0.009				
8.5			28785.097	0.018				
9.5			28784.699	-0.010				

$^2\Sigma^{(+)}_{1/2} - {}^2\Sigma^+$ **28957.2768(38) cm^{-1} band of C$_3$N.**

	P(N")				R(N")			
N''	P$_2$(N'')	obs.-calc.	P$_1$(N'')+P$_{12}$(N'')	obs.-calc.	R$_{21}$(N'')+R$_2$(N'')	obs.-calc.	R$_1$(N'')	obs.-calc.
0					28957.451	-0.014	28957.644	-0.005
1			28956.941	-0.006	28957.685	-0.010	28958.010	0.009
2	28956.454	-0.021	28956.669	0.011	28957.907	0.002	28958.318	-0.014
3	28956.037	-0.008	28956.360	0.011	28958.093	-0.003	28958.645	-0.001
4	28955.592	-0.004	28956.037	0.016	28958.271	0.004	28958.940	0.002
5	28955.132	0.006	28955.686	0.012	28958.441	0.022	28959.222	0.010
6	28954.633	-0.005	28955.316	0.009	28958.551	-0.000	28959.437	-0.029
7			28954.929	0.009			28959.711	0.010
8			28954.525	0.011			28959.927	0.012
9			28954.121	0.033				
10			28953.610	-0.033				
11			28953.032	-0.146				

$^{2}\Sigma^{(+)}_{1/2} - {}^{2}\Sigma^{+}$ **28973.3215(12) cm^{-1} band of C_3N.**

	P(N")				R(N")			
N''	P_2(N'')	obs.-calc.	P_1(N'')+P_{12}(N'')	obs.-calc.	R_{21}(N'')+R_2(N'')	obs.-calc.	R_1(N'')	obs.-calc.
0					28973.608	0.010	28973.665	0.002
1			28972.989	-0.003	28973.876	0.000	28973.967	-0.000
2	28972.613	0.005	28972.661	-0.001	28974.130	-0.007	28974.260	-0.005
3	28972.224	-0.002	28972.316	-0.001	28974.379	-0.001	28974.540	-0.005
4	28971.827	0.000	28971.956	0.000	28974.602	-0.004	28974.806	-0.001
5	28971.412	0.002	28971.579	0.002	28974.806	-0.010	28975.051	-0.002
6	28970.976	0.000	28971.174	-0.002	28975.015	0.001	28975.283	0.001
7	28970.531	0.005	28970.765	0.004	28975.183	-0.001	28975.486	-0.007
8	28970.060	0.002	28970.324	-0.006	28975.340	-0.001	28975.687	-0.001
9	28969.572	-0.001	28969.889	0.006				
10	28969.070	-0.001	28969.422	0.001				

$^2\Sigma^{(+)}_{1/2}-{}^2\Sigma^+$ **29049.0926(15) cm^{-1} band of C$_3$N.**

	P(N")				R(N")			
N''	P$_2$(N'')	obs.-calc.	P$_1$(N'')+P$_{12}$(N'')	obs.-calc.	R$_{21}$(N'')+R$_2$(N'')	obs.-calc.	R$_1$(N'')	obs.-calc.
0					29049.349	-0.002	29049.434	0.003
1			29048.758	-0.004	29049.620	-0.000	29049.754	0.000
2	29048.360	-0.002	29048.440	-0.001	29049.868	-0.002	29050.061	0.004
3	29047.976	0.006	29048.105	0.003	29050.098	-0.006	29050.333	0.010
4	29047.564	0.004	29047.746	0.000	29050.333	0.014	29050.614	0.003
5	29047.138	0.004	29047.368	-0.004	29050.514	-0.003	29050.858	-0.004
6	29046.688	-0.001	29046.982	0.002	29050.694	-0.003	29051.090	-0.005
7	29046.220	-0.006	29046.573	0.002			29051.306	-0.005
8	29045.748	0.001	29046.144	0.000				
9			29045.410	0.011				

$^2\Sigma^+-{}^2\Sigma^+$ **29144.2216(24) cm^{-1} band of C$_3$N.**

N''	P(N'')	obs.-calc.	R(N'')	obs.-calc.
0			29144.540	0.006
1	29143.885	-0.007	29144.832	0.004
2	29143.539	-0.005	29145.098	-0.006
3	29143.180	0.003	29145.368	0.005
4	29142.790	-0.004	29145.607	0.004
5	29142.398	0.006	29145.820	-0.007
6	29141.981	0.009	29146.018	-0.013
7	29141.539	0.004	29146.215	-0.003
8			29146.393	0.006

Chapter 5

Conclusions

In the present work, electronic spectra of large carbon chain molecules, C_4H (CCCCH), C_4D (CCCCD) and their isoelectronic molecule, C_3N (CCCN), have been reported by using laser induced fluorescence (LIF) spectroscopy. I have observed LIF spectra and dispersed fluorescence (DF) spectra for these three species.

(1) C_4H and C_4D

In the LIF spectra, $\tilde{B}^2\Pi_i - \tilde{X}^2\Sigma^+$ systems were observed in the region, 24000-25000 cm^{-1}(416.66 - 400 nm) for C_4H and C_4D. Twenty and seventeen vibronic bands of C_4H and C_4D have been observed , and rotational analyses of these bands and vibrational analysis were made for the $\tilde{B}^2\Pi_i$ states. The origins of $\tilde{B}^2\Pi_i$ were determined to be 24033.432(6) for C_4H and 24099.191(2) cm^{-1} for C_4D. Two types of ${}^2\Sigma-{}^2\Sigma$ bands were observed, ${}^2\Sigma^+-{}^2\Sigma^+$ and ${}^2\Sigma^{(\pm)}_{1/2}-{}^2\Sigma^+$, which belong to different bending modes with each other. ${}^2\Sigma^+$ vibronic states were those arise by excitation of bending modes with strong Renner-Teller effects and ${}^2\Sigma^{(\pm)}_{1/2}$ were those with weak Renner-Teller effect. Two bending modes were assigned, ν_6 CCC bending modes with the vibrational frequencies of ω_6=191 cm^{-1} for C_4H and 184 cm^{-1} for C_4D, where Renner parameters were very small, ε_6=-0.015 and -0.019, and ν_5 CCH bending modes, whose vibrational structures indicate that C_4H and C_4D have quasi-linearlities along ν_5 modes in the $\tilde{B}^2\Pi_i$ states. The ${}^2\Sigma-{}^2\Sigma$ band, although symmetry forbidden for $\tilde{B}^2\Pi_i - \tilde{X}^2\Sigma^+$ electronic transition, were vibronic allowed transition through $\tilde{A}^2\Pi_i - \tilde{X}^2\Sigma^+$ vibronic interaction. The strength of ${}^2\Sigma-{}^2\Sigma$ bands were very strong compared with symmetry allowed ${}^2\Pi-{}^2\Sigma$ bands. This results suggest the considerably strong vibronic interaction between the ground state, $\tilde{X}^2\Sigma^+$, and the first excited state, $\tilde{A}^2\Pi_i$, which were accidentally very close to $\tilde{X}^2\Sigma^+$.

Fluorescence time profiles consisted of two components for most of the observed vibronic states of $\tilde{B}^2\Pi_i$: the strong short time decay (τ=10-20 ns) and the very weak long time decay ($\tau > 2$ μs) components, where quantum beats were observed on the latter. This results indicate that fast internal conversions to highly vibrationally excited states of $\tilde{X}^2\Sigma^+$ and $\tilde{A}^2\Pi_i$ occur in the $\tilde{B}^2\Pi_i$ state, rather than dissociations.

In the DF spectra from the $\tilde{B}^2\Pi_i$ state, partial vibrational structure of the ground state, $\tilde{X}^2\Sigma^+$, and the low-lying first excited electronic state, $\tilde{A}^2\Pi_i$, have been observed. The lowest bending mode ν_7 (CCC bending) of $\tilde{X}^2\Sigma^+$ were assigned and vibrational frequencies were determined to be ν_7=118 cm^{-1} for C_4H and 114 cm^{-1} for C_4D, respectively. ν_6 progression of the $\tilde{A}^2\Pi_i$ were observed and vibrational frequencies were determined to 206 and 205 cm^{-1}, and the origins of $\tilde{A}^2\Pi_i$ were estimated to be 230 and 217 cm^{-1} for C_4H and C_4D, respectively.

(2) C_3N

LIF spectra of C_3N corresponding to $\tilde{B}^2\Pi_i - \tilde{X}^2\Sigma^+$ transition were observed in the region 28600-29200 cm^{-1} (349.65-342.47 nm). Six vibronic bands were observed and rotational analyses were made for these bands. The origin of the $\tilde{B}^2\Pi_i$ state was (tentatively) determined to be 28799.638(1) cm^{-1}. $^2\Sigma-^2\Sigma$ and $^2\Sigma^{(\pm)}_{1/2}-^2\Sigma^+$ bands were observed with the same intensities with a $^2\Pi-^2\Sigma$ band. This result indicate that the $\tilde{A}^2\Pi_i - \tilde{X}^2\Sigma^+$ vibronic mixing, which cause vibronic induced $^2\Sigma-^2\Sigma$ transition, is relatively weak compared with the case of C_4H or C_4D due to larger $\tilde{A}^2\Pi_i - \tilde{X}^2\Sigma^+$ energy gap.

Fluorescence time profiles of C_3N also consisted of two components, due to internal conversions to highly vibrationally excited states of $\tilde{X}^2\Sigma^+$ and $\tilde{A}^2\Pi_i$, similar to C_4H. However the short time decay (τ=120 ns) component were longer and the long time decay ($\tau > 2$ μs) components is much stronger, compared with the case of C_4H. This results can be explained qualitatively that the density of states of highly vibrationally excited states of $\tilde{X}^2\Sigma^+$ and $\tilde{A}^2\Pi_i$ of C_3N is smaller than those of C_4H.

DF spectra show clearly distinguishable structure into $\tilde{B}^2\Pi_i \rightarrow \tilde{X}^2\Sigma^+$ and $\tilde{B}^2\Pi_i \rightarrow \tilde{A}^2\Pi_i$ transitions. The origin of the $\tilde{A}^2\Pi_i$ state was determined to 1846 cm^{-1}. Both $\tilde{B}^2\Pi_i \rightarrow \tilde{X}^2\Sigma^+$ and $\tilde{B}^2\Pi_i \rightarrow \tilde{A}^2\Pi_i$ accompanied ν_5 progressions, and the vibrational frequencies were estimated to 133 cm^{-1} for $\widetilde{X}^2\Sigma^+$ and 120 cm^{-1} for $\widetilde{A}^2\Pi_i$.

Comparing the isoelectronic species, C_4H and C_3N, they have quite similar electronic structures and configurations as shown in Fig.5.1. Especially, both have the very low lying first excited electronic states, $\widetilde{A}^2\Pi_i$, which provide these isoelectronic molecules the special feature of electronic structure.

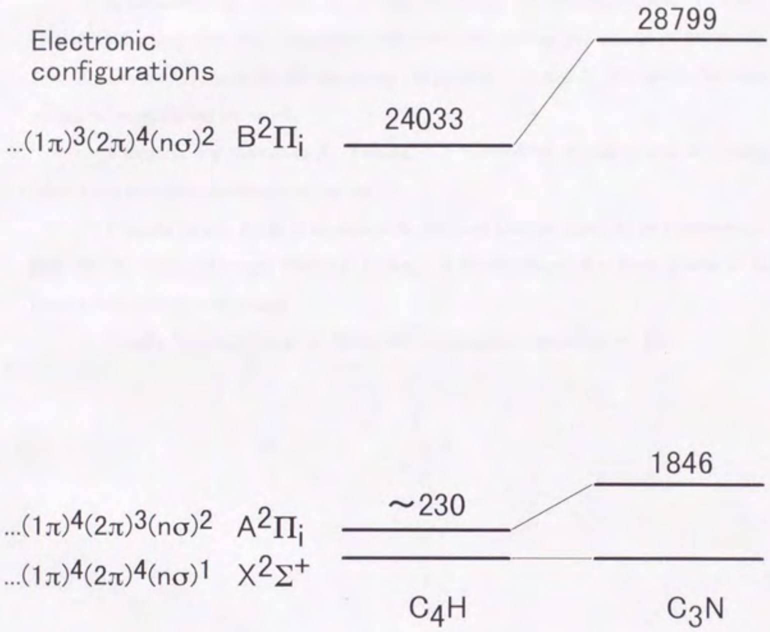

Fig.5.1 Electronic structure of C_4H and C_3N.

Acknowledgment

I wish to sincere thank Professor Y. Endo for his kind guidance and advice on this thesis. I would also like to thank Professor Y. Ohshima (Kyoto University) for his advice and comments on my work.

I acknowledge to Drs. H. Kohguchi (IMS), Y. Sumiyoshi and Y. Kasai (RIKEN) for their valuable discussions and kind helps during the course of my study. I would also like to thank Dr. H. Kanokogi (Microsoft Co.) and A. Mizoguchi for their technical supports on my work.

I express my thanks to K. Tanaka, A.J. Schoeffler, K. Seki, and all Endo's laboratory members for encouraging me.

I would like to thank to Professor K. Shibuya (Tokyo Institute of Technology) and Dr. K. Aoki (Yonago National College of Technology) for their guidance in research of laser spectroscopy.

Finally, I should thank my family for continuous supporting my life.

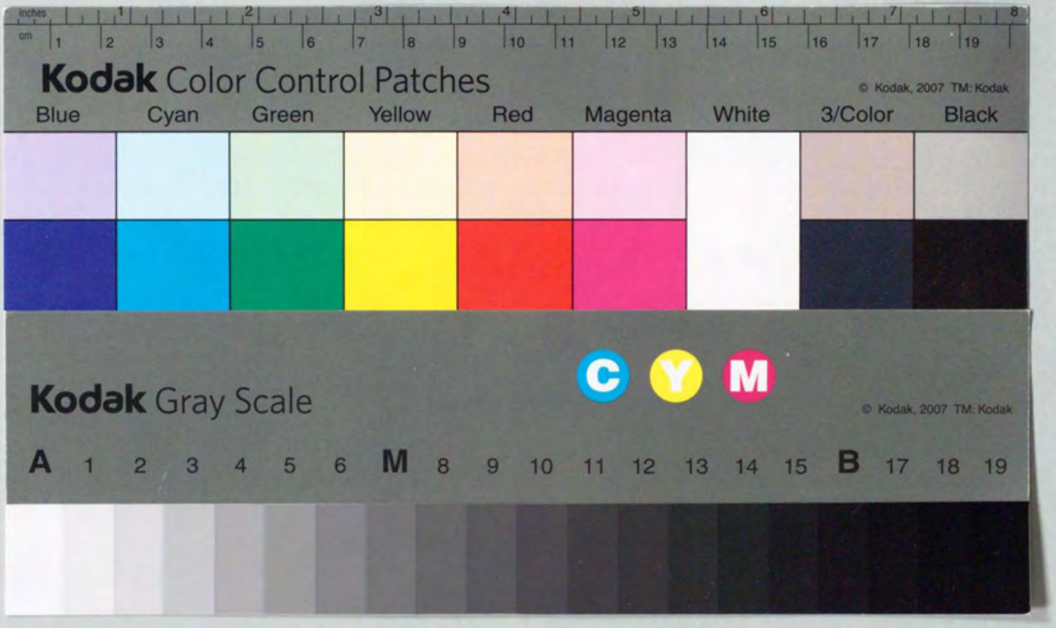
inches
cm
Kodak Color Control Patches
© Kodak, 2007 TM: Kodak
Blue
Cyan
Green
Yellow
Red
Magenta
White
3/Color
Black
Kodak Gray Scale
C
Y
M
© Kodak, 2007 TM: Kodak
A 1 2 3 4 5 6 M 8 9 10 11 12 13 14 15 B 17 18 19